Scholars' Mine

Masters Theses

Student Theses and Dissertations

Summer 2011

Morpho-tectonic analysis of the Tekeze and the Blue Nile drainage systems of northwestern Ethiopian Plateau, Ethiopia

Elamin Hassan Dai Ismail

Follow this and additional works at: https://scholarsmine.mst.edu/masters_theses

Part of the Geology Commons, and the Geophysics and Seismology Commons

Department:

Recommended Citation

Ismail, Elamin Hassan Dai, "Morpho-tectonic analysis of the Tekeze and the Blue Nile drainage systems of northwestern Ethiopian Plateau, Ethiopia" (2011). *Masters Theses*. 4974.
https://scholarsmine.mst.edu/masters_theses/4974

This thesis is brought to you by Scholars' Mine, a service of the Missouri S&T Library and Learning Resources. This work is protected by U. S. Copyright Law. Unauthorized use including reproduction for redistribution requires the permission of the copyright holder. For more information, please contact scholarsmine@mst.edu.

MORPHO-TECTONIC ANALYSIS OF THE TEKEZE AND THE BLUE NILE DRAINAGE SYSTEMS OF NORTHWESTERN ETHIOPIAN PLATEAU, ETHIOPIA

by

ELAMIN HASSAN DAI ISMAIL

A THESIS

Presented to the Faculty of the Graduate School of the

MISSOURI UNIVERSITY OF SCIENCE AND TECHNOLOGY

In Partial Fulfillment of the Requirements for the Degree

MASTER OF SCIENCE IN GEOLOGY AND GEOPHYSICS

2011

Approved by

Mohamed Abdelsalam, Advisor
Stephen Gao
David Rogers

© 2011
Elamin Hassan Dai Ismail
All Rights Reserved

DEDICATION

To

My late mother, late father and late brothers
Ismail and Agabna

To
My late friend Mansour M. Farag

To

My family

Siham, Sahar, Dali, Eiman and Mohamed

My aunt Fathia and my brothers and sisters

ABSTRACT

This study examines the morpho-tectonic evolution of the drainage system in the northwestern Ethiopian plateau by focusing on the Tekeze and the Blue Nile Rivers. The plateau is underlain by Precambrian crystalline rocks, overlain by Mesozoic sedimentary section that is topped with a 1-3 km thick pile of Oligocene-Quaternary volcanic rocks. It is bounded in the east and southeast by the Afar Depression (AD) and the Main Ethiopian Rift (MER). Satellite derived Digital Elevation Models are analyzed using ArcGIS and RiverTools to extract morpho-tectonic parameters of tributaries of the Tekeze and Blue Nile Rivers including Normalized Steepness Index (K_{sn}), Concavity (θ), Regression Fit (r^2), and spatial distribution of major and minor knickpoints and faults. Two end-member models have been previously proposed: 1) a steady-state rate of incision since the beginning of the development of these drainage systems (~30 Ma) or 2) a rate of incision that increased through time. This study shows that the incision history of these drainage systems is more complex than can be explained by these two end-member models. Nevertheless, the models are still valid explanations for specific regions of the plateau. The evolution of the drainage systems on the NW plateau is influenced by three tectonic and geological events: 1) The rising of the Afar mantle plume (~30 Ma) created a moderate increase in the incision rate of the entire plateau, 2) a localized increase in the incision rate associated with the shield volcanoes build-up event (~22 Ma) and lastly 3) a significant increase of the incision rate in the eastern part of the northwestern plateau due to rift-flank uplift on western escarpment of the AD and the northwestern escarpment of the MER. This uplift diminishes westward leaving the drainage system in the lower reaches of the Tekeze and Blue Nile Rivers relatively tectonically undisturbed, hence establishing a long-lived hydrological stability and reaching steady-state equilibrium.

ACKNOWLEDGEMENTS

I am grateful to my family, Siham Eltayeb, Sahar, Dali, Eiman and Mohamed for their patience and support. I would like to thank Dr. Mohamed Abdelsalam as advisor, friend and colleague for the effort and advice to complete this work and my appreciation to my committee members, Dr. Stephen Gao, Dr. John Hogan, Dr. Francisca Ikuenobe, Dr. David Wronkiewicz and Dr. David Rogers. My thanks to Dr. José Vicente Pérez-Peña from the Department of Geodynamics, University of Granada, Spain for providing me with CalHypso extension software he and his colleagues has developed, and for linking me with indispensible resources for tectonic geomorphology. I would like to thank the Geology and Geophysics Program at Missouri University of Science and Technology for the financial assistance they made available to me through the Radcliff endowment. I am very thankful for the Geological Engineering program and faculty for making my transition to the PhD program in Geological Engineering. Special thanks to my colleagues Dr. Kamal Sharafaldin Ali, Dr. Osama Awadelkarim and Dr. Mahgoub Ali for encouraging me to go back to school. Special thanks to Ahmed Elsheikh and to the remote sensing lab group for their support and advices. I am grateful to Dr. Lulu Tisege for his overwhelming assistance during my field work in Ethiopia and for all those in the Geological Survey of Ethiopia and the Tekeze Hydro-electric power project for making my field work in Ethiopia an unforgettable experience. Field work of this project was funded by the National Science Foundation (NSF) through a project entitled “Modeling Drainage Incision on the Ethiopian Plateau”.

TABLE OF CONTENTS

LIST OF ILLUSTRATIONS

LIST OF TABLES

Page

1. INTRODUCTION

1.1. STATEMENT OF THE PROBLEM AND OBJECTIVES

1.1.1. Statement of the Problem Significant research has been conducted to understand the interplay between geomorphology and tectonics in continental collision regimes such as the Alps, the Himalayas, the Tibetan plateau, and the Colorado plateau (e.g. Pederson et al., 2002; Clark et al., 2004; Schoenbohm et al., 2004; and McMillan et al., 2006). However, less research effort has been devoted to understand the morpho-tectonic evolution of drainage systems in active continental extensional regimes such as the Ethiopian plateau. The Ethiopian plateau (Figure 1.1) being one of the largest uplifted regions on Earth (the Wall of Africa) was formed during extensional tectonics associated with the Afar mantle plume and the opening of the East African Rift System which is represented in Ethiopia by the Afar Depression and the Main Ethiopian Rift (Figure 1.1). This region provides the geoscientific community with a unique opportunity to examine drainage evolution within non-orogenic tectonic regimes and to examine the relative roles of tectonic uplift, global climate change, and local structures in the evolution of long-lasting rivers. The Ethiopian plateau is underlain by Precambrian crystalline rocks and Mesozoic sedimentary rocks, and topped by ~2 km thick Oligocene – Quaternary volcanic rocks (Figure 1.2). Through time, rivers have incised deeply on the plateau forming in some places spectacular canyons that can be as deep as 1.5 km.

The plateau is dissected by the Afar Depression and the Main Ethiopian Rift into the northwestern plateau, dominated by the Tekeze River and Blue Nile drainage systems and a southeastern plateau occupied by Webi Shebelle and Ter Shet drainage system.

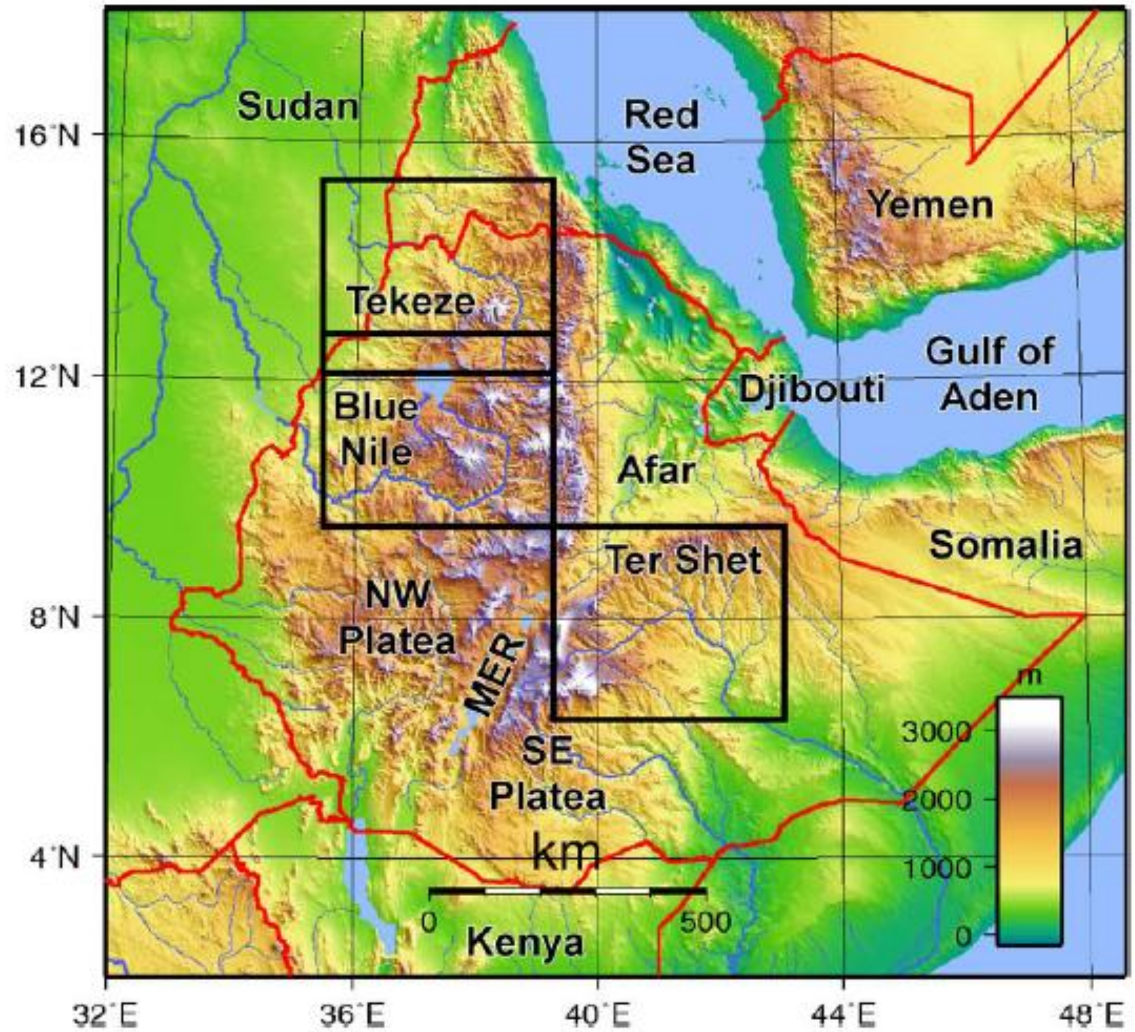

Figure 1.1: Digital Elevation Model (DEM) of Ethiopia showing topography, tectonic elements, and the drainage systems of the northwestern and southeastern Ethiopian plateaus, MER = Main Ethiopian Rift

(Figure 1.1). Few studies have been carried out to examine drainage evolution in the Ethiopian plateau (McDougall et al.., 1975; Weissel et al., 1995; Pik et al., 2003; Gani and Abdelsalam, 2006; and Gani et al., 2007). These studies have only focused on the Gorge of the Nile (Figure 1.1) which is arguably the rival of the Grand Canyon of the US.

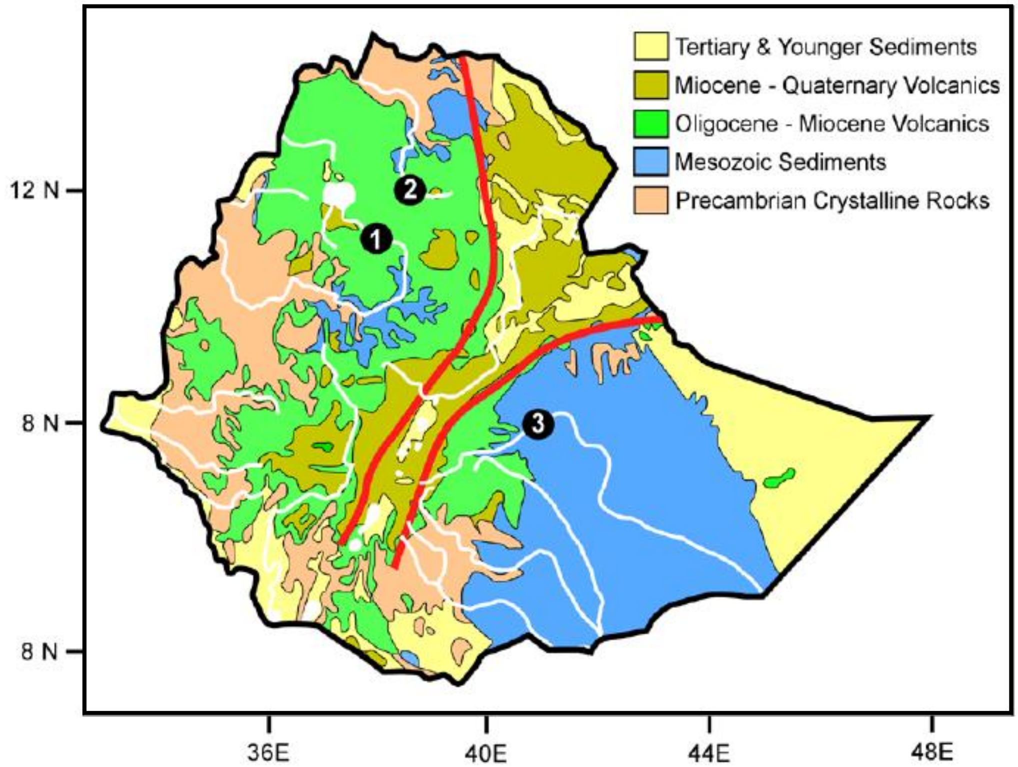

Figure 1.2: Geological map of Ethiopia showing the Ethiopian Plateau underlain by Precambrian crystalline rocks and topped with Oligocene – Quaternary volcanic rocks. 1 = Blue Nile and the Gorge of the Nile. 2 = Tekeze. 3 = Ter Shet. Red lines represent the approximate trends of the Afar Depression and Main Ethiopian Rift border faults.

Two contrasting end-member models have emerged from these studies: (1) Steady and constant rate of incision of the Blue Nile on the Ethiopian plateau since the beginning of the incision ~25-29 Ma ago (Pik et al., 2003); and (2) Significant increase in the rate of incision of the Blue Nile at ~10 and ~6 Ma (Gani et al., 2007).

The Pik et al. (2003) steady-steady model relies on results obtained from Apatite/He ages of samples collected from the Precambrian crystalline rocks. Pik et al. (2003) concluded that the upper Blue Nile drainage network went through long-term stability since the beginning of its incision ~25-29 Ma.

Additionally, Pik et al. (2003) suggested that the current hydrological characteristics of the Blue Nile drainage system were established early in the Oligocene time. This implies that the uplift of the Ethiopian plateau and its current physiographic features that control most of the present-day Blue Nile hydrology were established since the Oligocene (Pike et al., 2003).

Alternatively, Gani et al. (2007) suggested a pulsed plateau incision model. Gani et al. (2007) results are based on Geographic Information System (GIS) modeling of the Shuttle Radar Topography Mission (SRTM) Digital Elevation Model (DEM) data and ages of volcanic rocks that occur at different elevations in the Ethiopian plateau. In this model, Gani et al. (2007) proposed three tectonic uplift-driven phases of incision with an increased rate of incision through time. The first phase of incision, which dominated the period between 29–10 Ma, was characterized by slow and long-term incision that gradually increased from 53 m/Ma to 80 m/Ma. The second phase which occurred between 10 and 6 Ma was characterized by moderate rate of incision where the incision rate increased from 80 m/Ma to 120 m/Ma. The most recent incision phase occurred between 6 Ma and present where the long-term incision rates increased rapidly from 120 m/Ma to 320 m/Ma. Gani et al. (2007) concluded that much of the increase in the incision rate can be attributed to tectonic uplift, possibly associated with the rise of the Afar mantle plume, rather that climate change. This conclusion is based on that the timing of the increase of the incision rate of the Blue Nile in the Ethiopian plateau is out-of-phase with any enhanced precipitation in the region (Gani et al., 2007).

1.1.2. Objectives This present work recognizes the fundamental differences between the two end-member models of Pik et al. (2003) and Gani et al. (2007) and their subsequent implication in understanding the evolution of drainage system on the Ethiopian plateau. Hence, this work aims at understanding the morpho-tectonic evolution of the drainage systems in the northwestern Ethiopian plateau by focusing on the Tekeze River and the Blue Nile drainage systems. It relies on GIS analysis of DEMs extracted from the Advanced Spaceborne Thermal Emission and Reflection radiometer (ASTER) data, field studies, and published geological information to examine the morpho-tectonic evolution of the two drainage systems. Specifically, this work presents: (1) The geological context of the Tekeze River and the Blue Nile drainage systems;(2) Use morpho-tectonic analysis including: (A) The delineation of watershed of sub-basins or the tributaries of the two river and calculate their Normalized Steepness Index (K_{sn}) to evaluate the effect of tectonic uplift on the evolution of these sub-basins; (B) The extraction of the long profiles of these tributaries and evaluate their maturity through Regression Fit (r^2); (C) The computation of the Concavity (θ) values to evaluate the relative effect of tectonic uplift on the evolution of these tributaries; (D) The extraction of major and minor knickpoints from the long profiles to evaluate spatial distribution of potential tectonic uplift; and (3) Use these results to discuss the evolution of the Tekeze River and the Blue Nile on the northwestern Ethiopian plateau and evaluate the two-end members models.

1.2. OVERVIEW OF THE TEKEZE RIVER AND THE BLUE NILE

The River Nile is the longest in the world with total length of 6,650 km. Said (1993) divided the Nile River System into five regions including the Egyptian Nile, the Cataract Nile, the Central Sudan Nile, the Sudd Nile and Lake Plateau Nile. In his classification, Said (1993) included the drainage system in the Ethiopian plateau (the Tekeze River and the Blue Nile) within the Central Sudan Nile. Gani and Abdelsalam (2006) suggested separating the drainage system in the Ethiopian plateau from the Central Sudan Region because the two have different geological and geomorphological features that were shaped through different evolutionary paths.

The Tekeze and Blue Nile River basins are located in the northern part of northwestern Ethiopian plateau between latitudes ~8^{o} 30' and 15 ^{o} 00' N and longitudes ~36^{o} 00' and 40^{o} 00' E (Figure 1. 3). The length of Tekeze River in Ethiopia is ~608 km and its average elevation is ~1850 m above sea level (asl). The river flows in a north direction from its southernmost reaches, then circles Mount Ras Dashen in a semi-circular loop by flowing northeast, then north, then northwest before descending towards the low lands of the Sudan, (Figure 1.3; Tefera et. al., 2007). The Tekeze drainage system spans an area of ~69,000 km^2 bounded by the Axum-Adigrat lineament in the north, the western escarpment of Afar Depression in the east and the Simen ranges in the west, with an elevation ranging between 2500 and 4639 m (Figures 1.3 and 1.4a). The Simen ranges extend from Mount Ras Dashen (4639 m asl) in the north to Gondar and Mount Guna (4231 m asl) in the south and southeast respectively. These ranges continue to the east to Mount Abuna Yosef (4190 m asl) and merges into the flanks of the western escarpment of the Afar Depression. The southern elevated mountain ranges of Mount Guna separate the Tekeze River and the Blue Nile drainage basins (Figure 1.3).

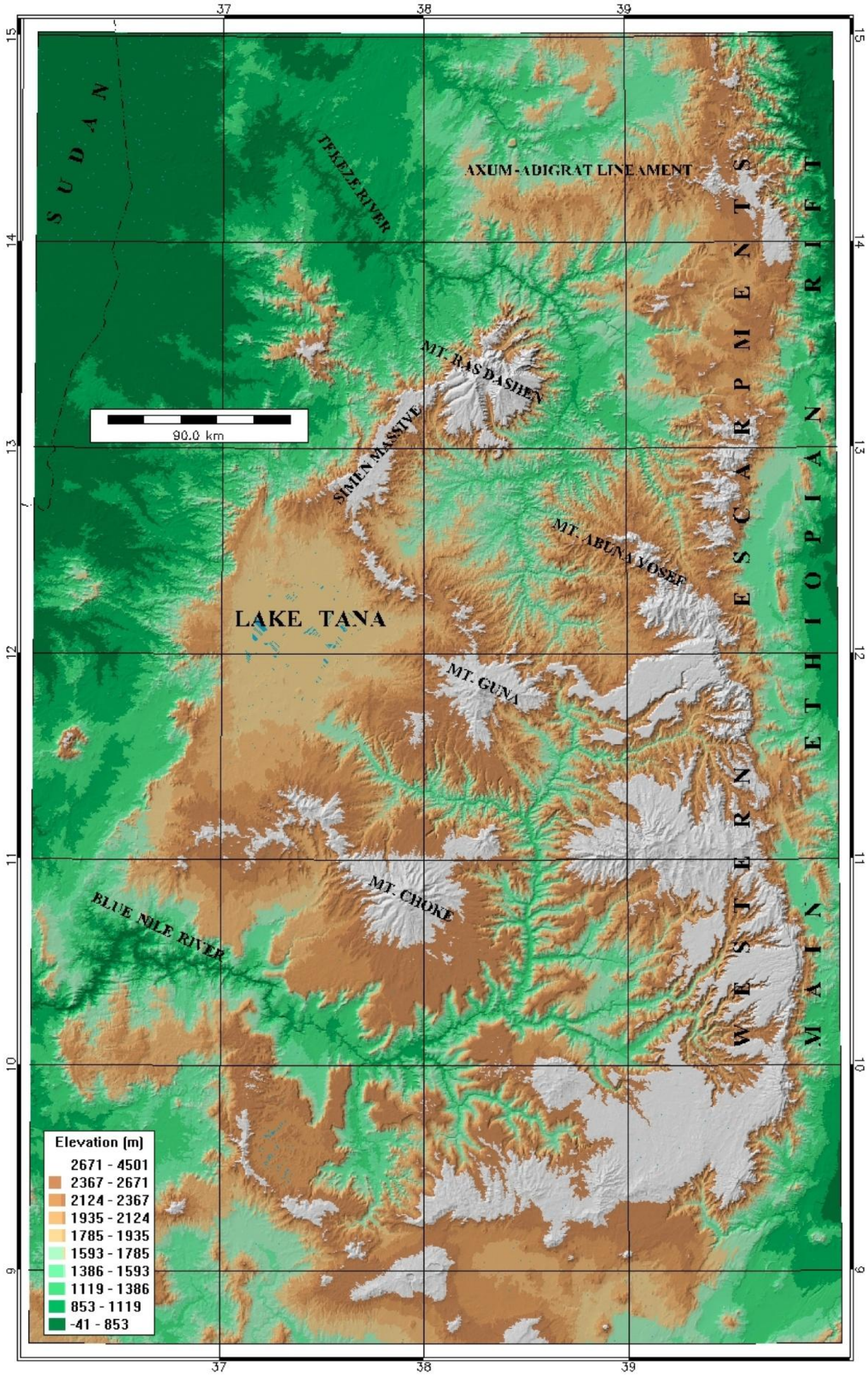

Figure 1.3: Location and physiographic setting of the Tekeze and the Blue Nile Rivers

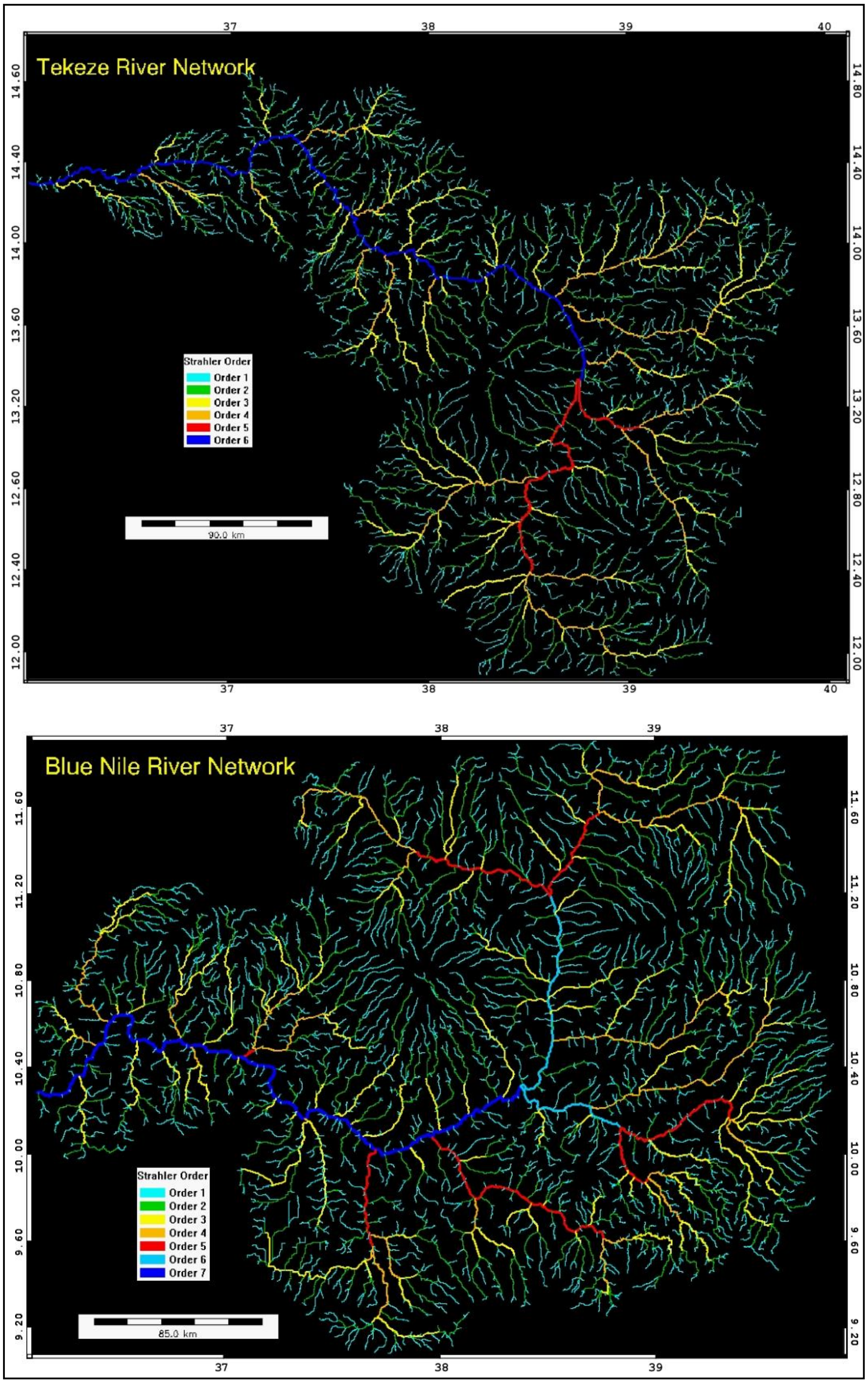

Figure 1.4: The Tekeze and Blue Nile Horton–Strahler Stream Order with pruning of three. The Tekeze River is a sixth order stream, and the Blue Nile is seventh order stream.

The Blue Nile originates from small riverlets in the Springs of Sakala which joins each others to from Gilgil Abay which flows northward to empty its water load in Lake Tana (Figure 1.3). The river emerges from Lake Tana as Abay or the Blue Nile where it makes a ~150 km radius loop around Mount Choke by flowing first southeast, then south, then southwest before ultimately travelling northwestward towards the low land of the Sudan (Figure 1.3; Gani and Abdelsalam, 2006). The total catchment area of the Blue Nile drainage system is estimated to be ~250,000 km^2 bounded between the elevated ranges of Mount Guna in the north, the western escarpment of the Afar Depression and the northwestern escarpments of the Main Ethiopian Rift in the southeast, and the Ambo lineament in the south (Figure 1.3; Gani and Abdelsalam, 2006; Gani et al., 2007).

1.3. TECTONIC SETTING

The Ethiopian plateau, with a mean elevation of 2.5 km, is divided by the tectonically-active Afar Depression and the Main Ethiopian Rift into the northwestern and the southeastern plateaus (Figure 1.1). The plateau was below sea level in the late Cretaceous as indicated by the presence of marine “Upper Limestone” formation overlain by Cretaceous continental fluvial sandstone (Gani and Abdelsalam, 2006; Gani et al., 2007, 2009). Today this contact is at an elevation of 2.2 km. The net rock uplift since ~150 Ma is thus over 2 km, much of which may have occurred in the past 30 Ma. The plateau was uplifted due to the combined effects of the rising Afar mantle plume and rift-flank uplift of the Afar Depression and the Main Ethiopian Rift (Collet et al., 1999; Sengor, 2001; Davis and Slack, 2002; Beyene and Abdelsalam, 2005). Sengor (2001) suggested that the Afar mantle plume reached the base of the African lithosphere by the

Middle Eocene resulting in regional uplift dominated by the Afar dome which reached a radius of ~1000 km. This was followed by outpouring of extensive (500–2000 m thick) flood basalts which were erupted at ~30 Ma over less than ~1 Ma period of time (Hoffmann et al., 1997). This volcanic pile was built over Precambrian crystalline rocks and Mesozoic sedimentary rocks (Figure 1.2). Gani et al. (2007) used a 1 km average thickness of the 30 Ma basaltic flow, an average density of 2800 kg/m^3 for the basalt, and 3300 kg/m^3 density for the mantle to estimate that such a volcanic pile would result in 0.85 km subsidence of the Ethiopian plateau in the absence of continued upwelling hot material to sustain topography. Gani et al. (2007) also estimated that the removal of geological material from the Ethiopian plateau through erosion (estimated to be ~93,200 km^3) would result in 0.3 km of isostatic rebound of the plateau. Hence, the net rock uplift of the Ethiopian plateau since 30 Ma is ~1.75 km.

The eruption of the ~30 Ma volcanic rocks covered an area of ~500,000 km^2 and it is inferred to mark the appearance of the Afar mantle plume (Mohr and Zanettin, 1988; Hofmann et al., 1997; Kieffer et al., 2004). Plume-related uplift caused deep-seated faults within the Ethiopian lithosphere, leading to the collapse of the Afar dome; a collapse that formed the Afar Depression at ~24 Ma (Capaldi et al., 1987; Beyene and Abdelsalam, 2005). This event was followed at ~22 Ma by shield volcano–building episodes (Kieffer et al., 2004). Wolfenden et al. (2004) suggested that the Main Ethiopian Rift started opening at ~11 Ma. However, Bonini et al. (2005) argued that extension forming the Main Ethiopian Rift started between 6 and 5 Ma. Another phase of shield volcano-building episodes took place at ~11 Ma (Kieffer et al., 2004) suggested to be related to the early phase of the Main Ethiopian Rift formation (Wolfenden et al., 2004).

1.4. GEOLOGY

Figure 1.5 is a generalized geological map of the Tekeze River and the Blue Nile. More research has been done on the geology of the Blue Nile sedimentary basin compared to the Tekeze River sedimentary basin, (Krenkel, 1926; Stefanini, 1933; Jespen and Athearn, 1961; Mohr, 1962; Ficcarelli, 1968; Kazmin, 1973, 1975; Merla et al., 1973; Beauchamp and Lemigne, 1975; Kalb and Oswald, 1974; McDougall et al., 1975; Canuti and Radrizzani, 1975; Beauchamp, 1974, 191977; Assefa, 1979, 1980, 1981, 1991; Chernet, 1988, Russo et al., 1994; Mangesha et al., 1996; Wood et al., 1997; Couile et al., 2003; Pik et al., 2003; Keiffer et al., 2004; Gani and Abdelsalam 2006; Gani et al., 2009). Gani et al. (2009) proposed that the Blue Nile is underlain by a NW-trending sedimentary basin most likely the continuation of the Blue Nile rift in the Sudan. Gani et al. (2009) proposed that the basin has in three main phases. The first phase (pre-sedimentation phase) occurred before rifting and was characterized by the peneplanation of the Neoproterozoic crystalline rocks, possibly during the Paleozoic time. The second phase dominated the Triassic to early Cretaceous and was characterized by the deposition of Mesozoic clastic and marine sedimentary formations. The third phase (post-sedimentation phase) was characterized by the extrusion of Early to Late Oligocene and Quaternary volcanic rocks, dominantly basalts. Figure 1.6 summarizes the stratigraphy of the Blue Nile sedimentary basin as proposed by Gani et al. (2009).

Beyth (1973) studied the Mekele outlier to the east of the Tekeze River (Figure 1.6) and concluded that it constitutes eight different formation; Precambrian meta-sedimentary rocks, Enticho sandstone, Edaga Arbi Glacials, lower Adigrat Sandstone, Augala shale, Antalo Limestone, upper Sandstone, and the Flood Basalts (Figure 1.6).

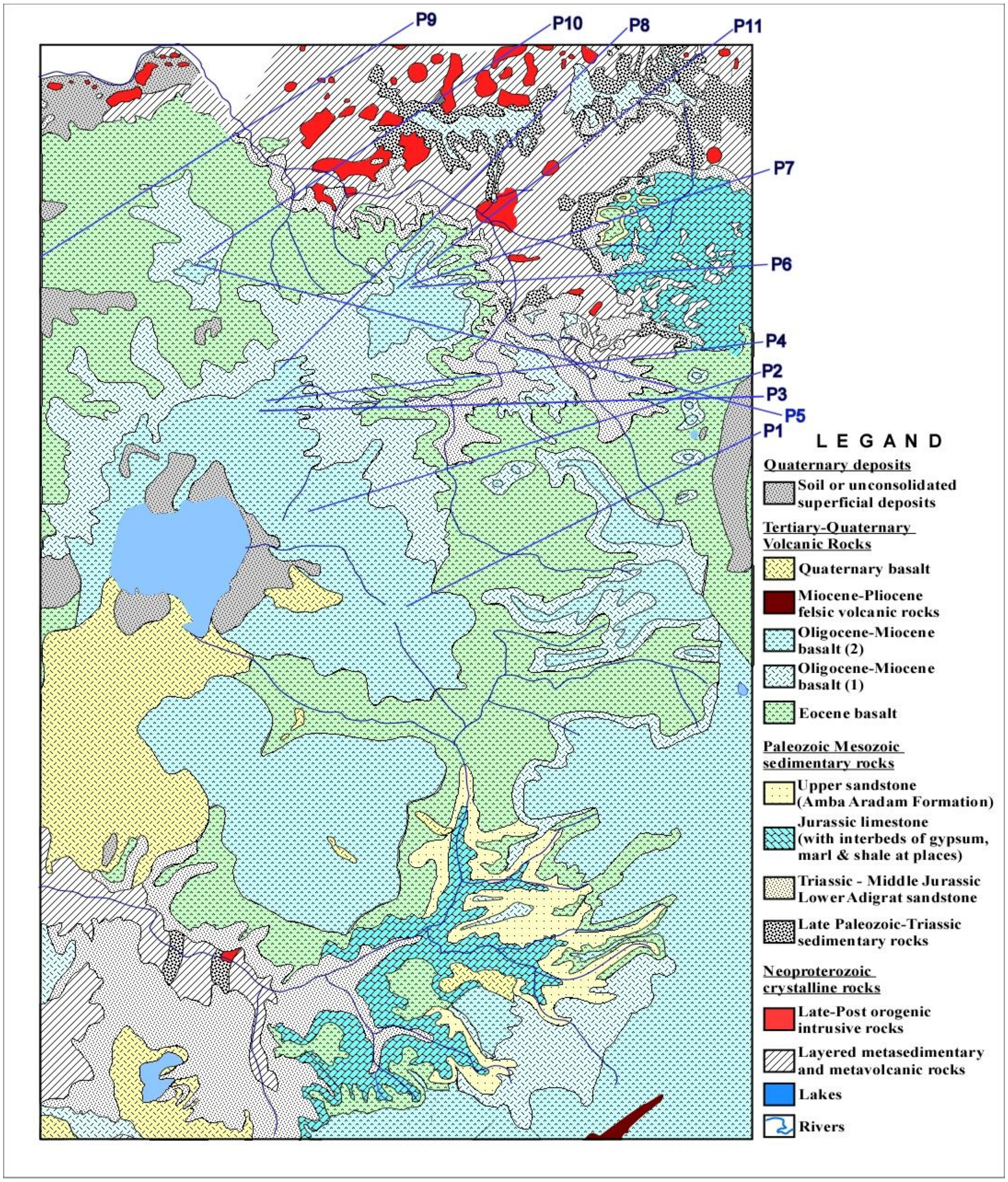

Figure 1.5: Geological map of the Tekeze and the Blue Nile River basins with the location of cross-sections shown as P1 to P11

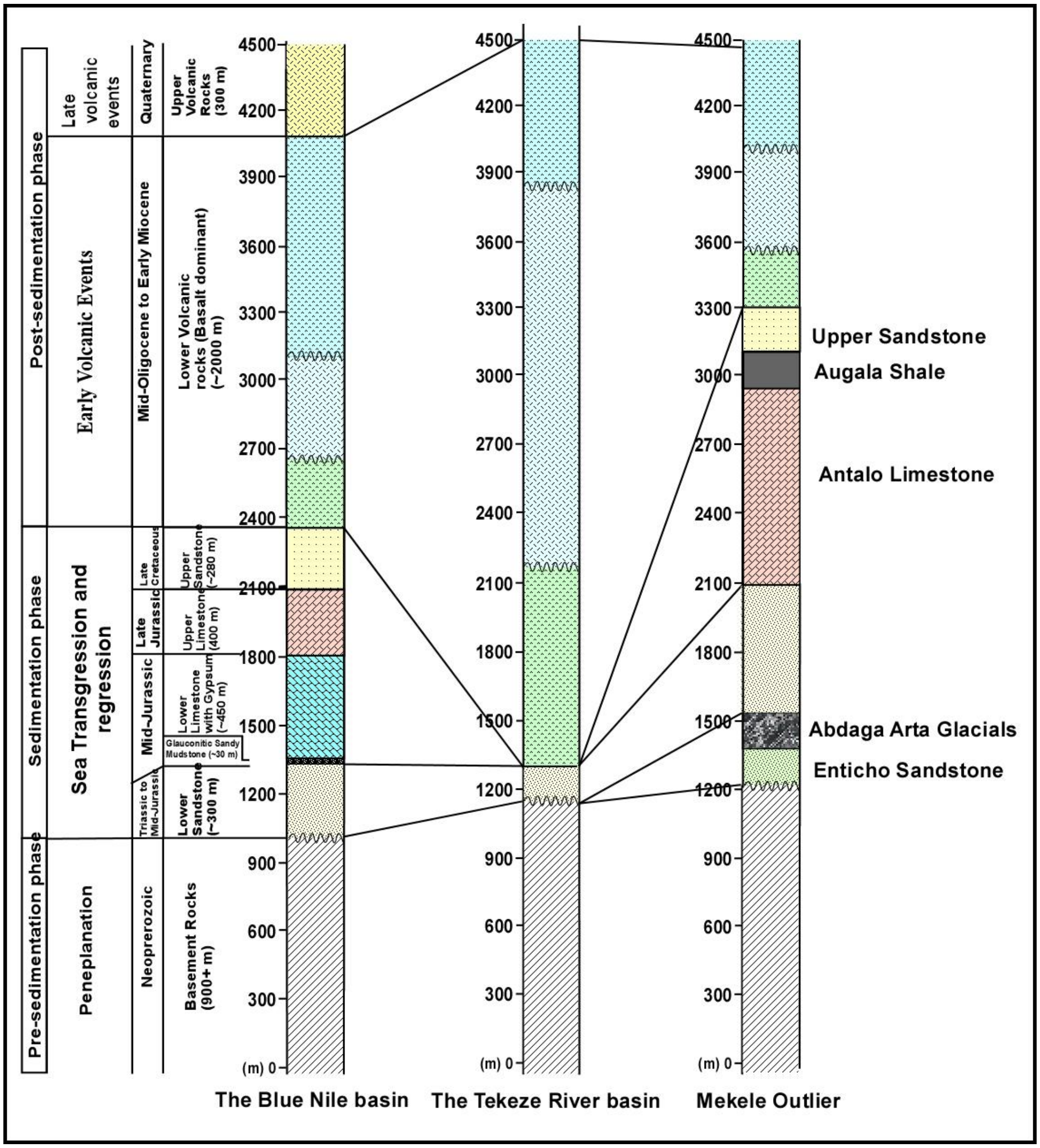

Figure 1.6: Stratigraphic columns comparing the stratigraphy of the Tekeze River (This Study) with those of the Blue Nile (Gani et al., 2009) and the Mekele Outlier (Beyth, 1973)

Since much more research was focused on the geology of the Blue Nile, this section will give a more detailed discussion on the geology of the Tekeze Rive and surroundings (Figure 1.5). This discussion relies on geological maps by the Ethiopian Geological Survey published in 1998 with scale of 1: 1,000,000 and the International

Geological Map of Africa (Sheet 3, 1/5,000,000) of the International Geological Mapping Bureau, published by the Commission for the Geological Mapping of the World (CGMW) and UNESCO, France in 1985. Additionally field work was conducted in the Tekeze River to delineate the contacts between different formations.

The geology of the Tekeze River differ from that of the Blue Nile basin and the Mekele outlier in that the Mesozoic sedimentary section is much thinner and most of the formations are missing with the exception of the Adigrat Sandstone. The Neoproterozoic crystalline rocks exposed along the Mekele River (Figure 1.6) are mainly slate, marble and meta-volcanic rocks. These layered rocks are highly deformed and show prominent N-trending foliation. They are also variably metamorphosed but the grade of metamorphism does not exceed the green schist facies. The slate is commonly grayish, rarely brownish, variegated in color and fine grained. It is graphitic in some places. The marble is black in color, fine grained, massive and jointed. It is laminated, contains quartz veins and veinlets that are strongly folded. It is stromatolitic in some places. The meta-volcanic rocks are of mafic composition and mainly exposed along both sides of the Tekeze River. These layered rocks are intruded by granitic bodies (Figure 1.5).

The Mesozoic sedimentary rocks are represented by the Adigrat sandstone which is well exposed along the Tekeze River. The maximum exposed thickness of the sandstone is about 50 meters (Figure 1.6) and pinches out to the west. It is ~ 700 m thick to the east at the Mekele outlier (Figure 1.6). The lowest exposed elevation of the Adigrat Sandstone is found in the Tekeze gorge at ~1052 m asl. The sandstone is medium-grained commonly reddish-brown and less commonly light-grey, whitish, purple and light-brownish in color. It is thinly-laminated and thinly-bedded rock. At its basal part close to the contact with the Neoproterozoic crystalline rocks it contains thin beds (~ 50 cm) of brownish siltstone. The contact between the weathered meta-volcanic rocks of the Neoproterozoic crystalline rocks and the sandstone is defined by a zone of about 1 meter thick indurated layer which contains angular fragments of the Neoproterozoic crystalline rocks cemented by yellowish matrix.

The Tertiary – Quaternary volcanic rocks divided into Eocene, Oligocene-Miocene, and Quaternary volcanic rocks which reach a maximum thickness of ~3000 m (Figure 1.6). These are dominantly exposed southwest of the Tekeze River (Figure 1.5). The lowest volcanic rocks (Eocene basalt) are deeply weathered and are dominantly alkaline basalts with rare intercalation of tuff. The Oligocene–Miocene basalts constitute a lower unit characterized by sub-alkaline basalts with infrequent intercalation of tuffs, rhyolites, and trachyte. This unit is overlain by alkaline basalts often found forming shield volcanoes. The Quaternary volcanic rocks are dominantly basalts with some rhyolites and these form outstanding plateaus.

2. DATA AND METHODS

2.1. DATA

ASTER imaging instrument boarded on Terra satellite which was launched in December 1999 by NASA as part of its Earth Observing System (EOS). ASTER is a joint effort between NASA, Japan’s Ministry of Economy, Trade and Industry (METI) and Japan's Earth Remote Sensing Data Analysis Center (ERSDAC). ASTER is being used to obtain high resolution data of land surface temperature, reflectance and elevation in fourteen bands, ranging from the visible and near-infrared (VNIR) to the shortwave infrared (SWIR) to the thermal infrared (TIR) wavelengths, as well as providing stereo viewing the DEM generation. These data have spatial resolution of 15 m in the VNIR region, 30 m in the SWIR and 90m in the TIR range. ASTER DEM covering both the Tekeze River and the Blue Nile was used as the main source for the data in this study. Along channel profiles, orthogonal profiles across both rivers and their tributaries, rivers networks and morpho-tectonic data, were all extracted from ASTER DEM.

2.2. METHODS

The ASTER DEMs are processed in Environment for Visualizing Images (4.5), ArcGIS 9.3.1 with CalHypso and Profiler 5.1 extensions, Matlab 2009 and RiverTools 3.03. ENVI is implemented in cropping the study area from an ASTER DEM and the extraction of topographic profiles orthogonal to the Tekeze River and utilized in the construction of the geological cross-sections. RiverTools is used to import the ASTER DEM of the study area for the extraction of the drainage networks and Strahler stream order, major and minor watersheds contributing to the over-all drainage, drainage areas, density, intensity and channel profiles. The ArcGIS 9.3.1 is a property of ESRI Inc. and it is a complete geographic information science for mapping and solutions (ESRI, 2011). ArcGIS9.3.1 utilized in this research in conjunction with Profiler 5.1 extension (Whipple et al. (2007), CalHypso module, written by Perez-Pena et al. (ESPL, 2009), and the HydroModeling extension written by Peter Isaacson.

ASTER DEM for the study area was saved in ENVI 4.5 as ASCII file and imported into ArcMap - ArcEditor as integer. Using Spatial Analysis tools in ArcMap, negative elevation values were removed, sinks were identified and filled and flow direction and flow accumulation raster images were created. Due to the large size of the study area, HydroModeling is used to delineate and create polygons for each individual watershed in the study area. The polygons extracted are used to clip each watershed DEM and flow accumulation. The clipped DEM's and flow accumulation ASCII files are imported into Matlab and converted into Matlab files. Channel profiles, major and minor kinckpoints, faults, and start and end of steep slopes along the profile are handpicked using Profiler 5.1 and assigned values of 1, 2, 5, 3 and 4 respectively. The stream profiles and handpicked data were imported into ArcMap as shape files including data tables containing description and figures of handpicked data.

CalHypso extension applied to each of the polygons and clipped watersheds. Subsequently, the hypsometric curves and hypsometric integral statistics for each basin are obtained. ArcGIS software is used to create shape files for major knickpoints, minor knickpoints, faults, rivers, basins and basin polygons.

3. RESULTS

3.1. RESULTS OF THE GEOLOGICAL ANALYSIS

To evaluate the potential geological and structural controls on the evolution of the Tekeze River, eleven geological cross-sections are constructed approximately orthogonal to the river (Figure 3.1). The locations of these geological cross-sections are shown in figure 1.5. Among other purposes, these geological cross-sections are produced to correlate stratigraphic units across the river. These geological cross-sections are produced through the extrapolation of topographic profiles from the ASTER DEM and the projection of geological boundaries shown in figure 1.5 onto these profiles. Since, there is no information about variation in the thickness of the formations cropping out along the Tekeze River, uniform thicknesses are assumed for all formations. Also, the geological contacts between these formations are assumed to be dominantly horizontal and change in the structural position of any formation is interpreted as due to faulting. Analysis of the geological cross-section suggests the following:

(1) The Tekeze River incises through progressively formations from its upper reaches in the south to its lower reaches in the north. From its source in the south, the river carves its way northwest and northward through Eocene basalts before exposing the Triassic – Middle Jurassic Adigrat formation (lower sandstone). The Tekeze River carves its channel through the Adigrat formation and then the Precambrian crystalline rocks by navigating its way around Mount Ras Dashen. In its northwestward flowing direction towards the lowlands of Sudan, the Tekeze River flow through dominantly Precambrian crystalline rocks.

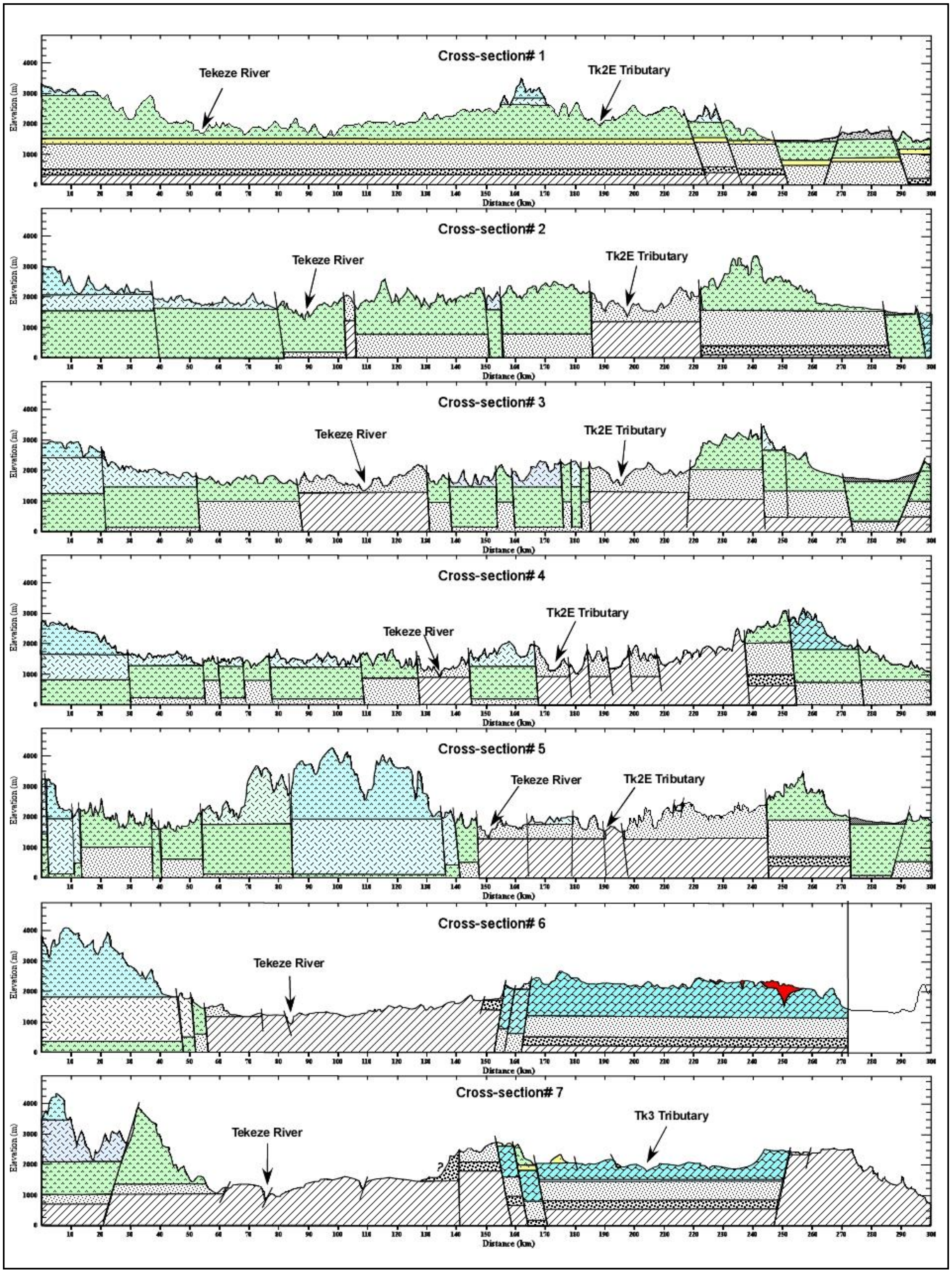

Figure 3.1: Geological sections across the Tekeze River.

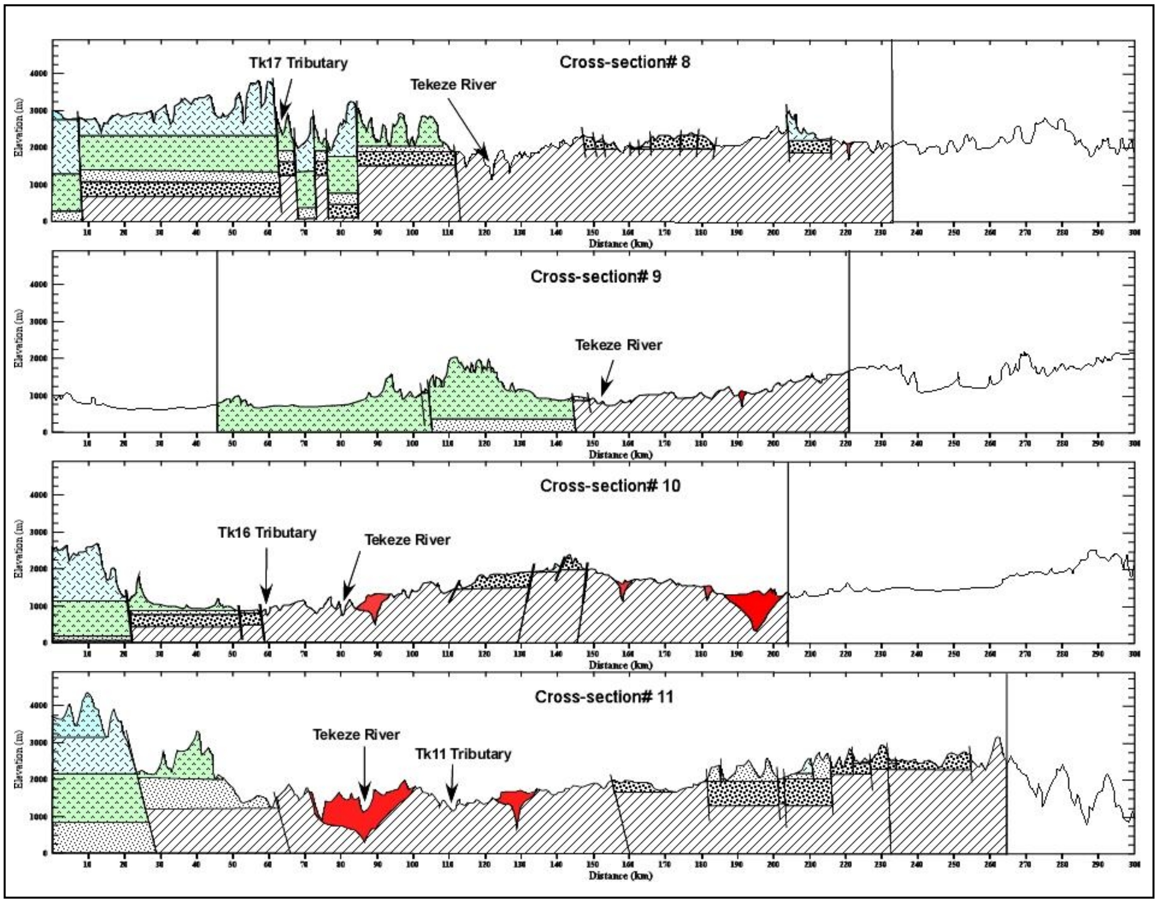

Figure 3.1: (Continued) Geological sections across the Tekeze River.

(2) Throughout much of its length, all stratigraphic units can be correlated across the Tekeze River and these units seem to maintain the same structural levels on both sides of the river. This suggests that for much of its length, the Tekeze River is not structurally-controlled. Nevertheless, numerous normal faults are suggested to exist on both sides of the Tekeze River to compensate for the vast differences in structural levels of different formations.

(3) Normal fault intensity seems to increase northward towards the Axum-Adigrat Lineament and eastward towards the western escarpments of the Afar Depression.

3.2. RESULTS OF MORPHO-TECTONIC ANALYSIS

Geomorphic indices and parameters have been widely used in studying local and regional active tectonics in collision regimes and in the incision history of fluvial rivers under different climatic and lithological constraints (Knuepfer, 2004; Harmar, 2006; Gani et al., 2007; Larue, 2007). Jordan et al., (2001; 2003) introduced the concept of Digital Terrain Analysis (DTA) which is a systematic approach for the extraction of morpho-tectonic information from the DEMs. Initially, Keller (1986) was the pioneer in using morpho-tectonic analysis in investigating active tectonics. Keller (1986) evaluated landforms using geomorphic indices such as the stream gradient index and the ratio of valley floor width to valley height. These indices provide insights into the adjustment of the geomorphologic elements of the terrain to the rates of tectonic activities. Subsequently, Yen-Chien (2003) applied stream gradient index and hypsometric analysis to highlight along-strike variations and to illustrate the relative activities in different tectonic regimes in the western foothills of Taiwan.

This study focuses on the extraction of morpho-tectonic parameters of the Tekeze River and the Blue Nile including: (1) The Normalized Steepness Index (K_{sn}); (2) The Regression Fit (r^2) of long profiles; (3) The Concavity (θ) values of the long profiles; and (4) The extraction of major and minor knickpoints from the long profiles to evaluate spatial distribution of potential tectonic uplift.

3.2.1. The Normalized Steepness Index (K_{sn}) The Normalized Steepness Index (**K_{sn}**) is calculated for all sub-basins of the Tekeze River and the Blue Nile (Figure 3.2). This index is used to quantify tectonic uplift rates on the basis of the agreement among researchers that the K_{sn} values are good approximation of tectonic uplift rates provided that the lithological and climate conditions are homogenous (Kirby, 2007, Wobus, 2005, Whipple, 2004, Koons, 1989, Burbank, 2004, Crosby, 2006, Bohon, 2009). The channel's K_{sn} value, which is a measure of the stream gradient normalized to the drainage area, is shown to be directly proportional to the rock uplift in a variety of landscapes (Cry et al., 2010). Many researchers identified the relation between longitudinal channel profiles, channel gradient and drainage area in response to changes in tectonic activity, climate change or lithology. The relationship can be derived from the power law equation $S = K_s A^{-\theta}$, where S is the channel slope, A is the upstream drainage area, K_s is the steepness and θ is the Concavity of the stream (Bohon, 2009). The K_{sn} values generally vary between 20 and 600 (Whipple, 2004). Generally high $\mathbf{K}_{sn}$ value are indicative of fast tectonic uplift whereas low $\mathbf{k}_{sn}$ values are associated with fluvial rivers that were not affected by tectonic uplift.

The K_{sn} values of the Tekeze river and the Blue Nile are as high as 162 and as low as 24.2 (Figure 3.2). These values can be explained as follows:

(1) The lowest K_{sn} values (24.2, 24.7 and 25.8) are found in the tributaries at the northwestern end of the Tekeze River on northeastern side of the river. This part of the river is close to the low lands of the Sudan and the tributaries originate from sources that have elevations just slightly higher than the river itself. The K_{sn} values progressively increase (ranging between 59 and 79.3) towards the southeast as the western escarpment of the Afar Depression is approached. This is suggestive of an increased tectonic uplift from west to east due to rift-flank uplift of the Afar Depression.

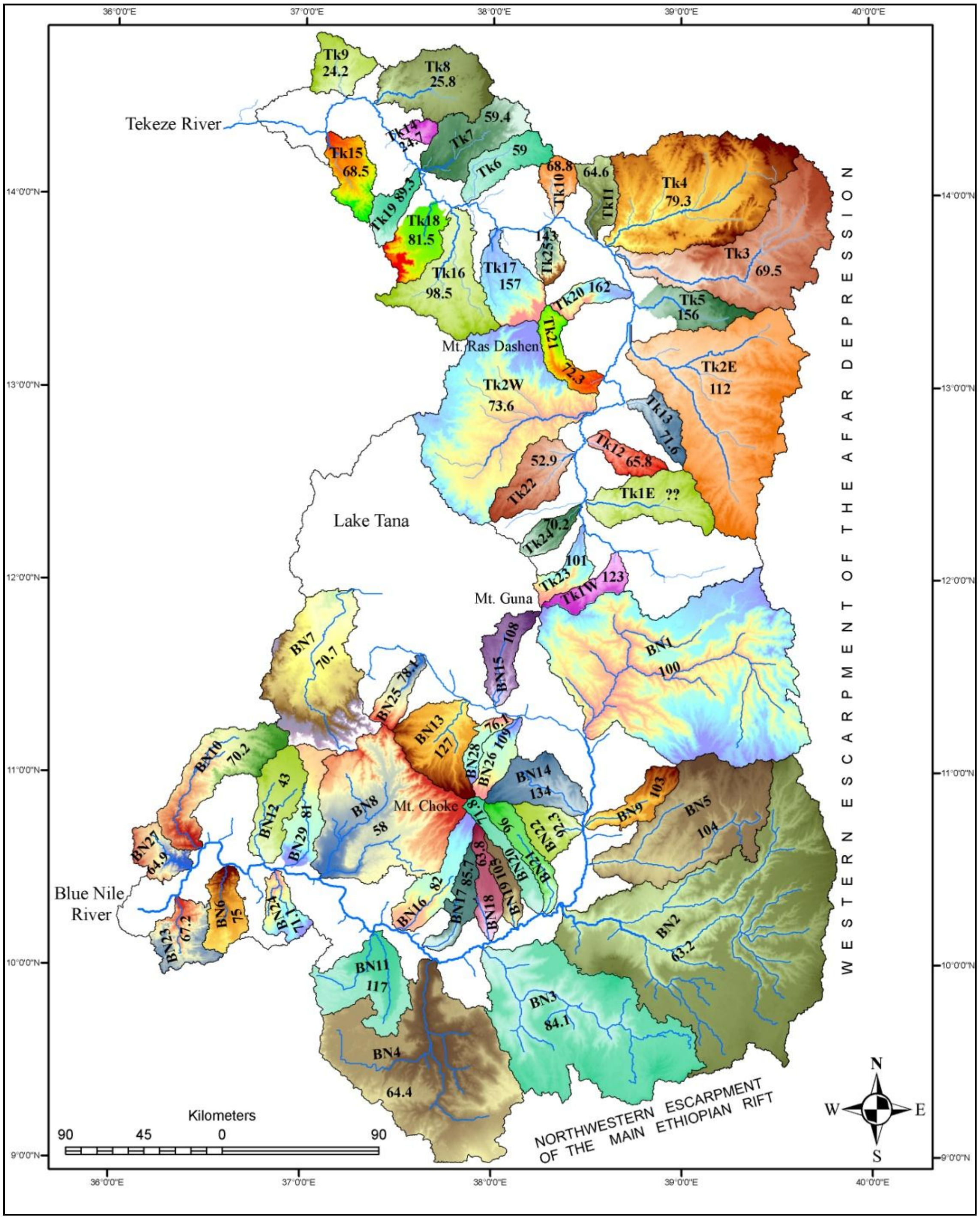

Figure 3.2: The spatial distribution of the channel Normalized Steepness Index ($\mathbf{K}_{sn}$) within the tributaries of the Tekeze River and the Blue Nile.

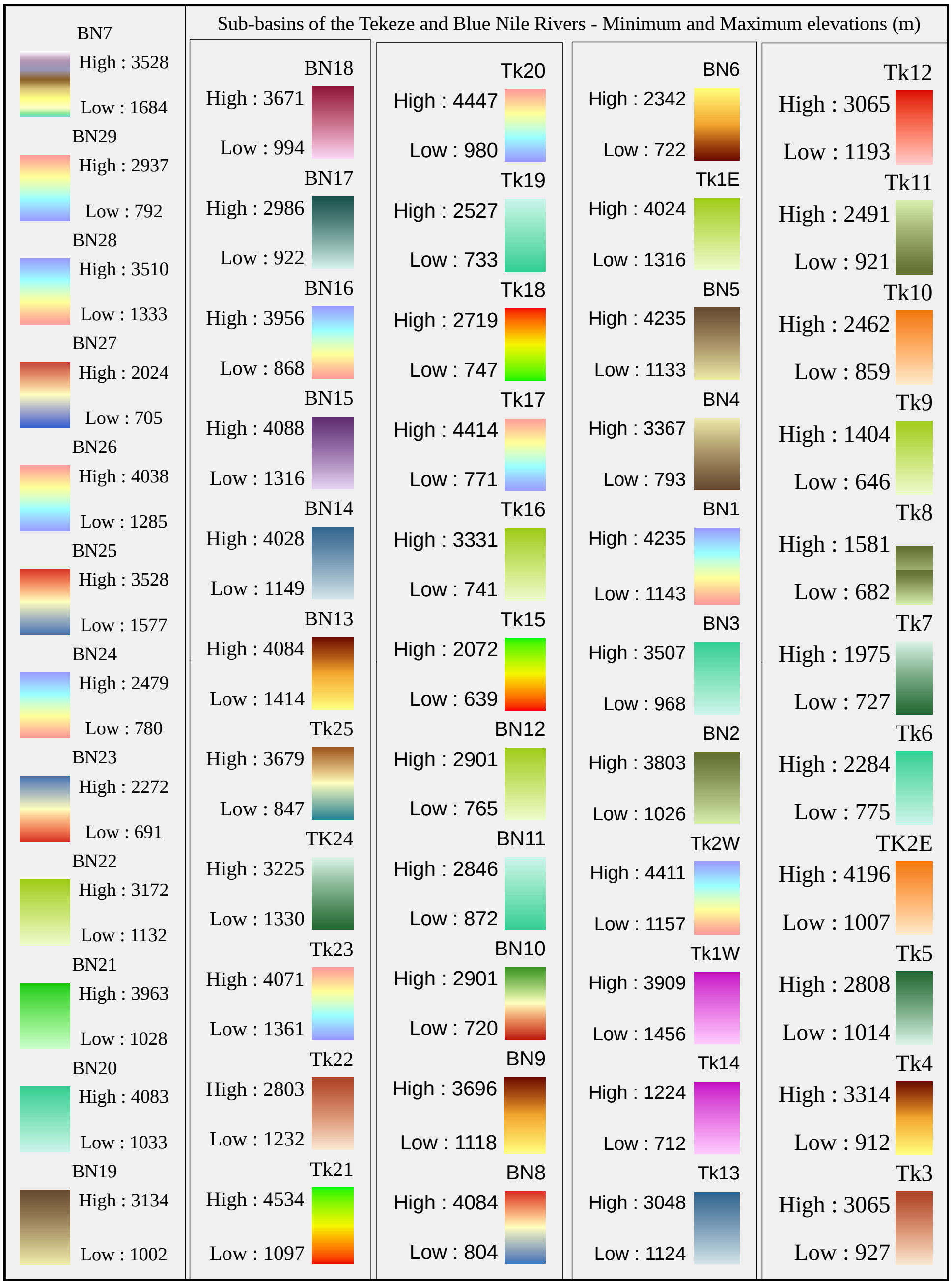

Figure 3.2: (Continued) Explanation of the color-coded DEM of each of the Tekeze River and the Blue Nile tributaries sub-basins.

(2) The tributaries on the southwestern side the Tekeze river is characterized by moderate K_{sn} values ranging between 68.5 and 81.5. The K_{sn} values on this side of the

river become higher (98.5 to 162) in the tributaries that originate from Mount Ras Dashen and Mount Guna. This increase in the K_{sn} values in this part of the Tekeze River is due to that the tributaries are originating from the highly elevated Mount Guna and Mount Ras Dashen.

(3) The tributaries on both sides of the Blue Nile are characterized by a relatively similar K_{sn} values (cluster between 43 and 84.1). However, higher Ksn values (ranging between 94 and 134) are present in the Blue Nile and these are associated with the rivers tributaries that originate from Mount Choke and Mount Guna.

(4) The tributaries of both the Tekeze River and the Blue Nile that originate from the western escarpment of the Afar Depression are characterized by a relatively high K_{sn} values (ranging between 100 and 156). However, the tributaries of the Blue Nile that originate from the northwestern escarpment of the Main Ethiopian Rift show relatively lower K_{sn} values (ranging between 63.2 and 84.1) compared to those originating from the western escarpment of the Afar Depression.

(5) The distribution of the K_{sn} values suggests that they have their highest values in the central part of the northwestern Ethiopian plateau. This might be due to a combination of tectonic uplift and the growth of the plateau through the build-up of shield volcanoes such as the Mount Ras Dashen, Mount Guna and Mount Choke. Also, relatively high K_{sn} values are encountered along the western escarpment of the Afar Depression suggesting significant rift-flank uplift. However, the K_{sn} values suggest that rift-flank uplift along the northwestern flank of the Main Ethiopian Rift is slower than that of the Afar Depression.

3.2.2. Results of Long Profiles Analysis of the shape of the rivers long profile is a powerful tool in determining the incision and the tectonic uplift history of a region (Weissel and Seidl, 1998; Schoenbohm et al., 2004; Clark et al., 2005; Crosby and Whipple, 2006; Pierre, 2007). The river's long profile that has abnormally high slope and non-lithological kinckpoints indicate major tectonic uplift. The combined presence of kinckpoints and the gradient of the river's long profiles are good geomorphologic indicators that can reveal tectonic influence even of weak amplitude (Pierre, 2007). The ideal shape of the river long profile is the logarithmic-decay curves. Deviations from the ideal shape are used to infer active uplift or subsidence associated with change in the base level caused by increase in uplift rate, faulting or stream capture. Nevertheless, kinckpoints origins and dynamics are debatable; hence caution is required when causes of knickpoint formation are interpreted as due to uplift, faulting, bedrock erodibility, or stream capture (Gani et al., 2007). Wobus et al. (2005) and Kirby et al. (2007) employed different methods to measure differences in rock uplift rates. These methods assume that landscape is in steady-state or dynamic equilibrium such that erosion and river incision are equal to rock uplift.

In this work, fifty five long profiles are extracted and analyzed for the tributaries of the Tekeze River and the Blue Nile. These tributaries are shown in figure 3.3. One example of these profiles is shown in figure 3.4. The rest of the profiles are included in appendix 1. All profiles are filtered with 500 m smoothing window, their contour intervals are fixed to 20 m, and all spikes are removed from the DEM data. Each plot contains three panels:

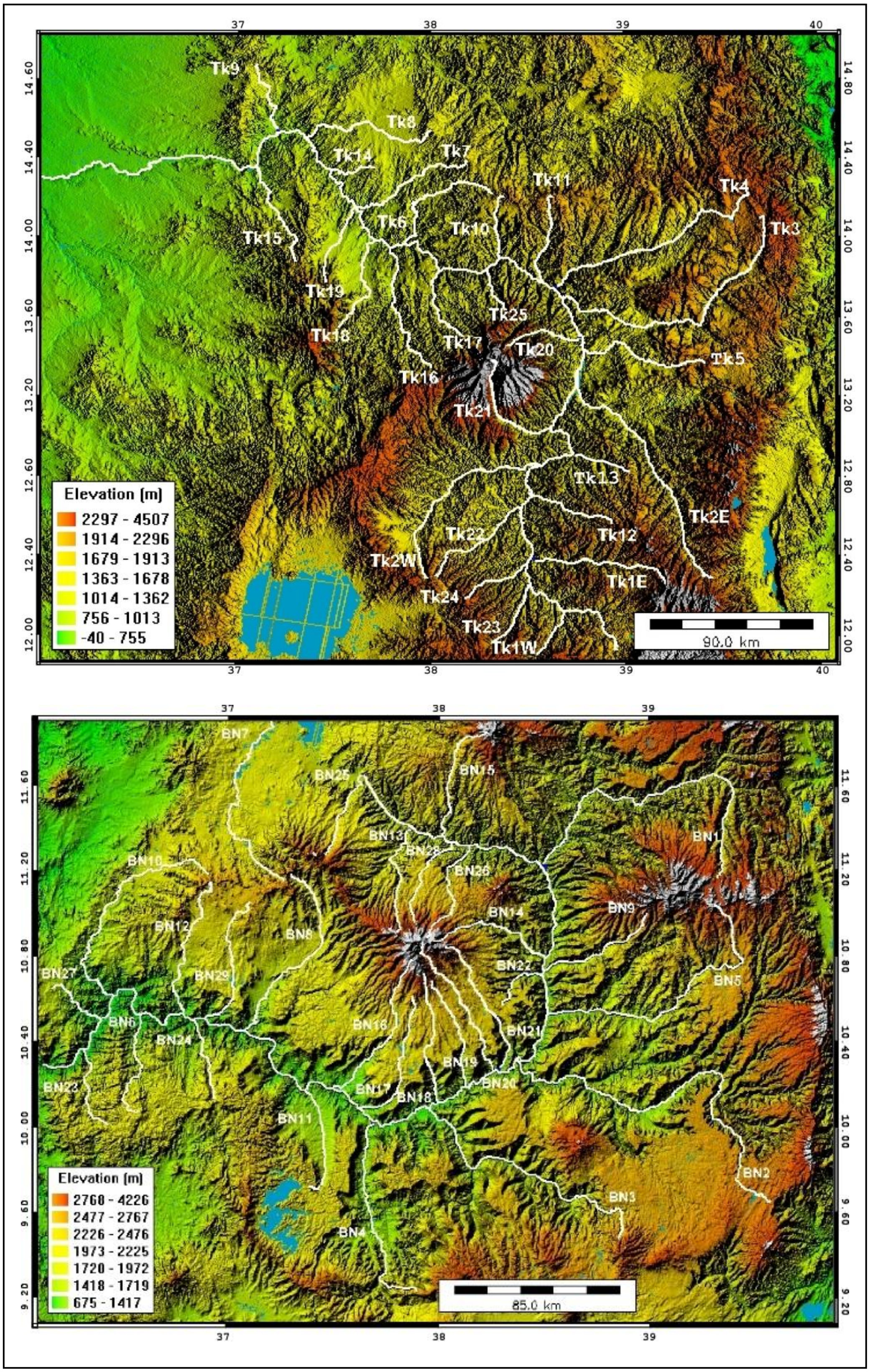

Figure 3.3: The location of the Tekeze River and the Blue Nile tributaries used in the channel long profile analysis

(1) The upper panel is the plot of the tributaries profiles where the X-axis represents the distance of the tributaries from either the Tekeze River or the Blue Nile (the value of zero indicates the confluence of the tributary with either river) and the Y-axis is elevation. The irregular line is the observed channel profile. The blue colored curve represents the predicted channel profile obtained from the regressed channel, where the concavity (θ) is derived from the regression fit. The cyan colored curve is the predicted channel profile obtained through the adoption of a reference concavity (θ_{ref}) of 0.45. The (+) symbols are the location of manually-selected knickpoints and faults.

(2) The middle panel is the plot of drainage area of the tributary sub-basin in m^2 (X-axis) versus the gradient of the tributary (Y-axis). The square symbols are the log bin averages of the steepness of the sub-basin minus area of the basin. The (+) is the gradient of the basin divided by the area of the basin (represents the spatial variation of steepness of each point on the channel profile). The (+) symbol contained in a circle define the location of the knickpoints and the faults along the tributary's longitudinal profile. Also given in this panel are the K_{sn} values of the tributary and its concavity (θ) value.

(3) The lower panel is the plot of the tributary gradient versus distance where the X-axis represents the distance of the tributaries from either the Tekeze River or the Blue Nile (the value of zero indicates the confluence of the tributary with either the Tekeze River or the Blue Nile) and the Y-axis is the gradient. The (+) symbol represents the calculated gradient along the tributary whereas the (+) symbol enclosed in a circle define the location of knickpoints and faults.

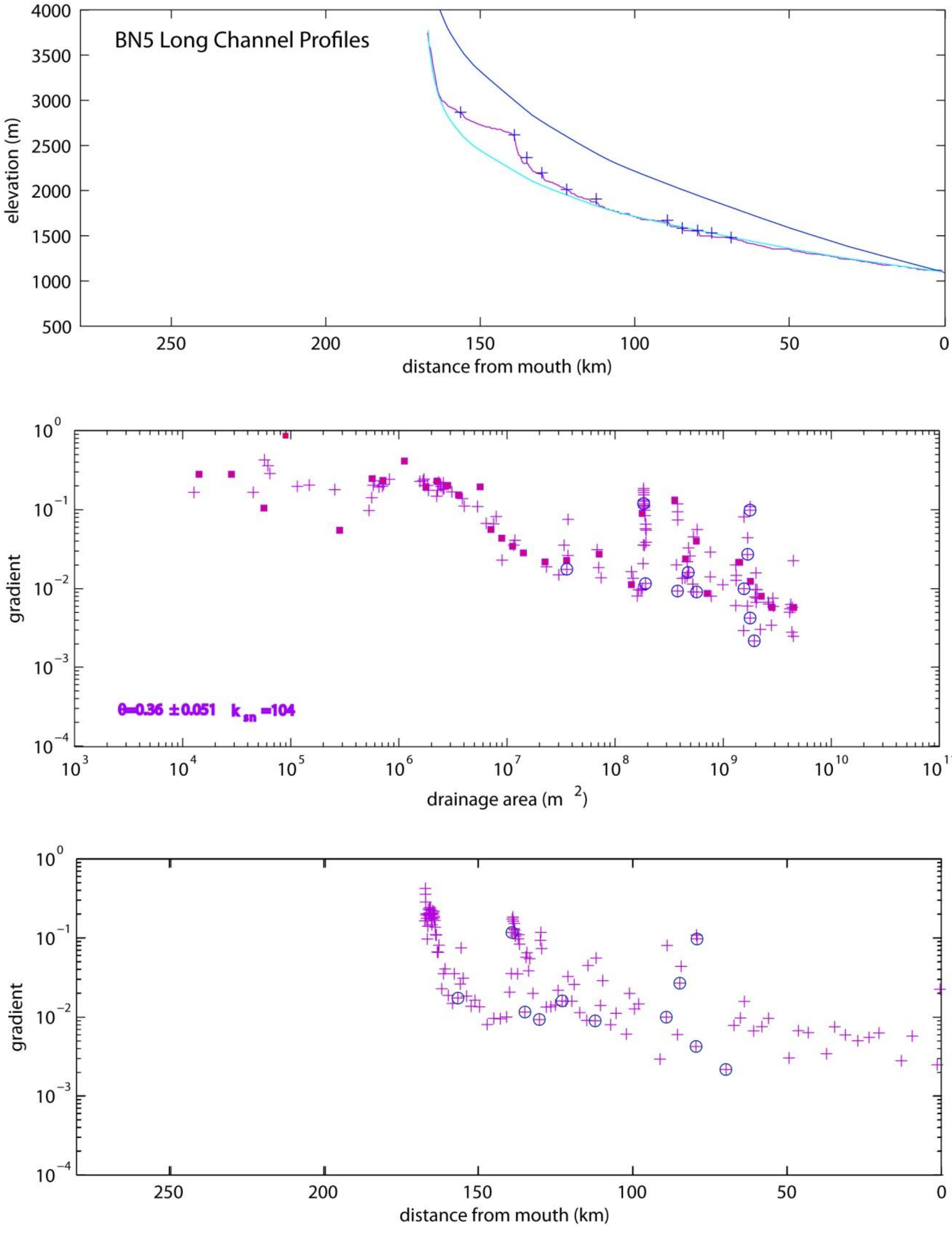

Figure 3.4: Example of Longitudinal Channel Profile analysis of tributary BN5 of the Blue Nile River. The rest of the profiles are presented in the appendix. See text for plot explanation.

The concavity (θ) values vary widely in different geological settings and can take negative values of less than one. These values have been divided by Whipple (2004) into low (< 0.4), moderate (0.4 - 0.7), high (0.7-1.0) and extremely high (>1.0). Low concavity (θ) values are associated with short and steep channels that are influenced by debris flow, downstream increase in incision rate, or by the rock strength which is commonly associated with knickpoints. Moderate concavity (θ) values are associated with channels incising in homogeneous lithology that is affected by homogeneous and actively uplift. High concavity (θ) values are associated with channels that are influenced by downstream decreases in rock uplift rate or rock strength indicating the transitioning to full fluvial conditions. Extreme concavity (θ) values (either negative values or values >1.0) are associated with channels that encounter the occurrence of abrupt knickpoints due to changes in the bedrock physical properties or due to temporal differences in bedrock uplift.

Most of the concavity (θ) values in the Tekeze River and the Blue Nile are either low or moderate (Table 3.1). However, in general the tributaries of the Tekeze River have a relatively higher concavity (θ) values compared to those of the Blue Nile. Also, with the exception of a few tributaries of the Tekeze River and the Blue Nile, most of the tributaries show channel profiles that deviate from the predicted channel profile from the regressed channel, where concavity (θ) is derived from the regression fit. Usually the close similarity between the observed and predicted channel profile indicates channel maturity.

Table 3.1: The concavity (θ), Normalized Steepness Index (**K_{sn}**) and the Regression Fit (r^2) of the tributaries of the Tekeze River and the Blue Nile.

Tekeze River				**Blue Nile**			
Trib	θ	K_{sn}	r^2	Trib	θ	K_{sn}	r^2
TK1	0.23	101		BN1	0.24	100	0.22
TK1E				BN2	022	71.8	0.14
TK 1W		101	0.34	BN3	0.18	63.8	0.11
TK2E	0.41	112		BN4	0.17	65.7	0.16
TK2W	0.37	73.6	0.64	BN5	0.36	104	0.60
TK3	0.19	69.5	0.20	BN6	0.061	70.2	0.03
TK4	0.33	79.3	0.67	BN7	0.21	43	0.19
TK5	0.31	156	0.25	BN8	0.25	81	0.58
TK6	0.31	59	0.46	BN9	0.29	103	0.65
TK7	0.35	59.4	0.46	BN10	0.27	75	0.39
TK8	0.27	25.8	0.47	BN11	0.19	117	0.096
TK9	0.16	24.2	0.22	BN12	0.19	71.1	0.32
TK10	0.32	68.8	0.62	BN13	0.24	127	0.43
TK11	0.19	64.6		BN14	0.30	134	0.50
TK12	0.33	65.8	0.86	BN15	0.27	108	0.37
TK13	0.33	71.6	0.79	BN16	0.20	62	0.15
TK14	0.24	24.7	0.55	BN17	0.15	64.4	0.00097
TK15	0.38	68.5	0.79	BN18	0.097	84.1	0.044
TK16	0.53	98.5	0.92	BN19	0.42	63.2	0.0035
TK17	0.31	157	0.29	BN20	0.16	105	0.11
TK18	0.49	61.5	0.90	BN21	0.17	96	0.12
TK19	0.42	89.3	0.57	BN22	0.14	92.3	0.061
TK20	0.34	162	0.79	BN23	0.20	67.2	0.10
TK21	0.27	72.3	0.68	BN24	0.12	70.7	0.10
TK22			0.94	BN25	0.32	78.1	0.65
TK23	0.32	123	0.55	BN26	0.18	109	0.20
TK24	0.38	70.2	0.94	BN27	0.20	64.9	0.49
TK25	0.38	143	0.65	BN28	0.11	76.1	0.69
				BN29	0.094	58	0.051

Analysis of the long profiles suggests the following:

(1) Some of the long profiles of the tributaries originating from the western escarpment of the Afar Depression and the northwestern escarpment of the Main Ethiopian Rift display “bump” shapes, which are explained as areas of deposition, and most probably represent locations of landslides. Another feature exhibited by these profiles is the

presence of widely-spaced knickpoints or a cluster of them. Such spacing is inductive of changes in the channel base level due to tectonic uplift or alternatively due lithological variation. These profiles also exhibit sharp gradient drop at or close to the convolution with the Tekeze River or the Blue Nile.

(2) The tributaries of the Tekeze River and the Blue Nile which originate from the western escarpment of the Afar Depression and the northwestern escarpments of the Main Ethiopian Rift (Labeled TK1E, TK2E, TK3, TK5, BN1 and BN6 in figure 3.3) show very low Regression Fit (r^2) (Table 3.1) suggesting that these rivers channels have been continuously modified by rift-flank uplift of the western escarpment of the Afar Depression and the northwestern escarpment of the Main Ethiopian Rift.

(3) The tributaries in the lower reach of the Tekeze River close to the low-lands of the Sudan (labeled TK6, TK7, TK9, TK15, TK16, TK18) have high Regression Fit (r^2) (Table 3.1) suggesting that these are mature rivers and they are not affected by the tectonic activities to the east in the Afar Depression and the Main Ethiopian Rift.

(4) The tributaries originating from Mount Ras Dashen to join the Tekeze River (labeled TK17, TK20, TK21, TK25 in figure 3.3) have moderate Regression Fit (r^2) (Table 3.1) suggesting moderate influence development of this shield volcano on shaping the channel geometry of these rivers. However, the tributaries originating from of Mount Choke to join the Blue Nile (Labeled BN13, BN15, BN19, BN21, BN26, and BN28) have a relatively low Regression Fit (r^2) (Table 3.1) suggesting a more influence of the development of the shield volcano in shaping the channel geometry of these rivers.

3.2.3. Spatial Distribution of Knickpoints and Faults Figure 3.5, 3.6, and 3.7 shows the spatial distribution of the major and minor knickpoints and faults in the Tekeze River and the Blue Nile. The classification of these knickpoints into major, minor and faults is based on the magnitude and shape of the change on the long profiles. Major Knickpoints are characterized by a significant drop in the elevation of the profile, but this drop occurs within a long distance creating a less steep drop. Minor knickpoints have same topological features as the major knickpoints, but the change in the elevation is subtle. On the other hand, faults are characterized by a high and steep drop in the elevation of the profile. Below is a summary of the nature of spatial distribution of major knickpoints:

(1) Major Knickpoints are distributed along a linear zone sub-parallel to western escarpment of the Afar Depression. These knickpoints concentrate at elevations ranging between 2500 and 3000 m. Generally, these knickpoints are more apparent in the southern part of the western escarpment to the east of the Blue Nile compared to its southern part east of the Tekeze River. No major knickpoints cluster is apparent to be parallel to the northwestern escarpment of the Main Ethiopian Rift.

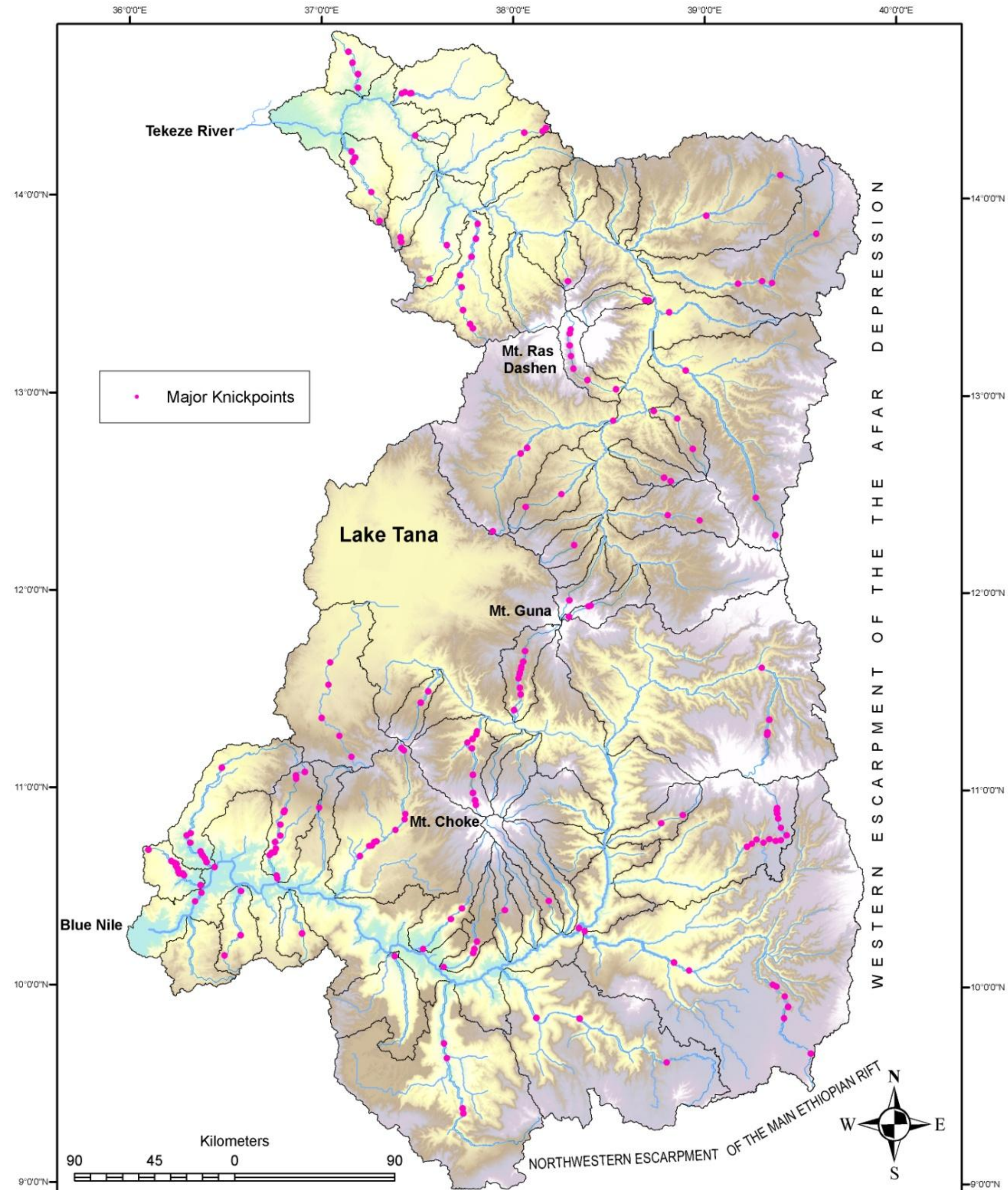

Figure 3.5: Spatial distribution of major knickpoints in the Tekeze and the Blue Nile River Systems

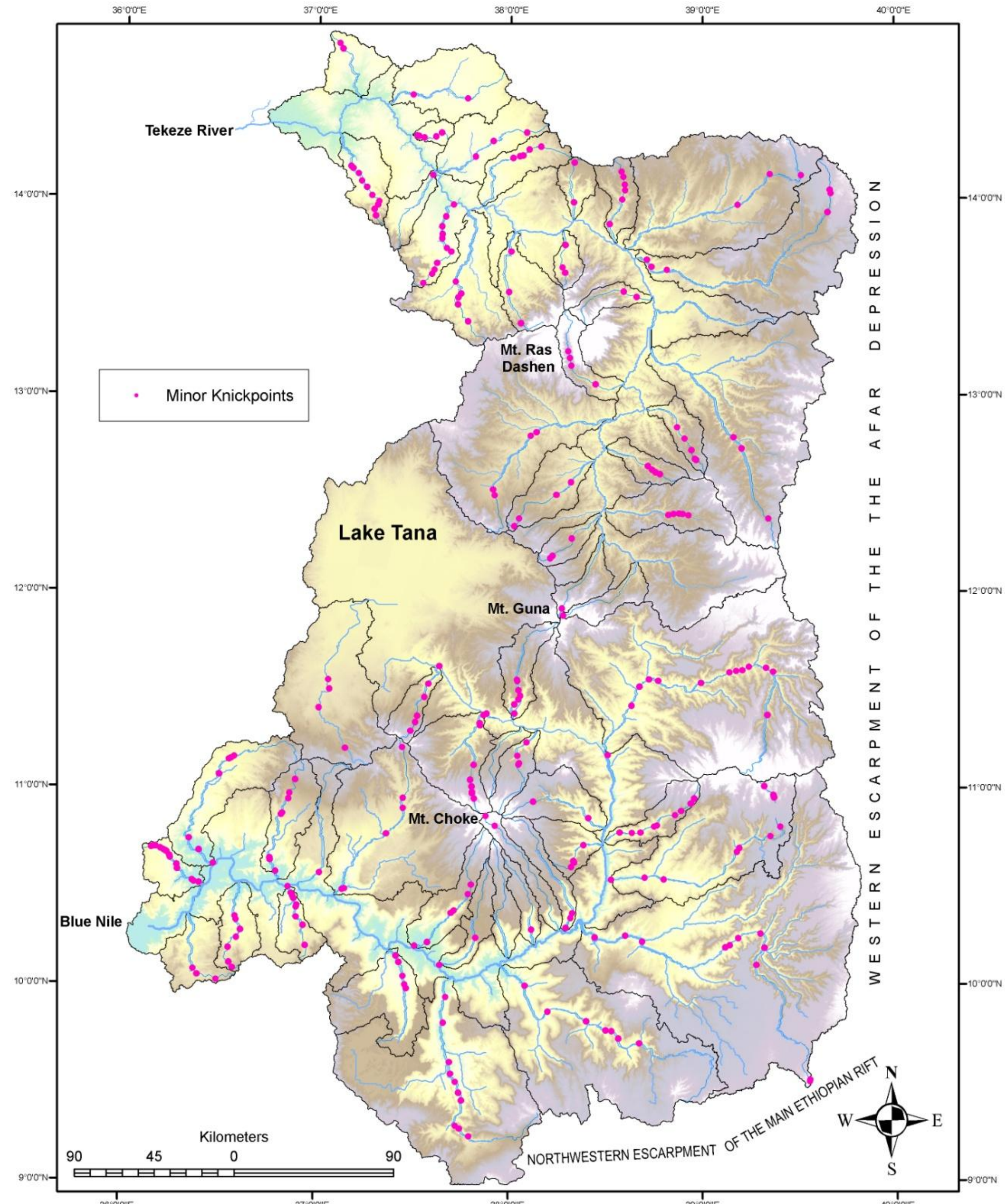

Figure 3.6: Spatial distribution of minor knickpoints in the Tekeze and the Blue Nile River Systems

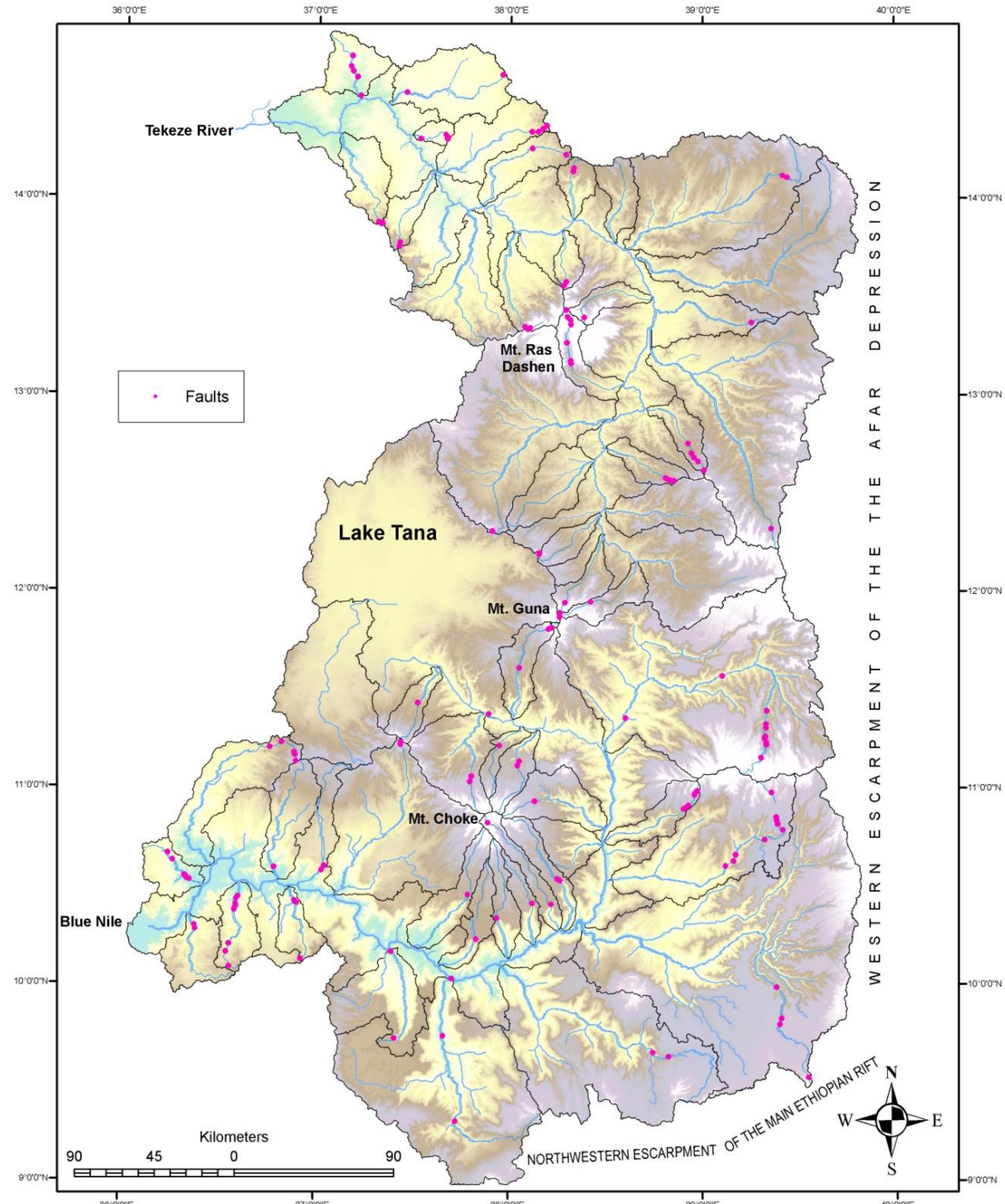

Figure 3.7: Spatial distribution of faults in the Tekeze and the Blue Nile River Systems

(2) There appears to be a concentric pattern of major knickpoints around Mount Choke. These major knickpoints occur at 2000-2500 m elevation. Similar, but less apparent clusters appear to occur around Mount Guna and Mount Ras Dashen. The presence of these major knickpoints can be attributed to an enhanced incision due to the build-up of these shield volcanoes.

(3) There are clusters of knickpoints that appear to align in N-S direction at the lower reaches of the Tekeze River and the Blue Nile close to the low land of the Sudan. These major knickpoints are likely due to sediments flux carried from the upper reaches of these tributaries and deposited when relatively less-steep relief is encountered.

The distribution of miner knickpoints in the Tekeze and the Blue Nile (Figure 3.6) suggests the presence of four linear patterns for minor knickpoints. There is no apparent pattern for the distribution of these minor knickpoints. However, it is apparent that they are less dominant in the eastern part of the Tekeze River and the Blue Nile drainage basin (close to the western escarpment of the Afar Depression) as compared to the central and western parts of the basin. Hence, the minor knickpoints seems to be found at a lower elevation (900 m to 2600 m) compared to the major knickpoints. Different formations of the Mesozoic sedimentary section crop out at these elevations. Hence, many of these miner knickpoints might be due to variation in the rock resistance to erosion rather than increase in the rate of incision.

The spatial distribution of faults in the Tekeze River and the Blue Nile (Figure 3.7) suggest that these faults occur in the upper reaches of Tekeze River at elevations ~2000 m to 3000 m. Also, these faults appear too clustered in the upper reaches of the Blue Nile at elevation between 2000 m to 2500 m. These faults might be associated with the build-up of shield volcanoes such as Mount Ras Dashen and Mount Choke. In addition, these faults appear to occur along a N-S trending zone sub-parallel to the western escarpment of the Afar Depression at an elevation ranging between 2500 and 3000 m. These faults might have developed in association with the rift-flank uplift on the western escarpment of the Afar Depression.

4. DISCUSSION

Morpho-tectonic analysis of the Tekeze River and the Blue Nile suggest that the incision history of these drainage systems on the northwestern Ethiopian plateau is much more complicated that to be explained by either the steady-state incision model of Pik et al. (2003) or the increased incision rate through time that is suggested by Gani et al. (2007). However, this work is in agreement with the notion that the incision of the Tekeze River and the Blue Nile on the northwestern Ethiopian plateau started shortly after the eruption of the ~30 Ma flood basalts which resulted in the burial of all drainage systems that preceded this volcanic event. It is suggested here that the incision history of these drainage systems was influenced by a number of tectonic and geological events including: (1) Long wavelength regional uplift that resulted in the uprising of the entire Ethiopian plateau, but this was centered in the region that divides the Tekeze River drainage system from the Blue Nile drainage system. This long wavelength uplift might be due to the rise of the Afar mantle plume which reached the base of the Ethiopian lithosphere shortly before the out-pouring of the ~30-29 Ma flood basalts (Hoffman et al., 1997); (2) This long wavelength regional uplift was superimposed by a shorter wavelength event that produced regions of localized positive topography in association with the build-up of shield volcanoes such as Mount Ras Dashen, Mount Guna and Mount Choke. This event might have occurred at ~22 Ma as suggested by Keiffer et al. (2004). (3) The topography that resulted from these two events was subsequently modified by the rift-flank uplift on the western escarpment of the Afar Depression and the northwestern escarpments of the Main Ethiopian Plateau. This uplift might have accompanied the opening of the Main Ethiopian Rift at ~11 Ma as suggested by

Wolfenden et al. (2004) or at 6-5 Ma as suggested by Bonini et al. (2005). This uplift diminishes progressively in a west and northwest directions away from the Afar Depression and the Main Ethiopian Rift, respectively.

The long wavelength uplift of the northwestern Ethiopian plateau might have triggered an overall slow to moderate increase in uplift of Tekeze River and the Blue Nile. This evident from the relatively moderate K_{sn} values that dominate the central part of the northwestern Ethiopian plateau (except around the shield volcanoes), the low Concavity (θ) values, and the moderate Regression Fit (r^2) values. This notion is further supported by the lack of major knickpoints (other than around the shield volcanoes) and the domination of miner knickpoints.

The short wavelength events that produced localized positive topography in association with the build-up of the shield volcanoes might have resulted in an additional increase in the rate of incision. This is evident from the relatively high K_{sn} values encountered around Mount Ras Dashen, Mount Guna and Mount Choke as well as the concentration of major knickpoints around these shield volcanoes. In addition, the low to moderate Concavity (θ) values and moderate Regression Fit (r^2) values characterizing the tributaries of the Tekeze River and the Blue Nile origination from these shield volcanoes further support this proposition.

A significant increase of the incision rate might have occurred in association with the rift-flank uplift, especially on the western margin of the Afar Depression. This is particularly evident from the linear north-south trending pattern exhibited by knickpoints on the long profiles of the tributaries that originate from this escarpment to join the Blue Nile. These knickpoints are likely to be associated with tectonic uplift rather that changes of the bedrock erodibility because they occur of a region dominated by one rock type (the Oligocene-Miocene basalts). This is further supported by the relatively high Normalized Steepness Index (K_{sn}) values, the relatively high Concavity (θ) values, and the relatively low Regression Fit (r^2) values of these tributaries.

The Pik et al (2003) steady-state model and the long-lived established hydrological stability of the drainage system in the northwestern Ethiopian plateau, especially the Blue Nile, should not be completely disregarded. This might be true for the tributaries at the lower reaches of the Tekeze River and the Blue Nile. It is certain that some morpho-tectonic parameters of these tributaries suggest that these drainages are mature and they have not been affected by tectonic disturbances for a long time. This is evident from the low Normalized Steepness Index (K_{sn}) values and the high regression Fit (r^2) values of many of these rivers. It worth mentioning here that Pik et al (2003) study was conducted in the lower reaches of the Blue Mile close to the low lands of the Sudan. Such long-lived stability can be attributed to that these tributaries were incised in the western part of the plateau far away from the disturbance of the rift-flank uplift that occurred further east along the western margin of the Afar Depression and the northwestern margin of the main Ethiopian Rift. This stability is also suggestive of head-ward incision before drainage reversal.

Equally, the Gani et al. (2007) model that advocates for an increased rate of incision through time is certainly true, but for only parts of the drainage system on the northwestern Ethiopian plateau. This is certainly the case for the drainage that emerges from the western escarpments of the Afar Depression as indicated by the high K_{sn} values and the very low Regression Fit (r^2) values of the tributaries that originate from the western escarpment of the Afar Depression to join the Tekeze River and the Blue Nile. Also, this notion is further supported by the presence of linear zone of major knickpoints concentration that runs parallel to the western escarpment of the Afar Depression. Gani et al. (2007) study identified three incision phases based on preserved major knickpoints on the tributaries Gudar (corresponds to BN4 in figure 3.3) and Birr (corresponds to BN8 in figure 3.3). Tributary Gudar originates from the northwestern escarpment of the Main Ethiopian Rift to join the Blue Nile. Hence, it is likely that the presence of knickpoints along the profile of this tributary reflects an increased rate of incision due to rift-flank uplift. On the other hand, tributary Birr emerges from Mount Choke to join the Blue Nile. Hence, the presence of knickpoints along the profile of this tributary might be associated with an increased incision due to the build-up of this shield volcano.

5. CONCLUSIONS

The analysis of DEM from ASTER data through the Profiler, CalHypso, HydroModel, RiverTools, and ArcMap to extract morpho-tectonic parameters of tributaries of the Tekeze River and the Blue Nile including the Normalized Steepness Index (K_{sn}), Concavity (θ), Regression Fit (r^2), and spatial distribution of major and minor knickpoints and faults revealed that the evolution of the Tekeze River and the Blue Nile drainage systems on the northwestern Ethiopian plateau is influenced by three tectonic and geological events.

(1) The first event which is manifested by moderate increase in the incision rate on the entire plateau was associated with long wavelength uplift of the plateau, likely due to rising of the Afar mantle plume, that started ~30 Ma.

(2) The second event resulted in localized increase in the incision rate in association with shield volcanoes build-up event at ~22 Ma.

(3) The third event resulted in a significant increase of the incision rate in the eastern part of the northwestern Ethiopian plateau due to rift-flank uplift on western escarpment of the Afar Depression and the northwestern escarpment of the main Ethiopian Rift. This uplift diminishes westward left the drainage system in the lower reaches of the Tekeze River and the Blue Nile relatively tectonically undisturbed, hence establishing a long-lived hydrological stability and reaching steady-state equilibrium.

APPENDIX

LONGITUDINAL PROFILES OF THE TRIBUTARIES OF THE TEKEZE AND THE BLUE NILE RIVERS

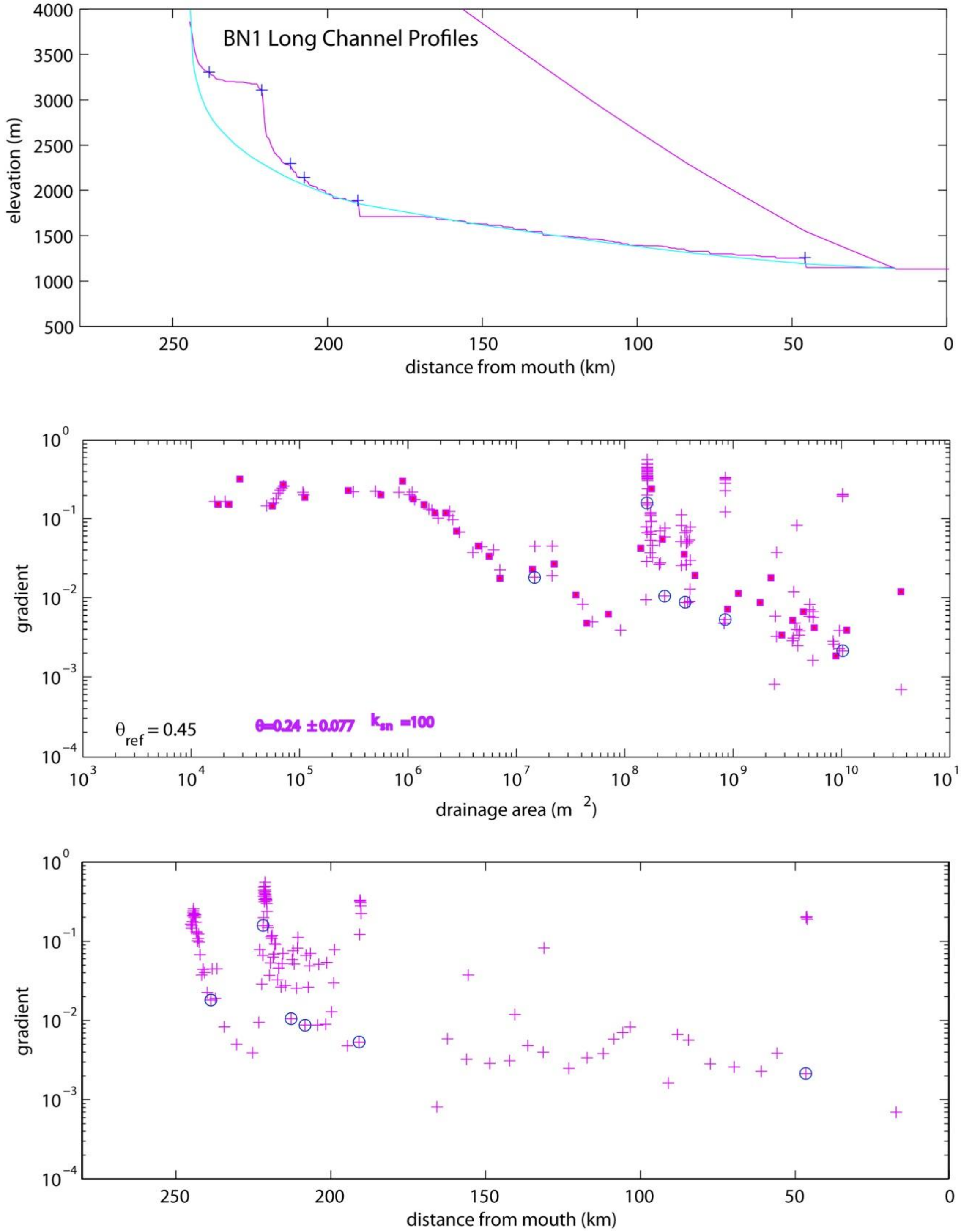
BN1 Long Channel Profiles
elevation (m)
distance from mouth (km)
gradient
θref = 0.45
θ=0.24 ± 0.077 ksn =100
drainage area (m 2)
gradient
distance from mouth (km)

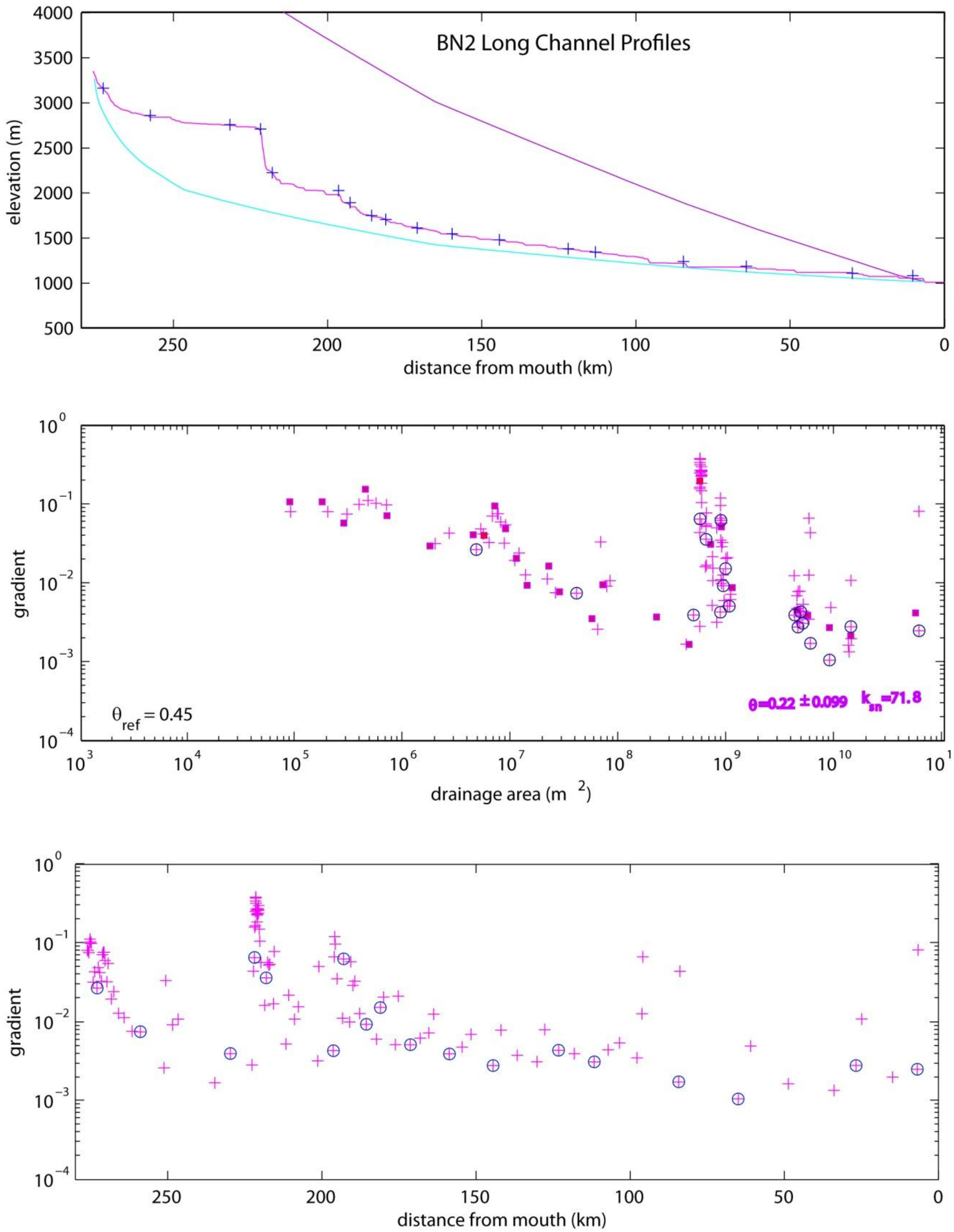
BN2 Long Channel Profiles
elevation (m)
distance from mouth (km)
gradient
drainage area (m 2)
θ=0.22 ±0.099 k_sn=71.8
θ_ref = 0.45
gradient
distance from mouth (km)

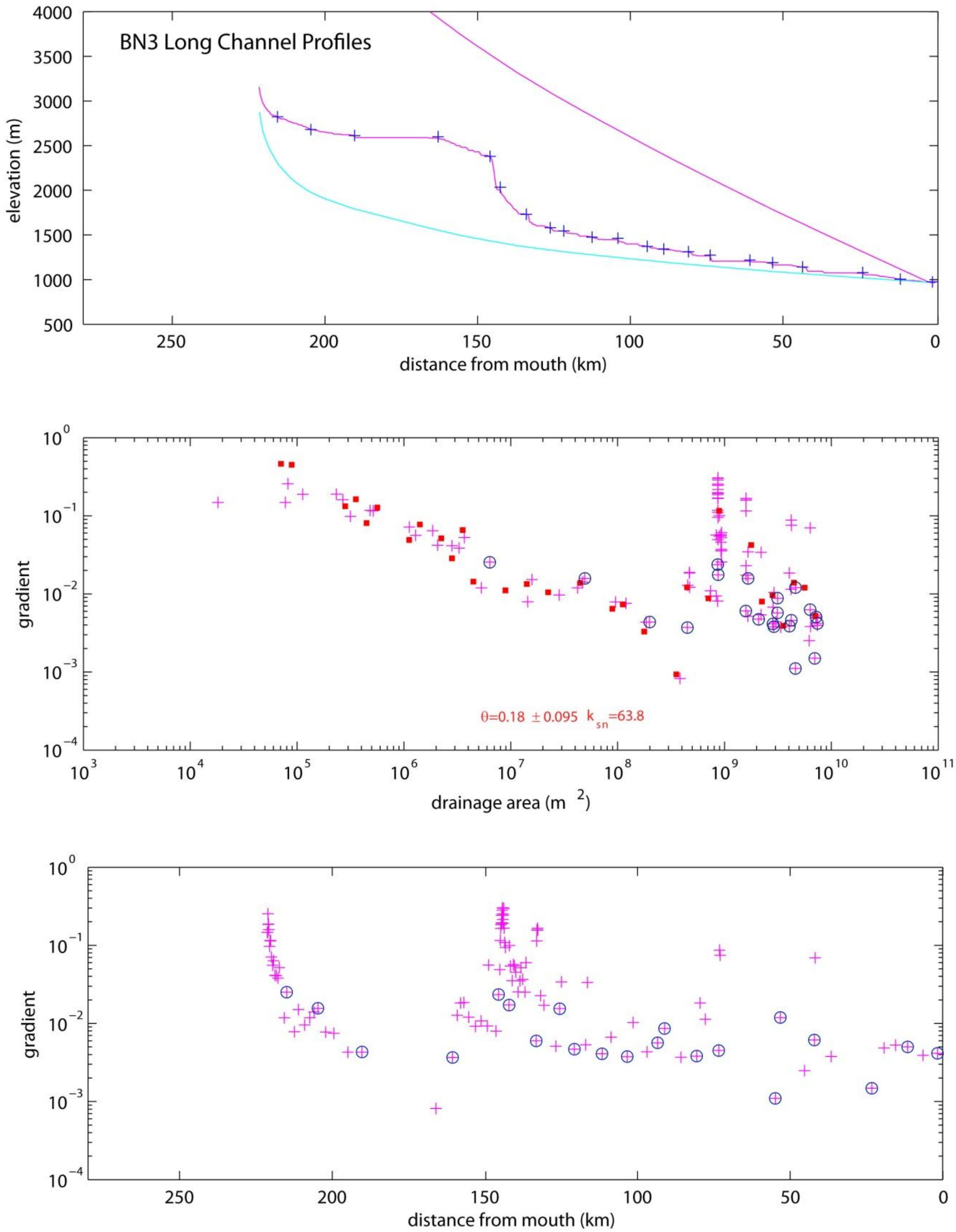
BN3 Long Channel Profiles
elevation (m)
4000
3500
3000
2500
2000
1500
1000
500
250
200
150
100
50
0
distance from mouth (km)
gradient
θ=0.18 ± 0.095 k sn=63.8
drainage area (m 2)
gradient
distance from mouth (km)

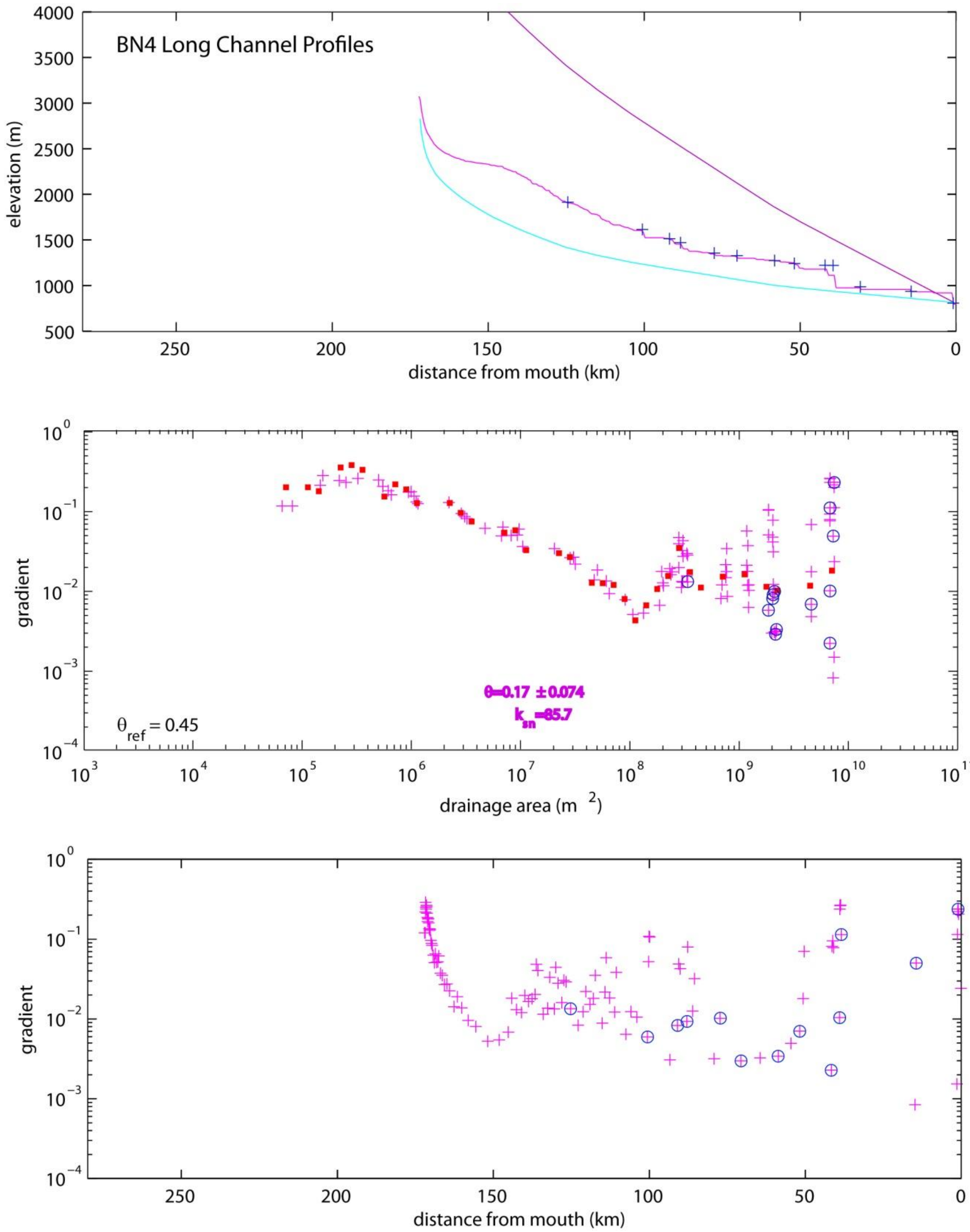
BN4 Long Channel Profiles
elevation (m)
distance from mouth (km)
gradient
drainage area (m 2)
θ=0.17 ±0.074
ksn=85.7
θref = 0.45
gradient
distance from mouth (km)

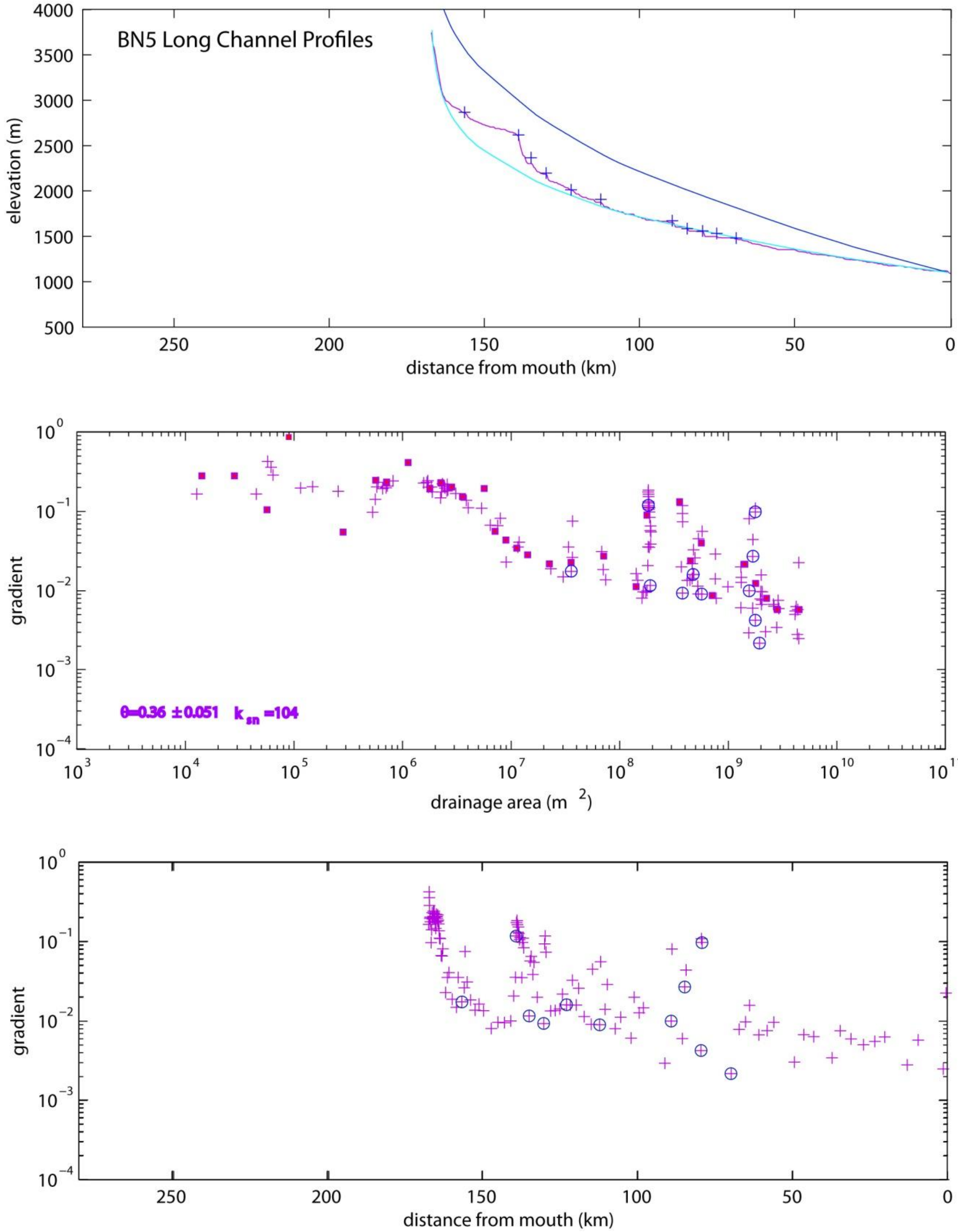

BN5 Long Channel Profiles
elevation (m)
distance from mouth (km)
gradient
drainage area (m 2)
θ=0.36 ±0.051 k sn =104
gradient
distance from mouth (km)

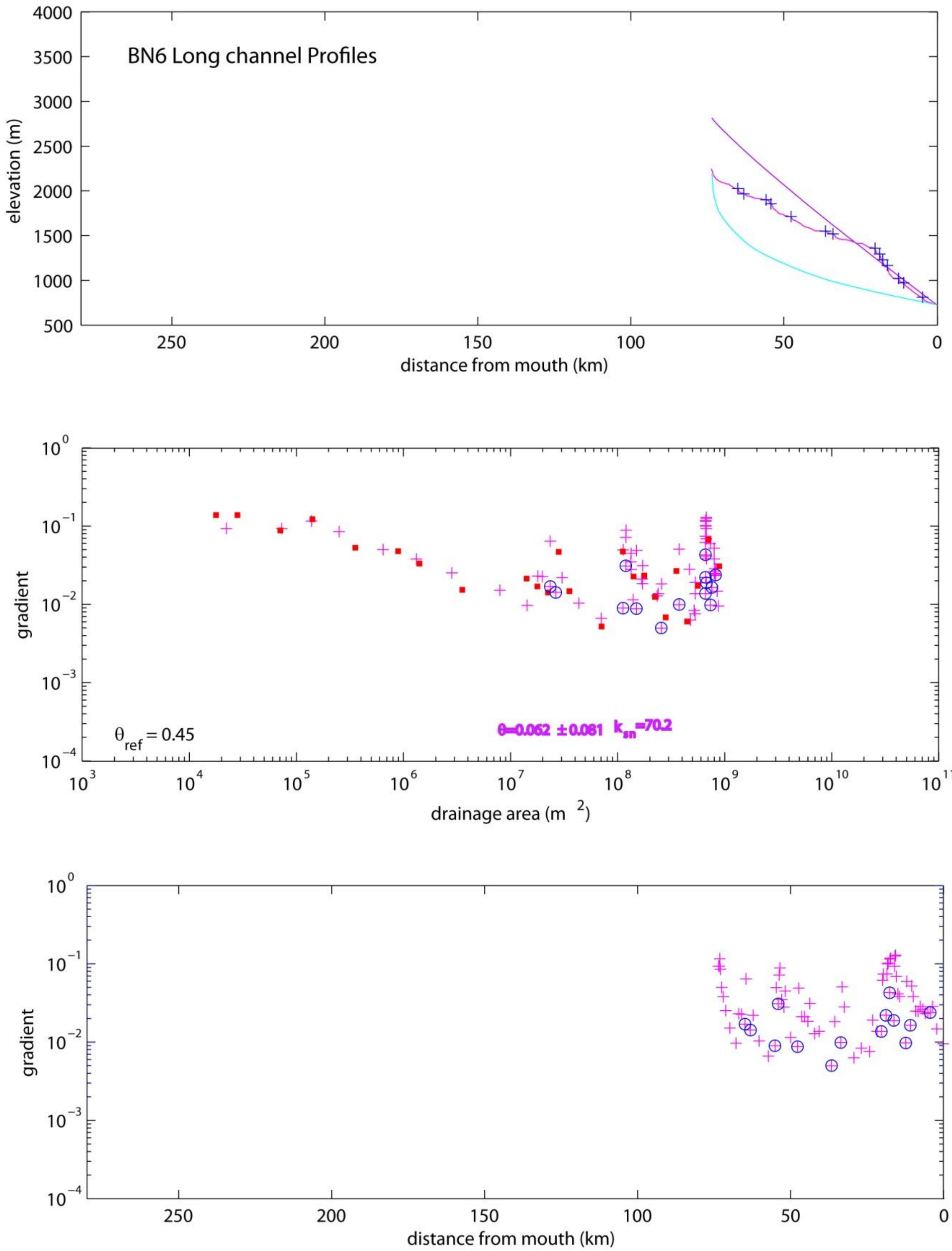
BN6 Long channel Profiles
elevation (m)
4000
3500
3000
2500
2000
1500
1000
500
250
200
150
100
50
0
distance from mouth (km)
gradient
10^0
10^-1
10^-2
10^-3
10^-4
θref = 0.45
θ=0.062 ±0.081 ksn=70.2
10^3
10^4
10^5
10^6
10^7
10^8
10^9
10^10
10^11
drainage area (m 2)
gradient
10^0
10^-1
10^-2
10^-3
10^-4
250
200
150
100
50
0
distance from mouth (km)

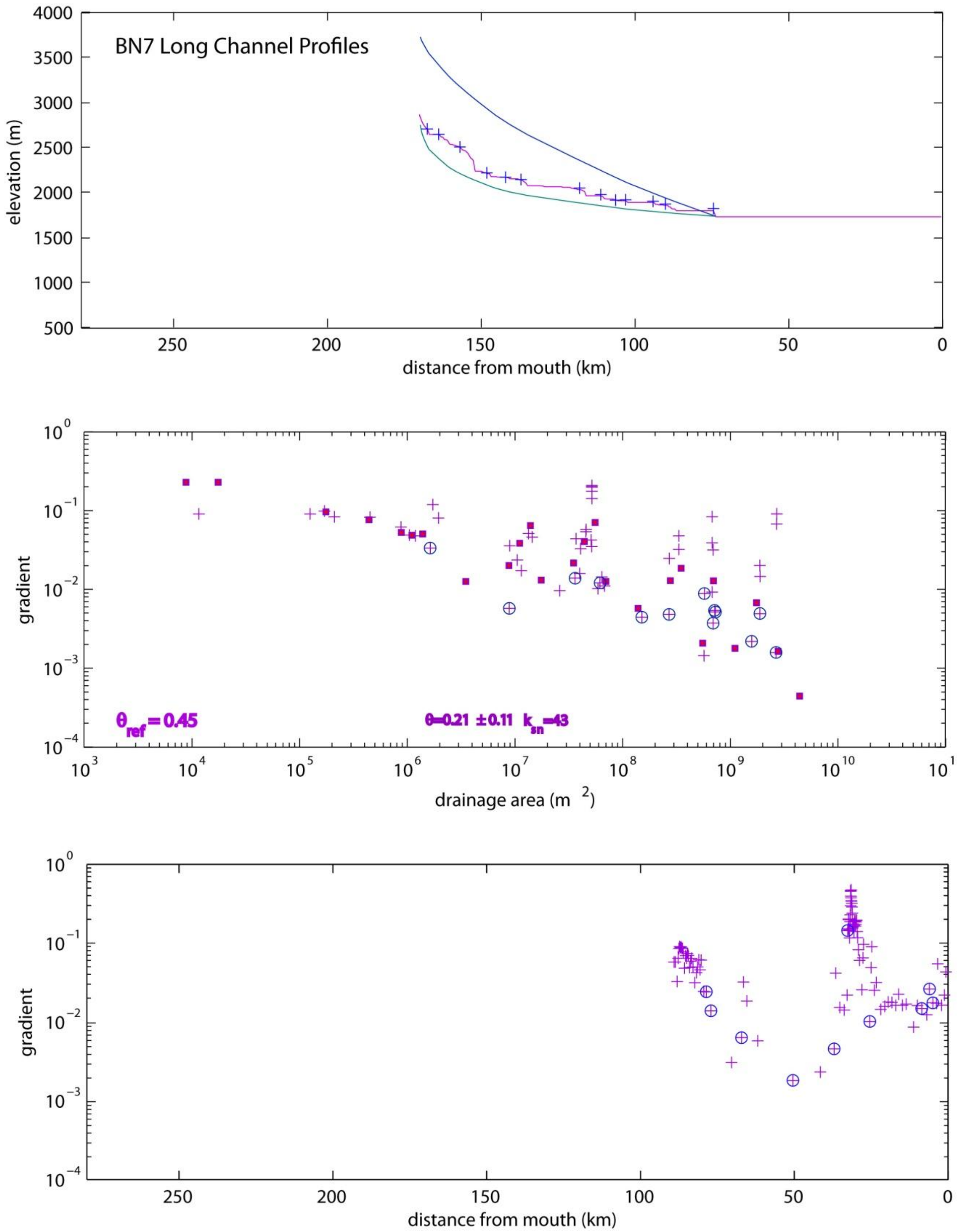
BN7 Long Channel Profiles
elevation (m)
distance from mouth (km)
gradient
drainage area (m 2)
θref = 0.45
θ=0.21 ±0.11 ksn=43
gradient
distance from mouth (km)

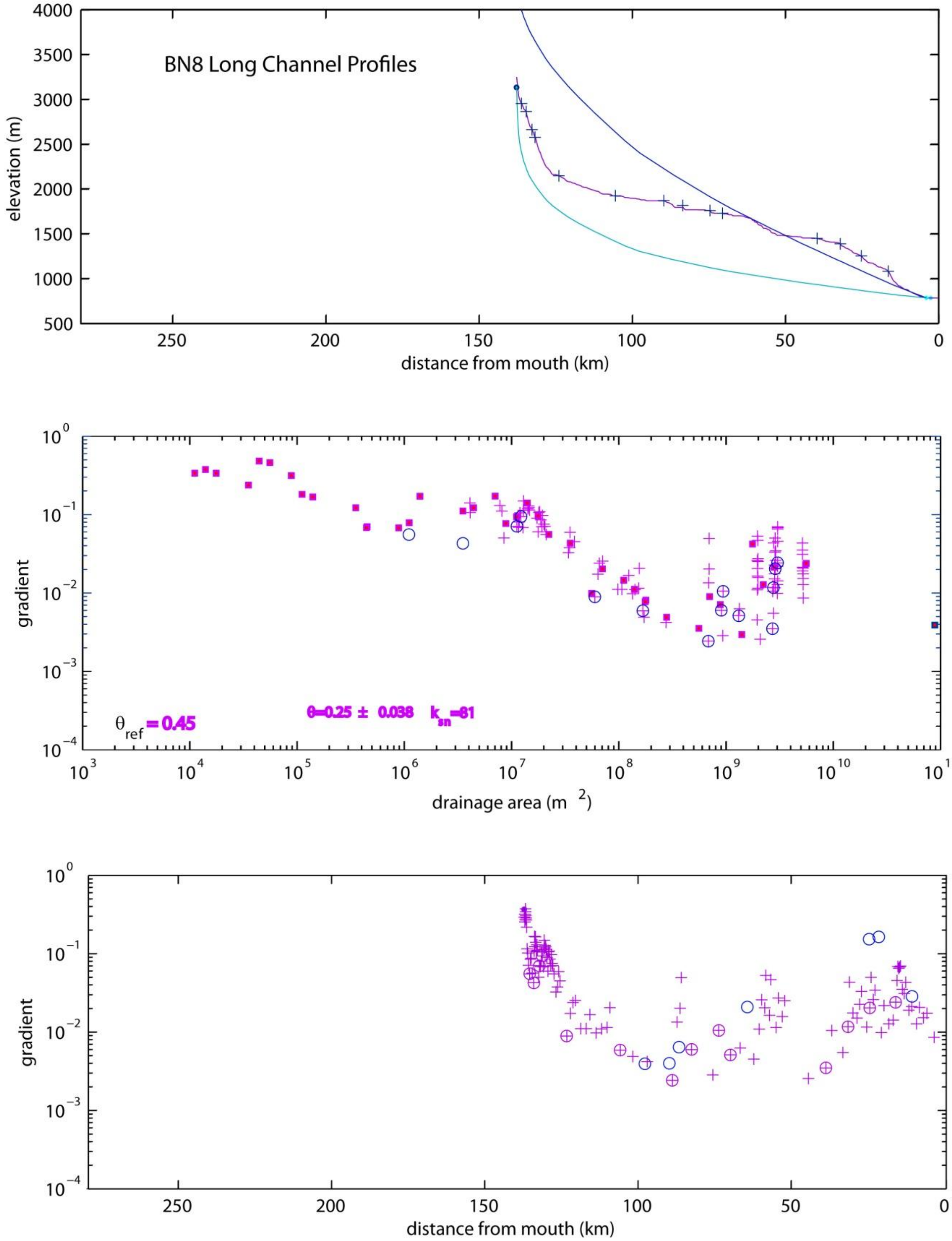
BN8 Long Channel Profiles
elevation (m)
distance from mouth (km)
gradient
drainage area (m 2)
θref = 0.45
θ=0.25 ± 0.038 ksn=81
gradient
distance from mouth (km)

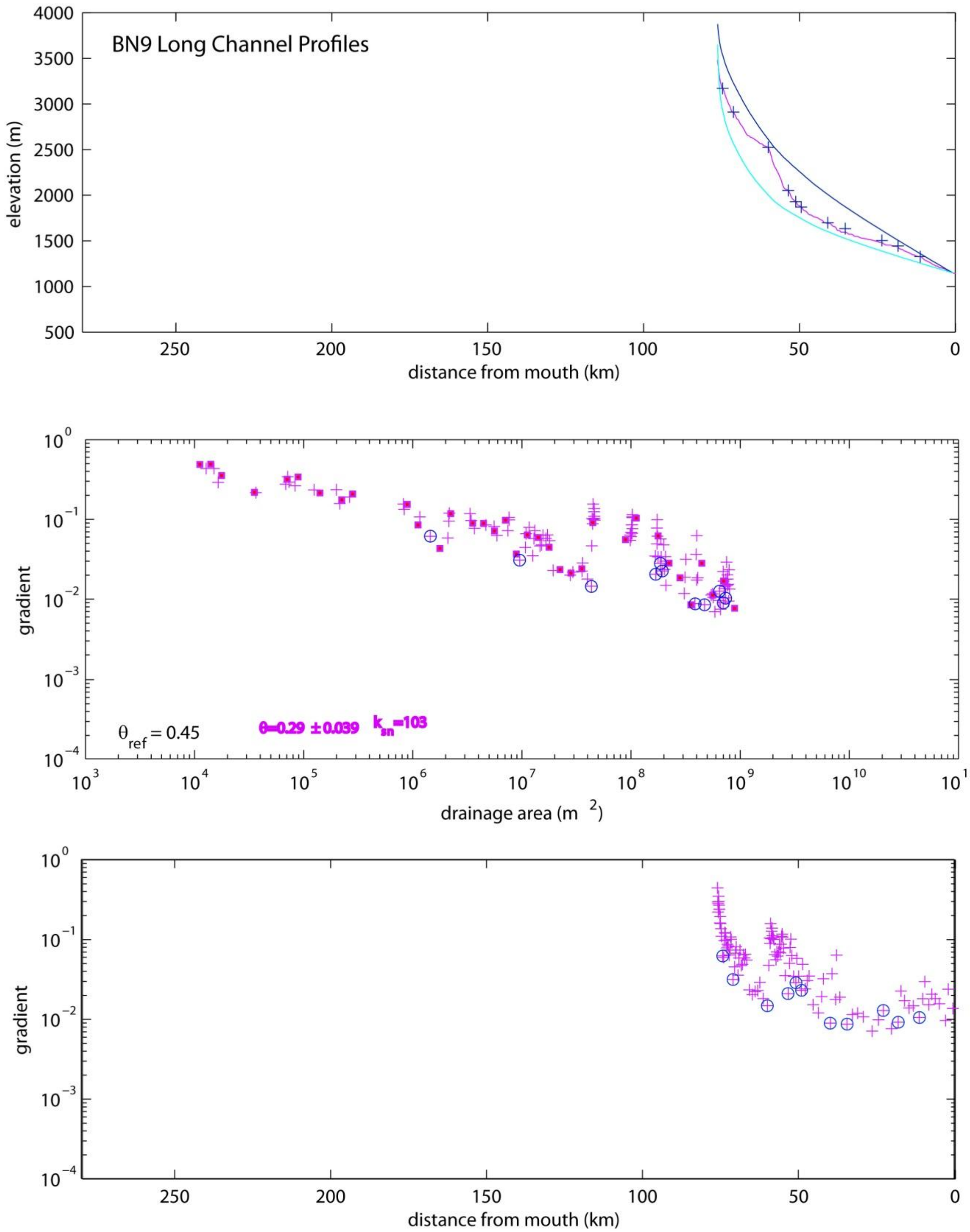
BN9 Long Channel Profiles
elevation (m)
distance from mouth (km)
gradient
θ_{ref} = 0.45
θ=0.29 ± 0.039
k_{sn}=103
drainage area (m 2)
gradient
distance from mouth (km)

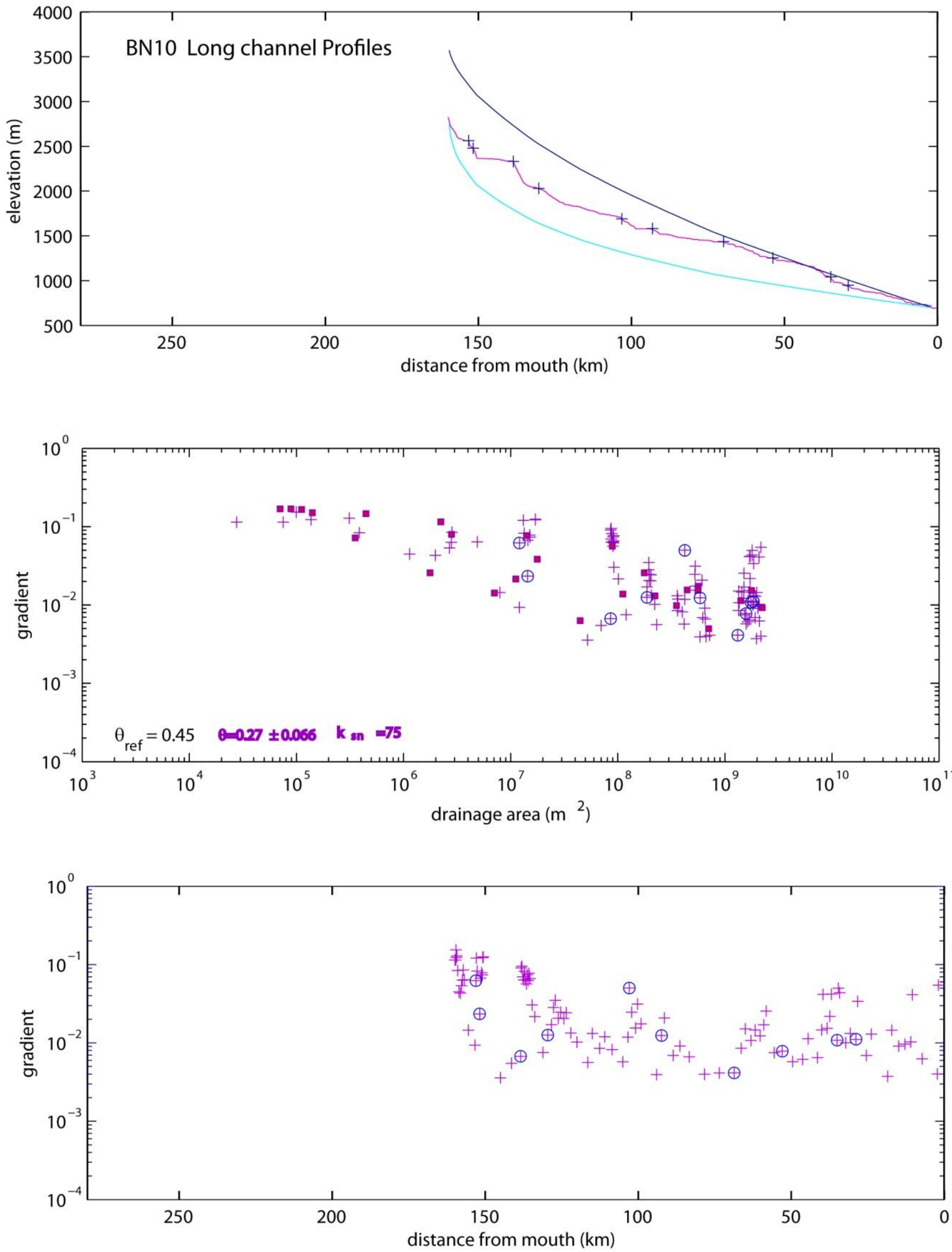

BN10 Long channel Profiles
elevation (m)
distance from mouth (km)
gradient
drainage area (m 2)
θref = 0.45
θ=0.27 ±0.066
k sn =75
gradient
distance from mouth (km)

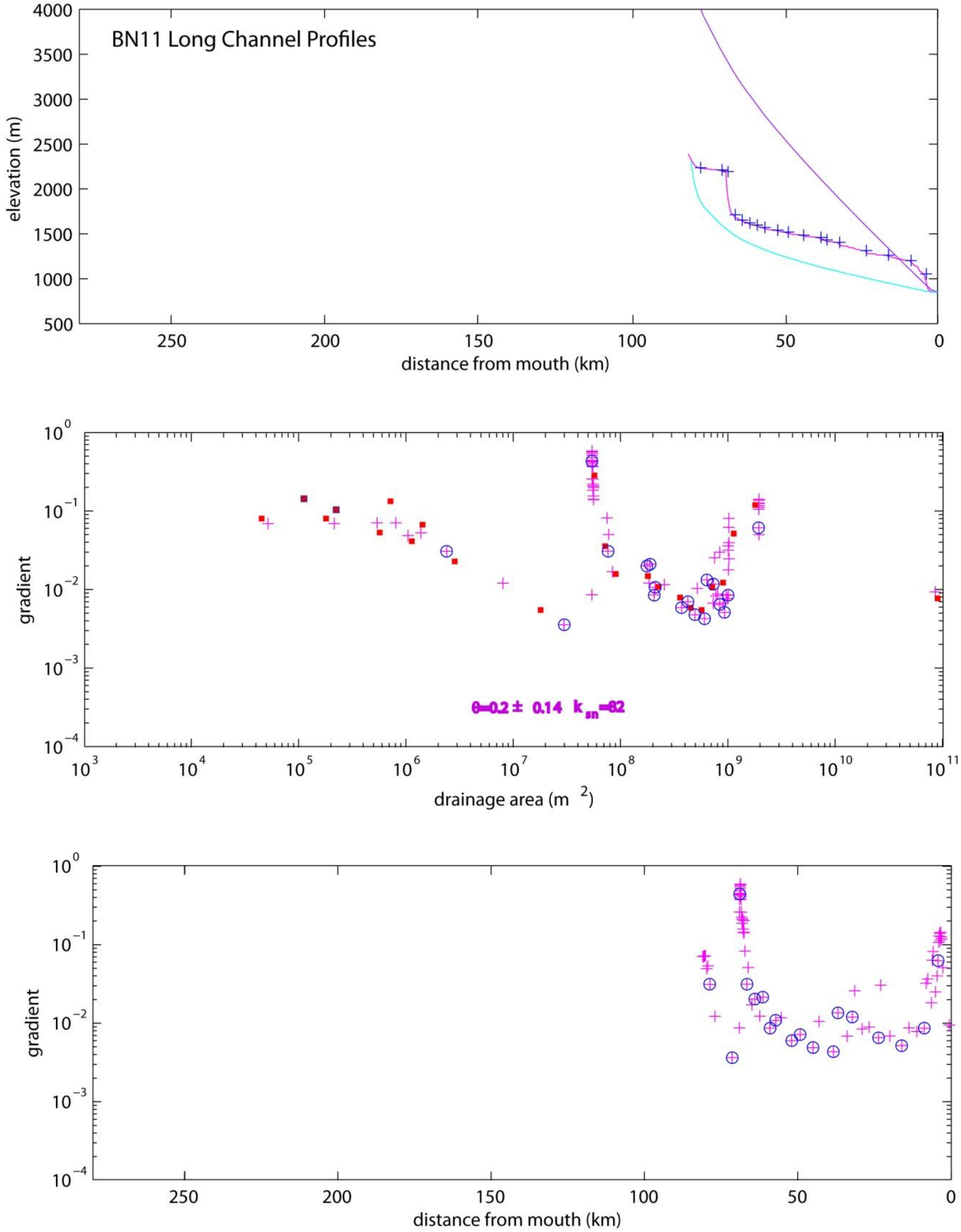
BN11 Long Channel Profiles
elevation (m)
distance from mouth (km)
gradient
drainage area (m 2)
θ=0.2 ± 0.14 ksn=82
gradient
distance from mouth (km)

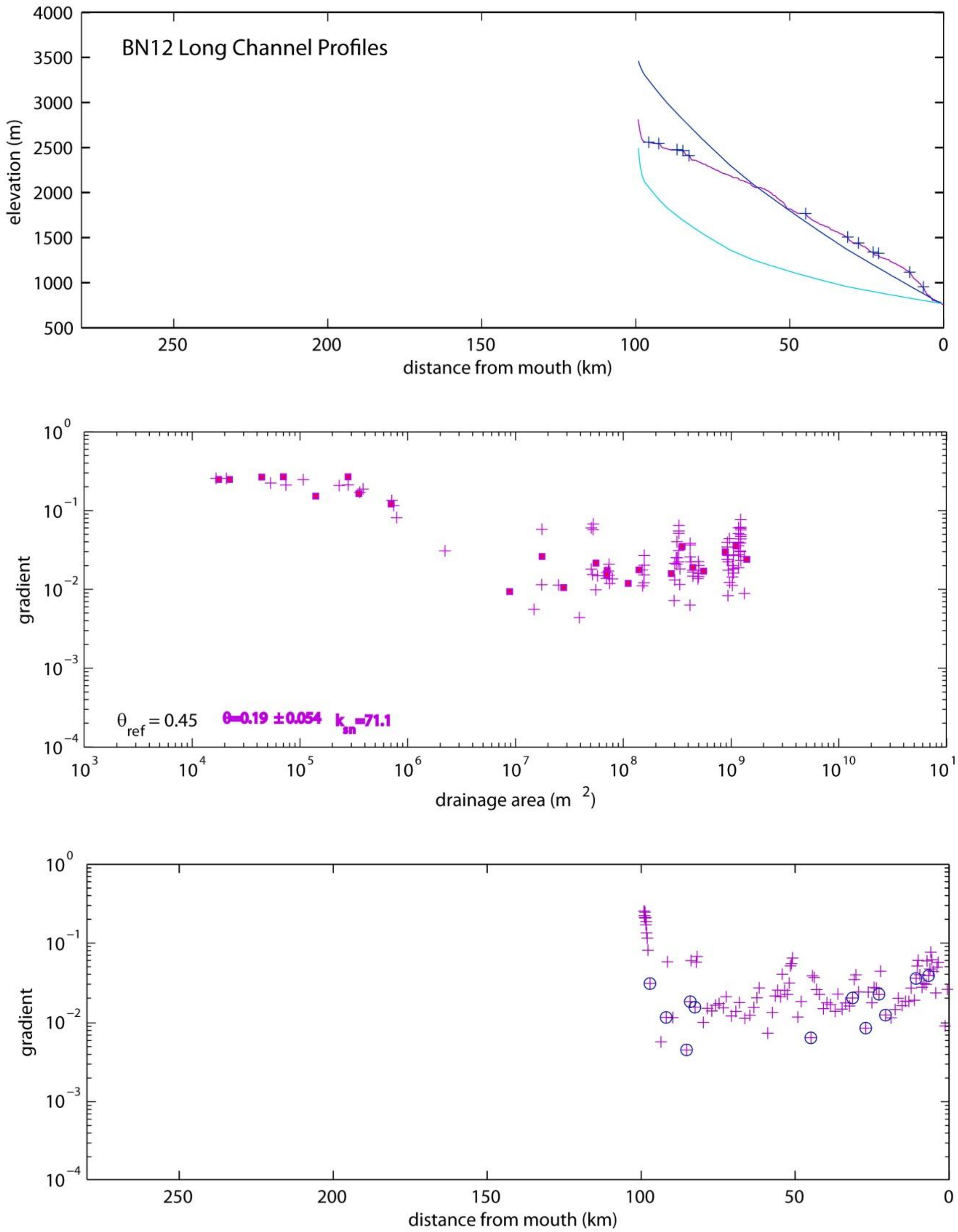
BN12 Long Channel Profiles
elevation (m)
distance from mouth (km)
gradient
θref = 0.45
θ=0.19 ±0.054
ksn=71.1
drainage area (m 2)
gradient
distance from mouth (km)

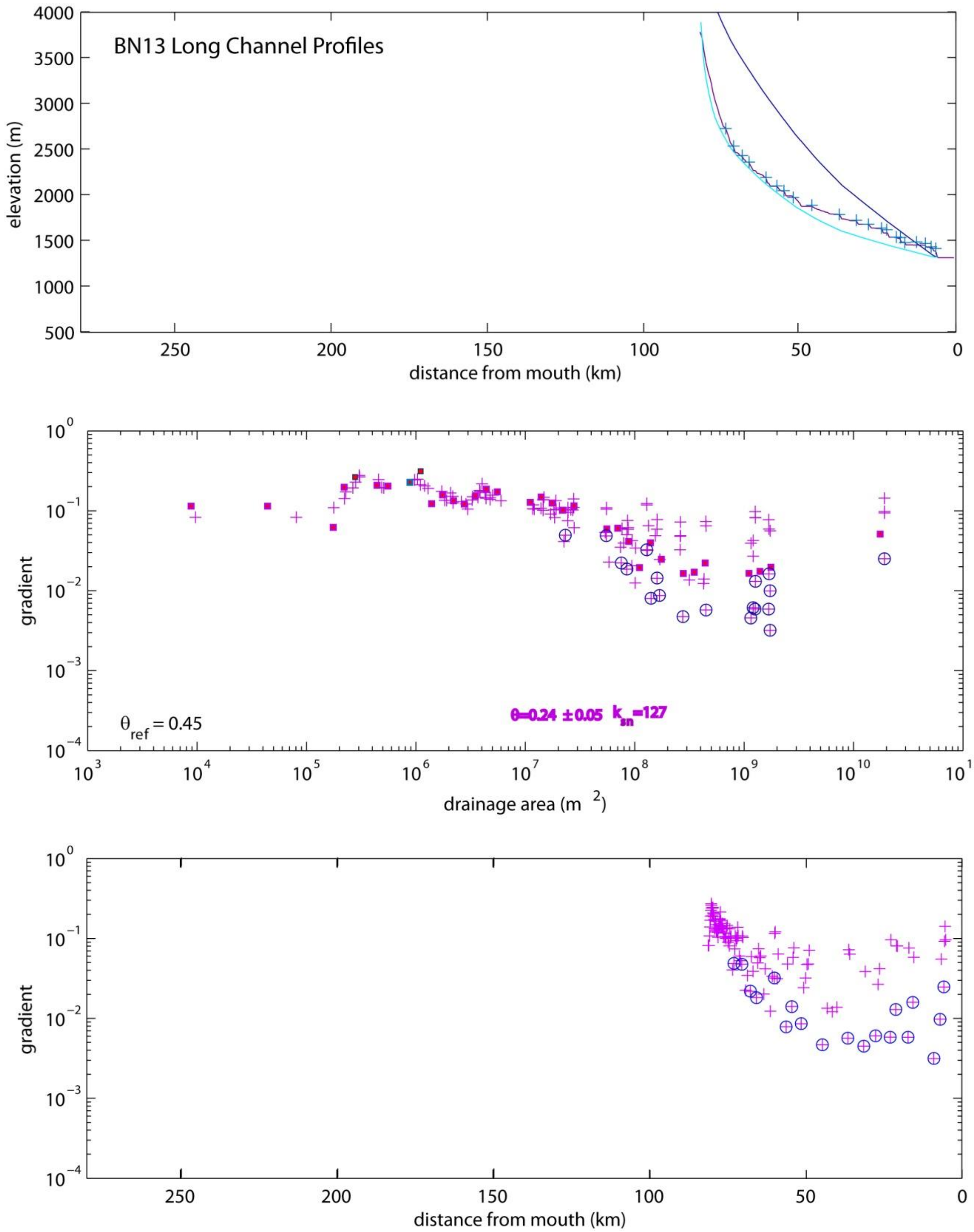
BN13 Long Channel Profiles
elevation (m)
distance from mouth (km)
gradient
θref = 0.45
θ=0.24 ±0.05 ksn=127
drainage area (m 2)
gradient
distance from mouth (km)

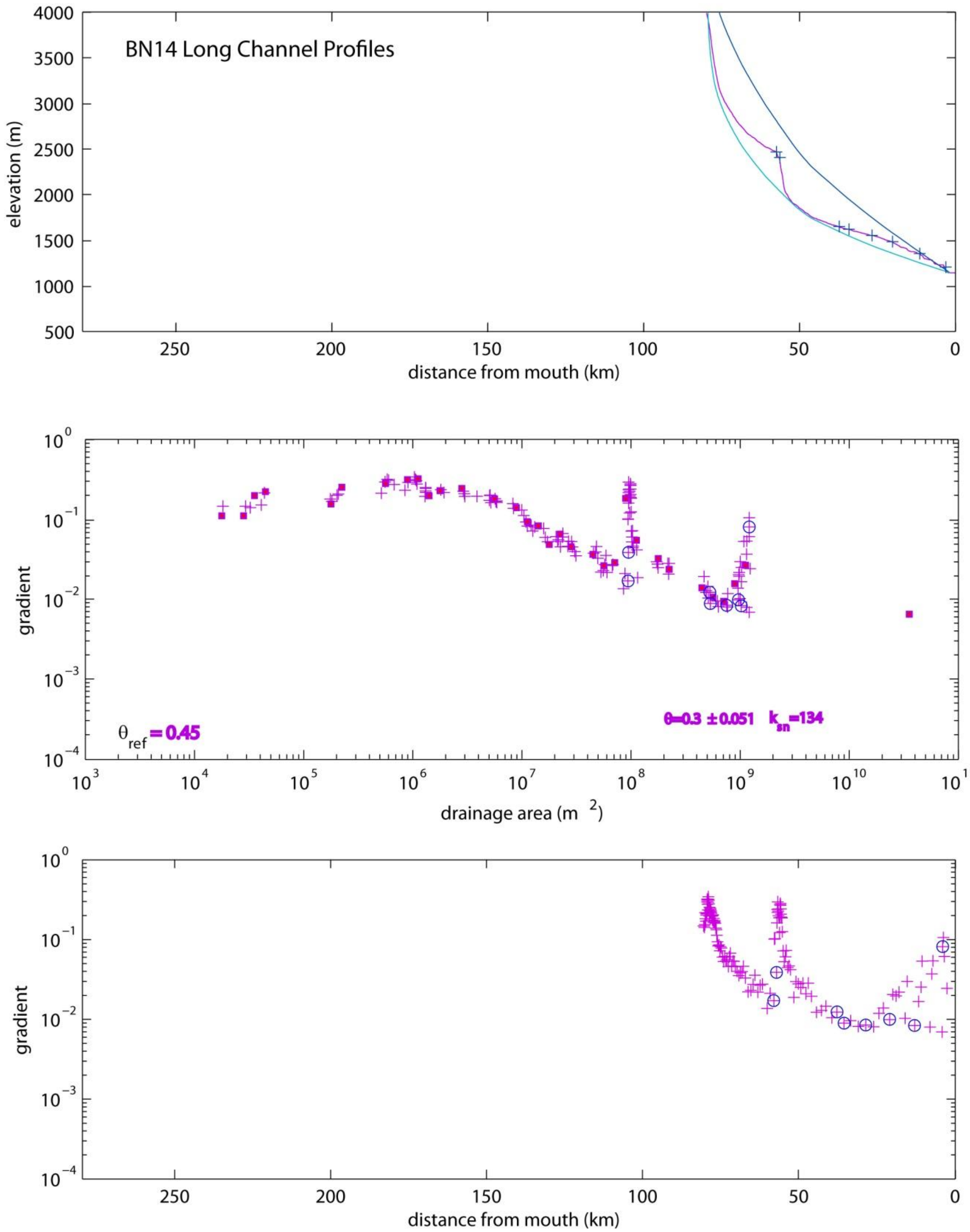
BN14 Long Channel Profiles
elevation (m)
distance from mouth (km)
gradient
drainage area (m 2)
θref = 0.45
θ=0.3 ±0.051 ksn=134
gradient
distance from mouth (km)

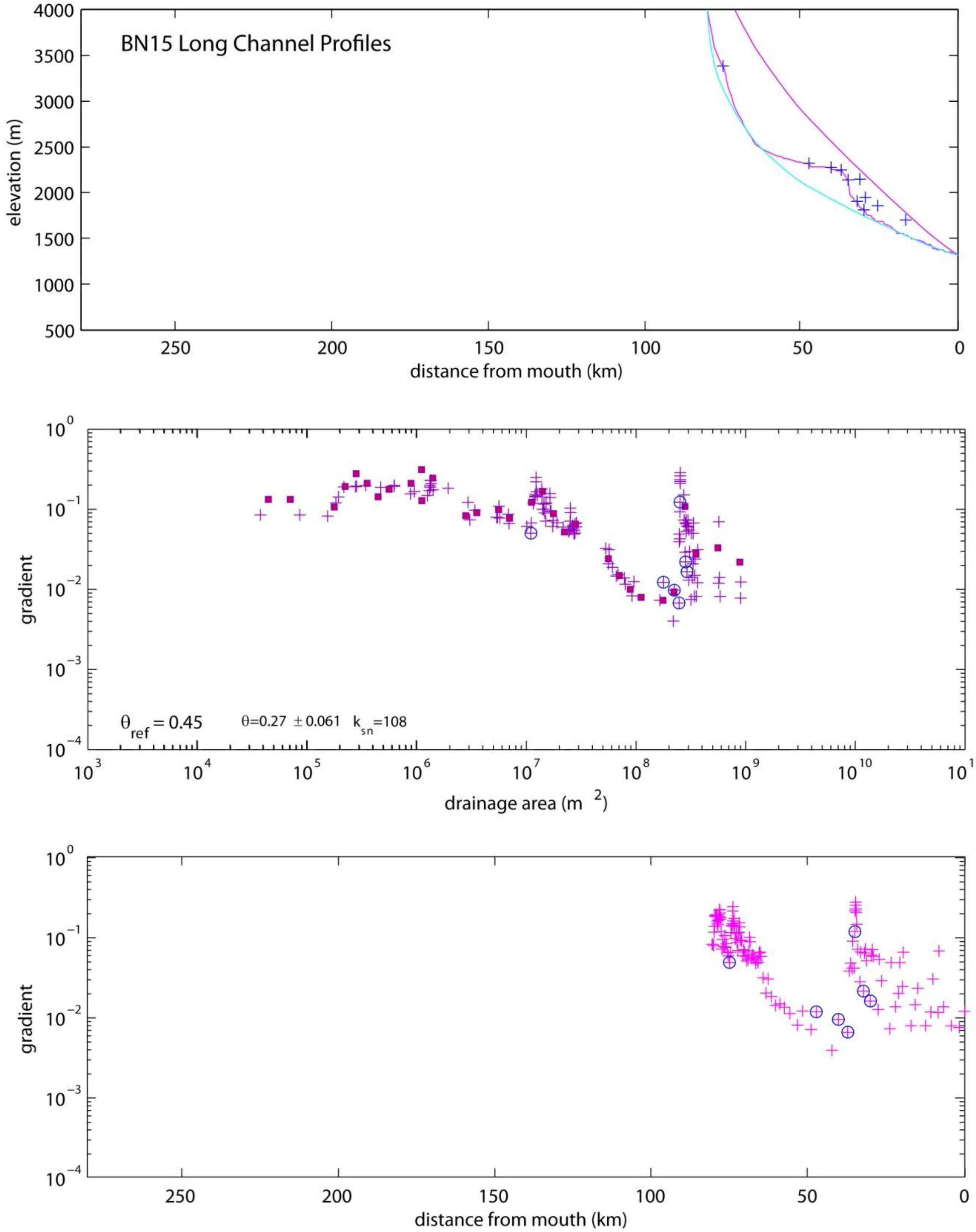
BN15 Long Channel Profiles
elevation (m)
distance from mouth (km)
gradient
drainage area (m 2)
θ_{ref} = 0.45
θ=0.27 ± 0.061 k_{sn}=108
gradient
distance from mouth (km)

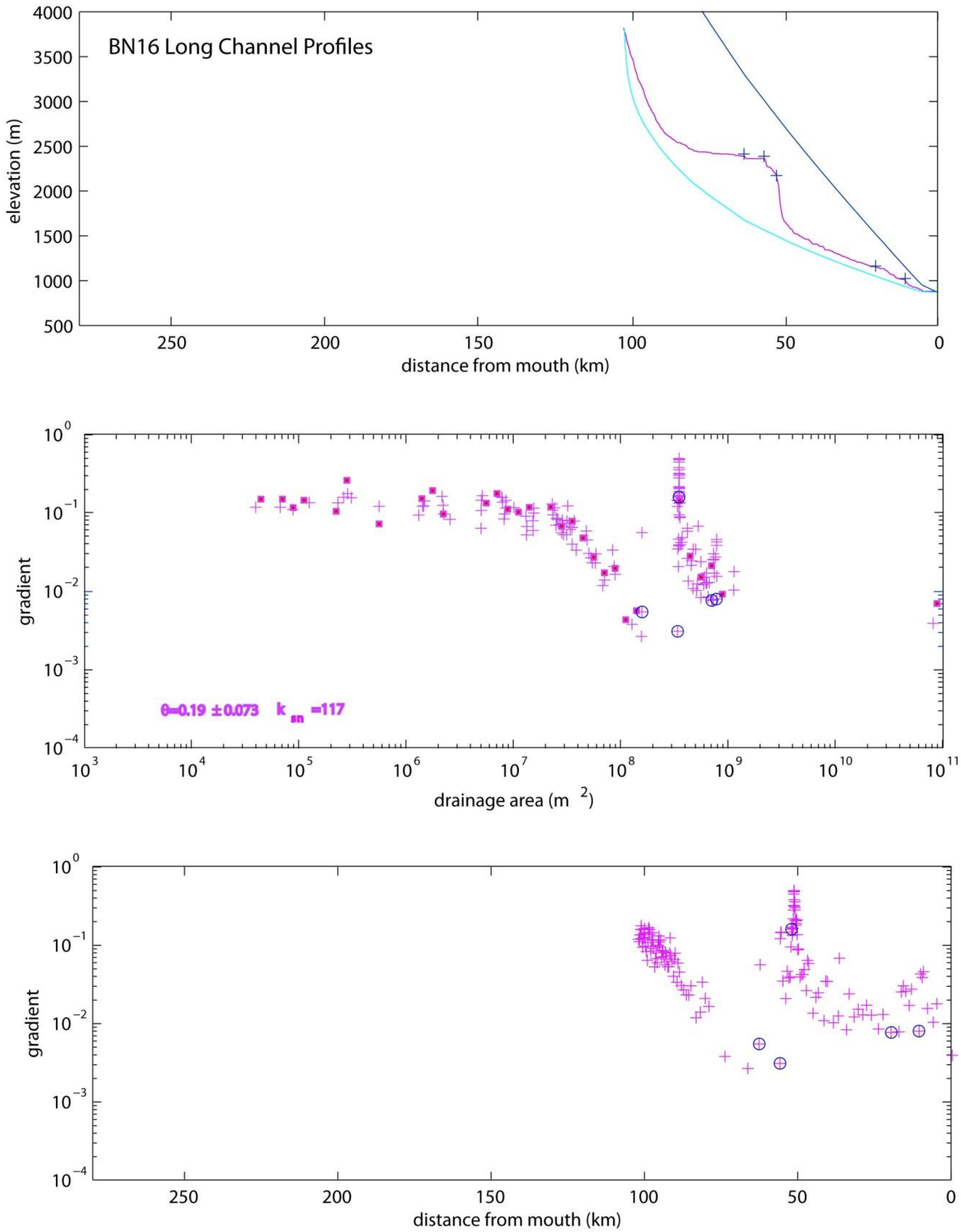
BN16 Long Channel Profiles
elevation (m)
4000
3500
3000
2500
2000
1500
1000
500
250
200
150
100
50
0
distance from mouth (km)
gradient
θ=0.19 ± 0.073 k sn =117
drainage area (m 2)
gradient
distance from mouth (km)

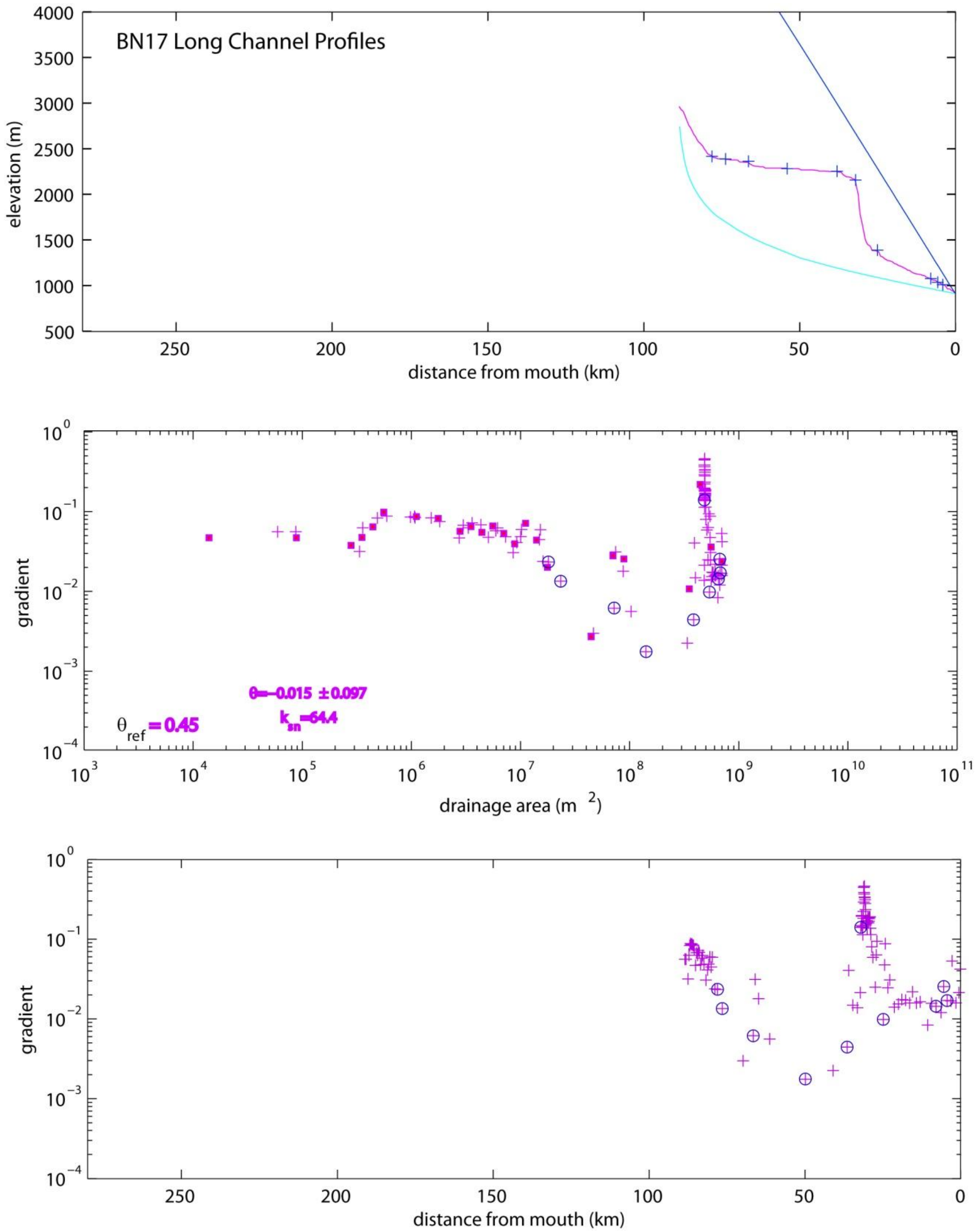

BN17 Long Channel Profiles
elevation (m)
distance from mouth (km)
gradient
drainage area (m 2)
θ=-0.015 ±0.097
ksn=64.4
θref = 0.45
gradient
distance from mouth (km)

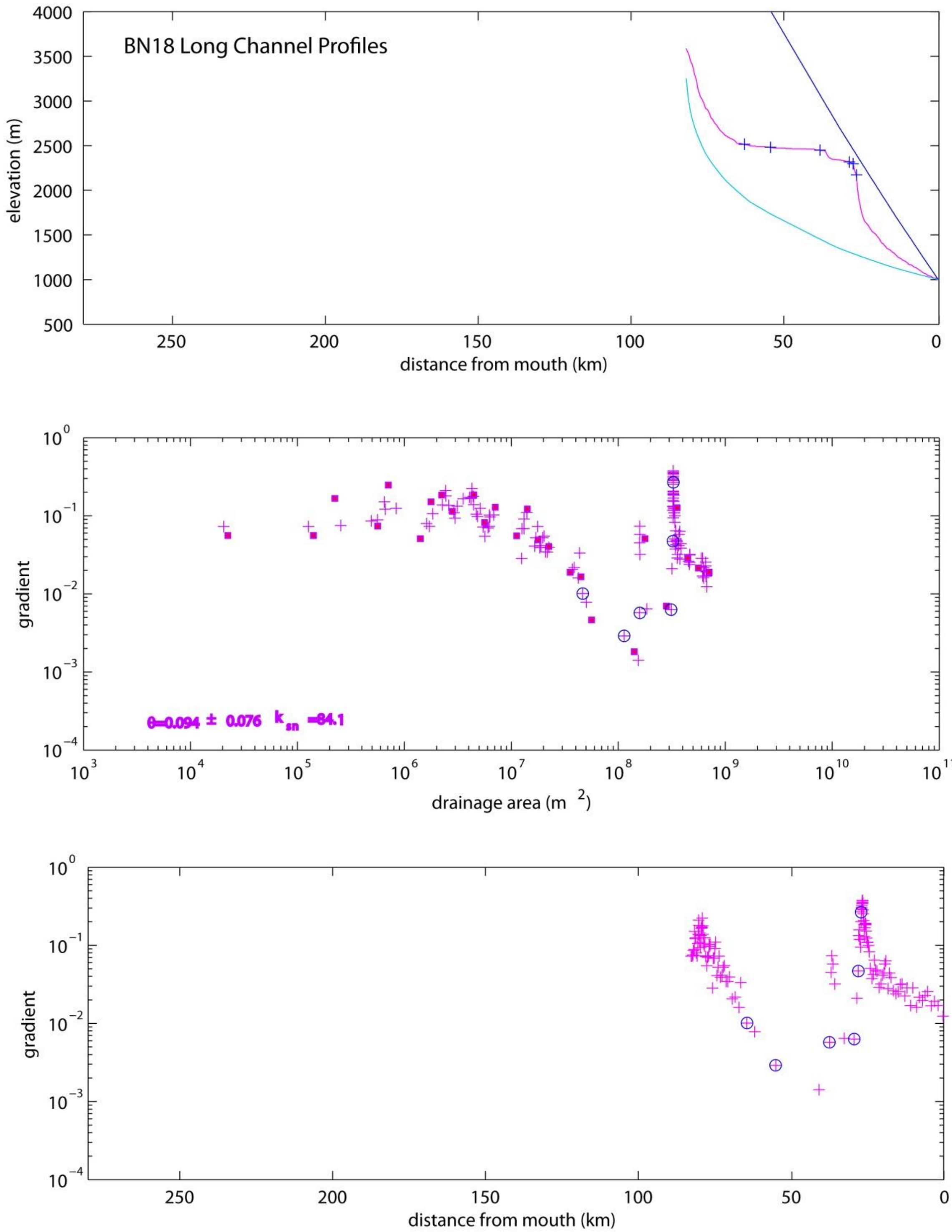
BN18 Long Channel Profiles
elevation (m)
distance from mouth (km)
gradient
drainage area (m 2)
θ=0.094 ± 0.076 k sn =84.1
gradient
distance from mouth (km)

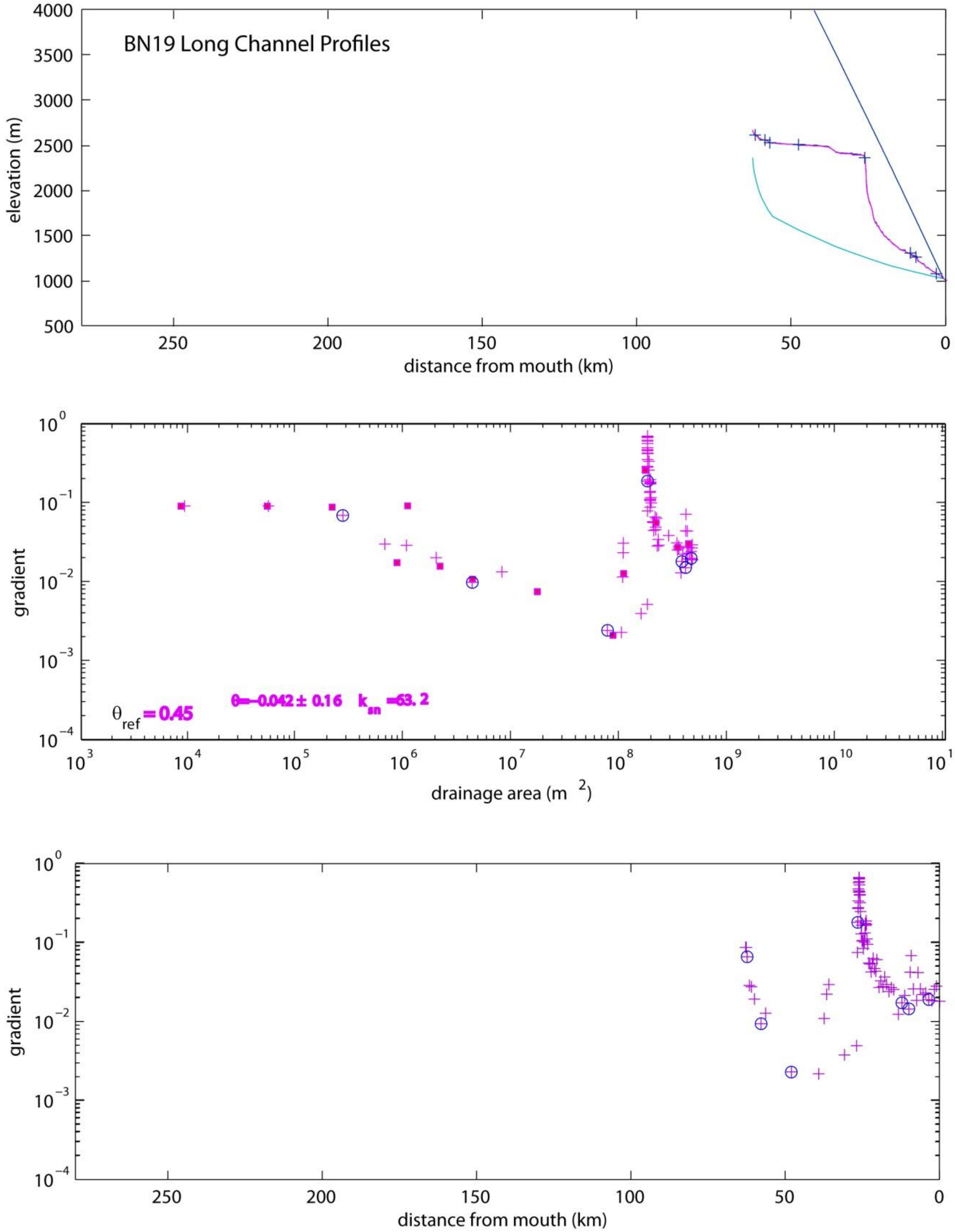
BN19 Long Channel Profiles
elevation (m)
distance from mouth (km)
gradient
drainage area (m 2)
θref = 0.45
θ=-0.042 ± 0.16 ksn =63. 2
gradient
distance from mouth (km)

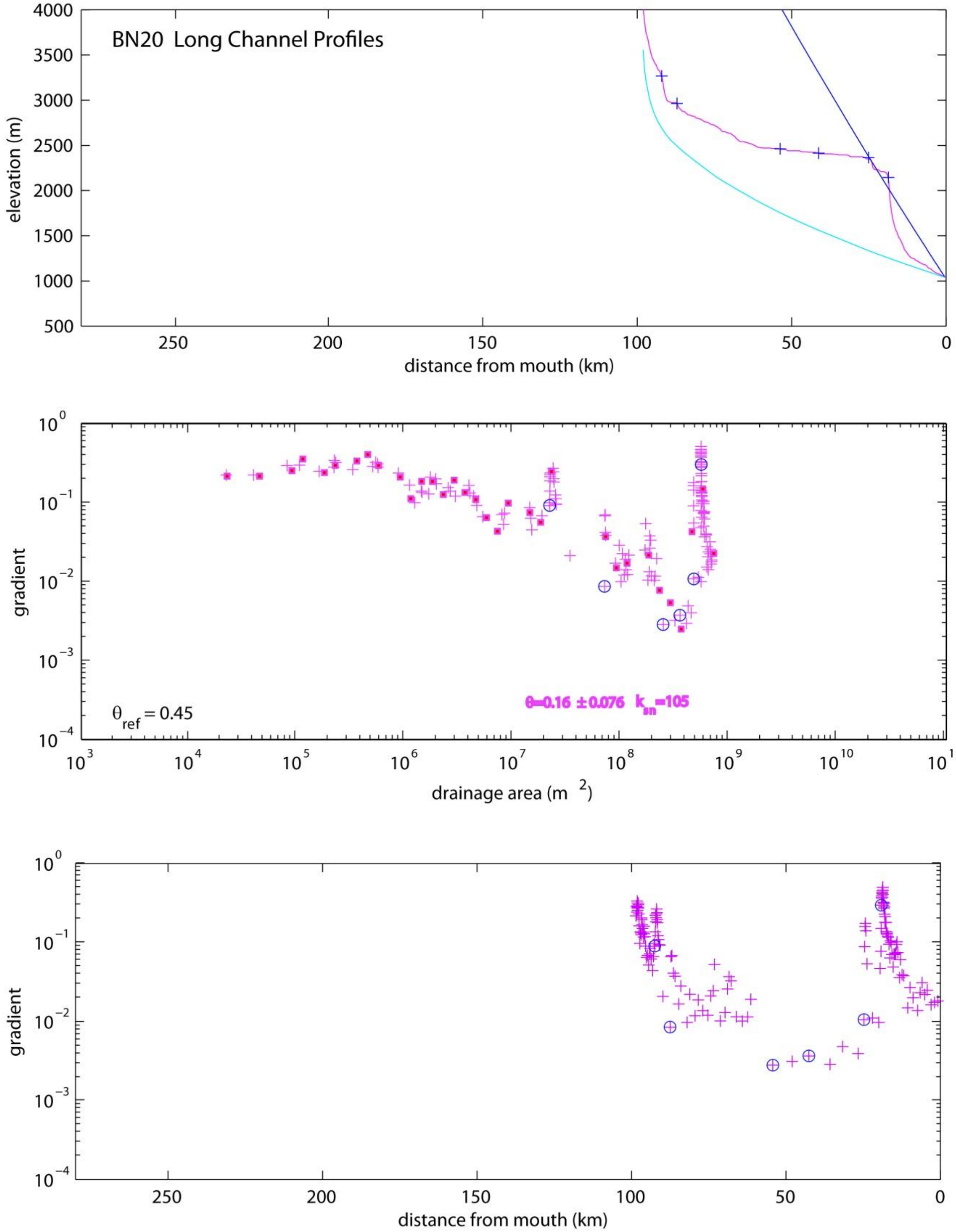
BN20 Long Channel Profiles
elevation (m)
distance from mouth (km)
gradient
drainage area (m 2)
θref = 0.45
θ=0.16 ±0.076 ksn=105
gradient
distance from mouth (km)

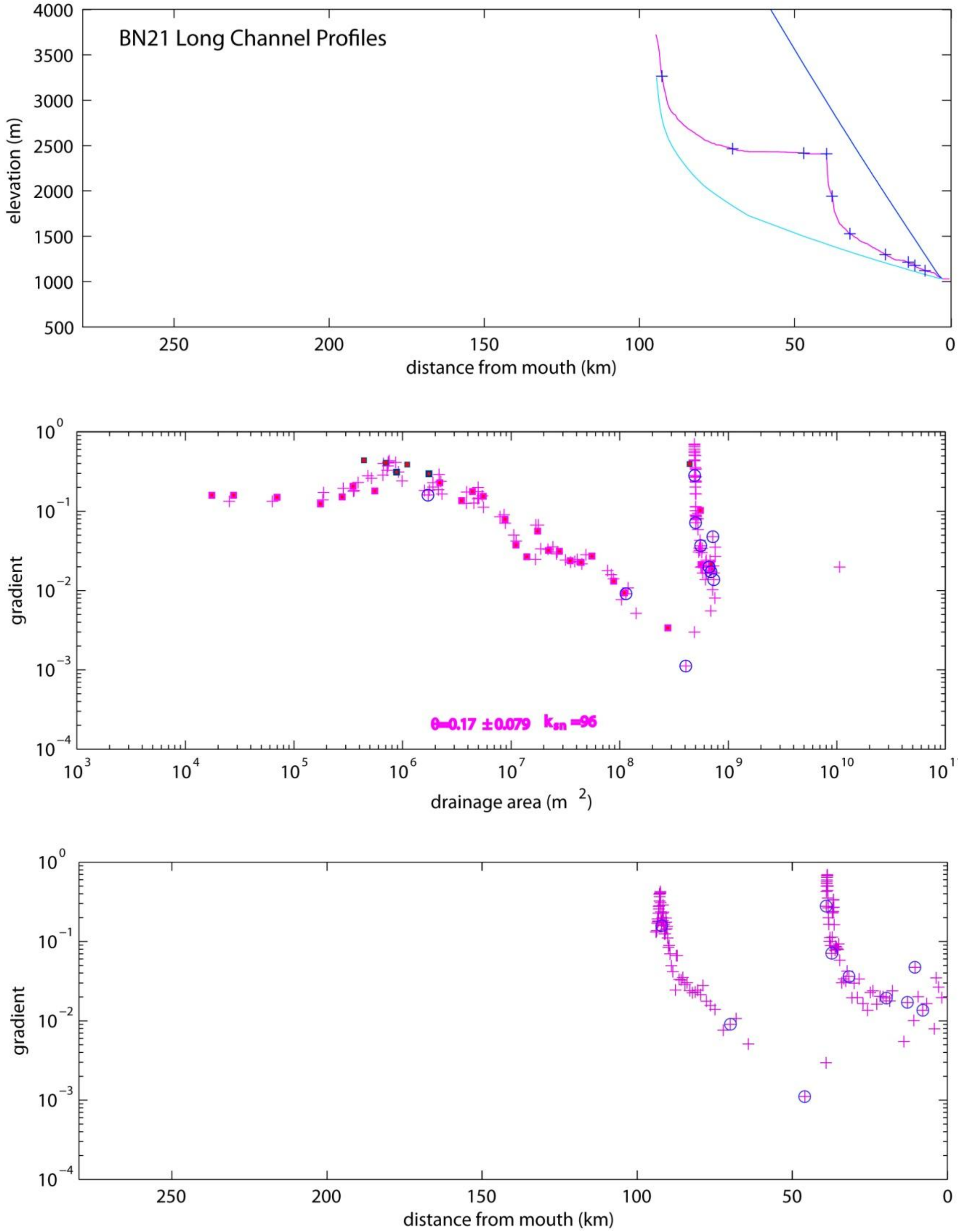
BN21 Long Channel Profiles
elevation (m)
distance from mouth (km)
gradient
drainage area (m^2)
θ=0.17 ± 0.079 k_{sn} =96
gradient
distance from mouth (km)

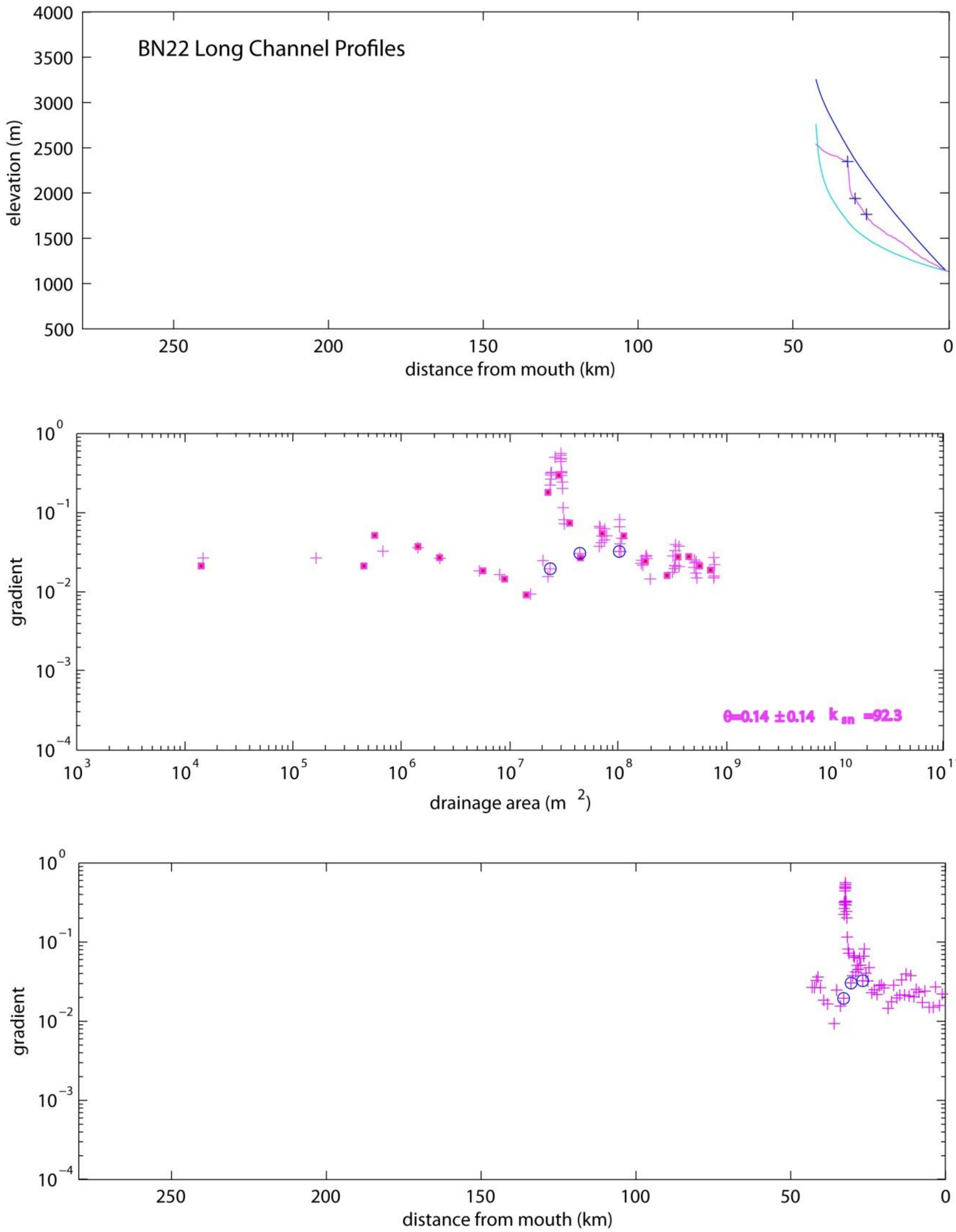
BN22 Long Channel Profiles
elevation (m)
4000
3500
3000
2500
2000
1500
1000
500
250
200
150
100
50
0
distance from mouth (km)
gradient
10^0
10^-1
10^-2
10^-3
10^-4
θ=0.14 ±0.14 k sn =92.3
10^3
10^4
10^5
10^6
10^7
10^8
10^9
10^10
10^11
drainage area (m 2)
gradient
10^0
10^-1
10^-2
10^-3
10^-4
250
200
150
100
50
0
distance from mouth (km)

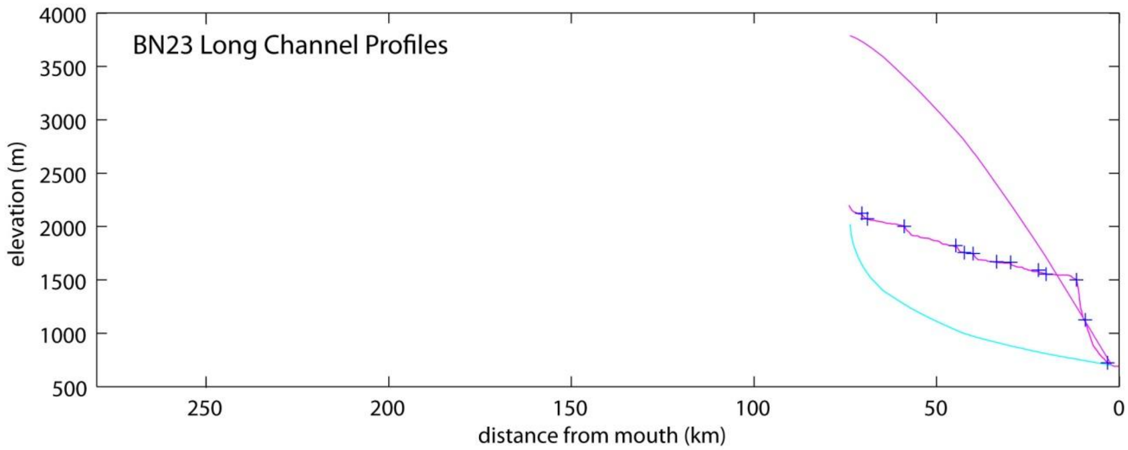
BN23 Long Channel Profiles
elevation (m)
distance from mouth (km)

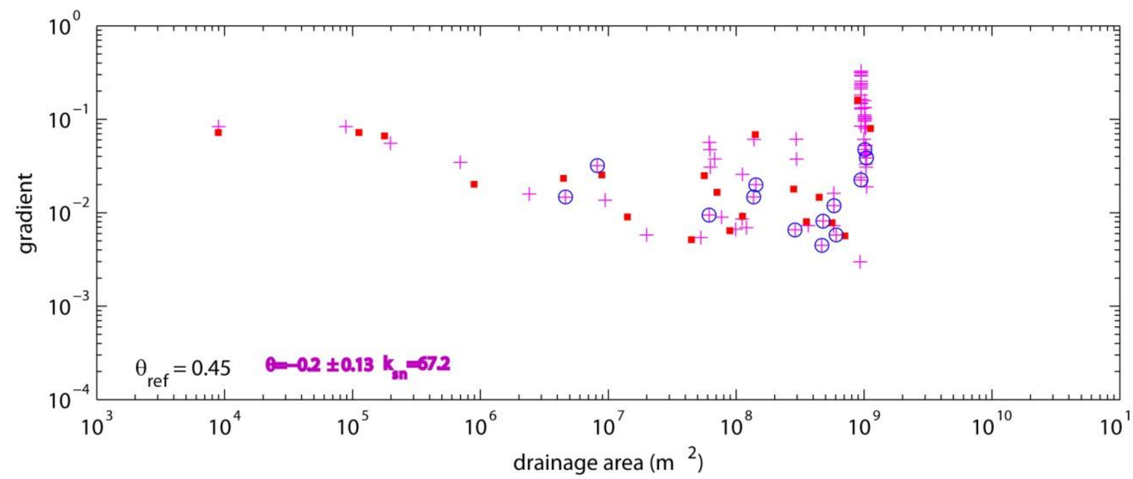
gradient
drainage area (m 2)
θref = 0.45
θ=-0.2 ±0.13 ksn=67.2

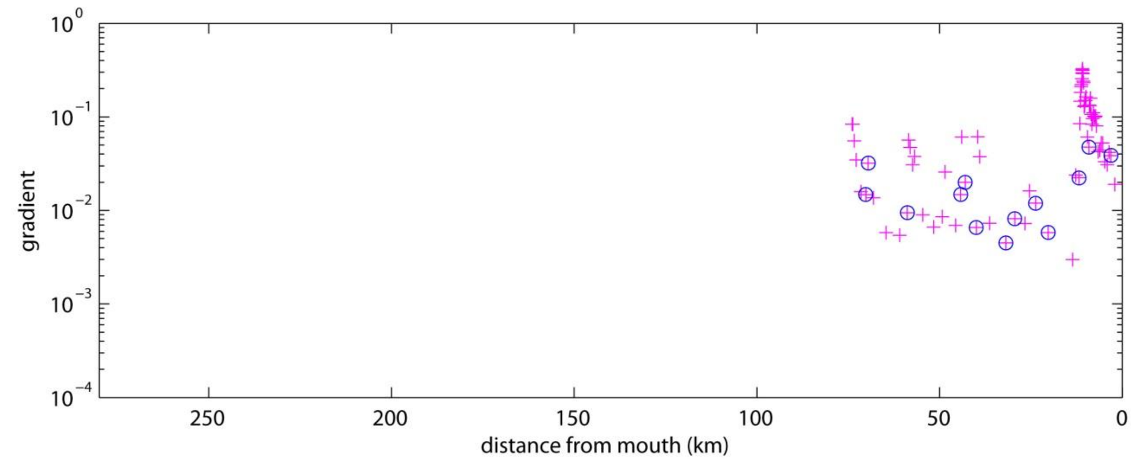
gradient
distance from mouth (km)

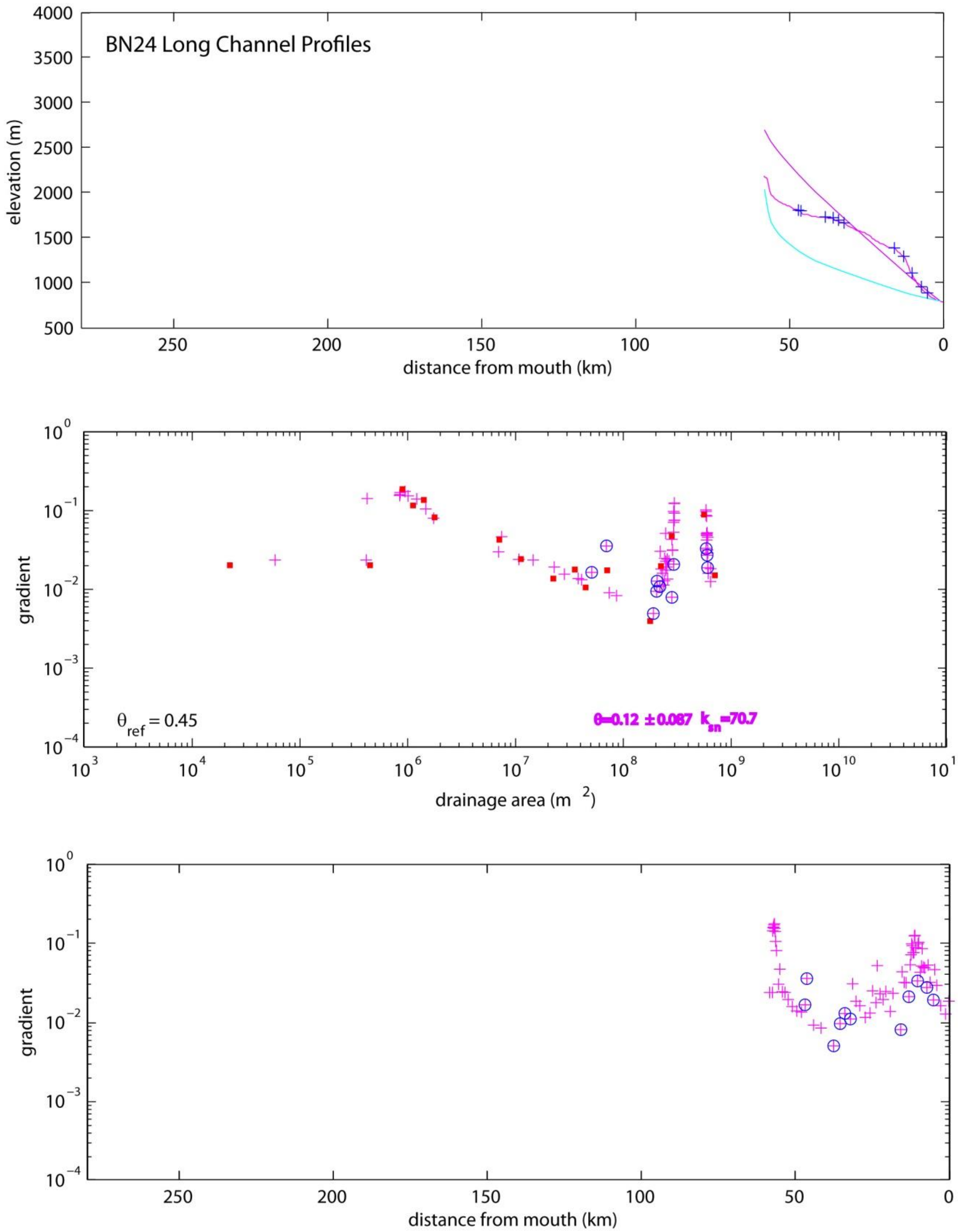
BN24 Long Channel Profiles
elevation (m)
distance from mouth (km)
gradient
drainage area (m 2)
θref = 0.45
θ=0.12 ± 0.087 ksn=70.7
gradient
distance from mouth (km)

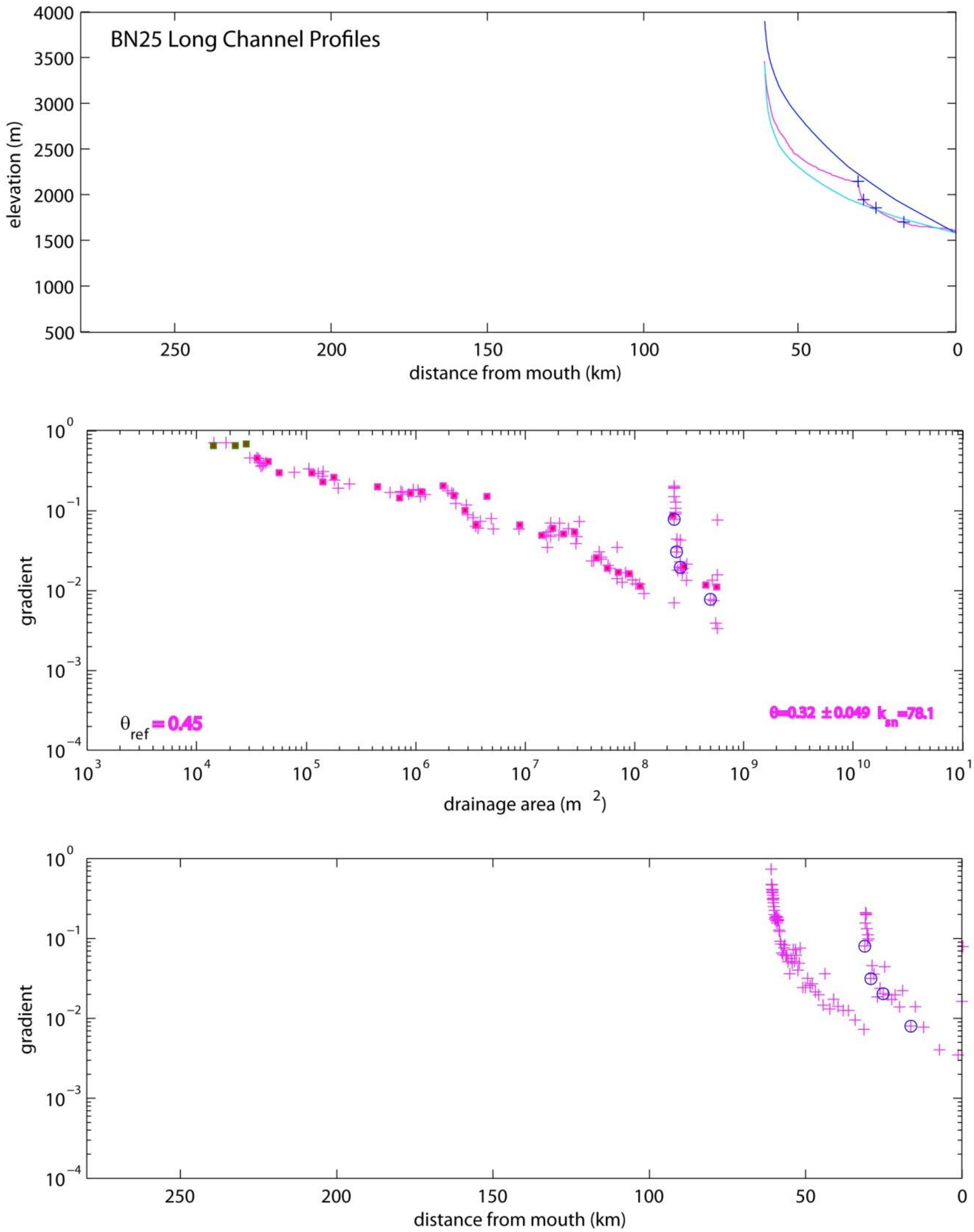

BN25 Long Channel Profiles
elevation (m)
distance from mouth (km)
gradient
drainage area (m 2)
θref = 0.45
θ=0.32 ± 0.049 ksn=78.1
gradient
distance from mouth (km)

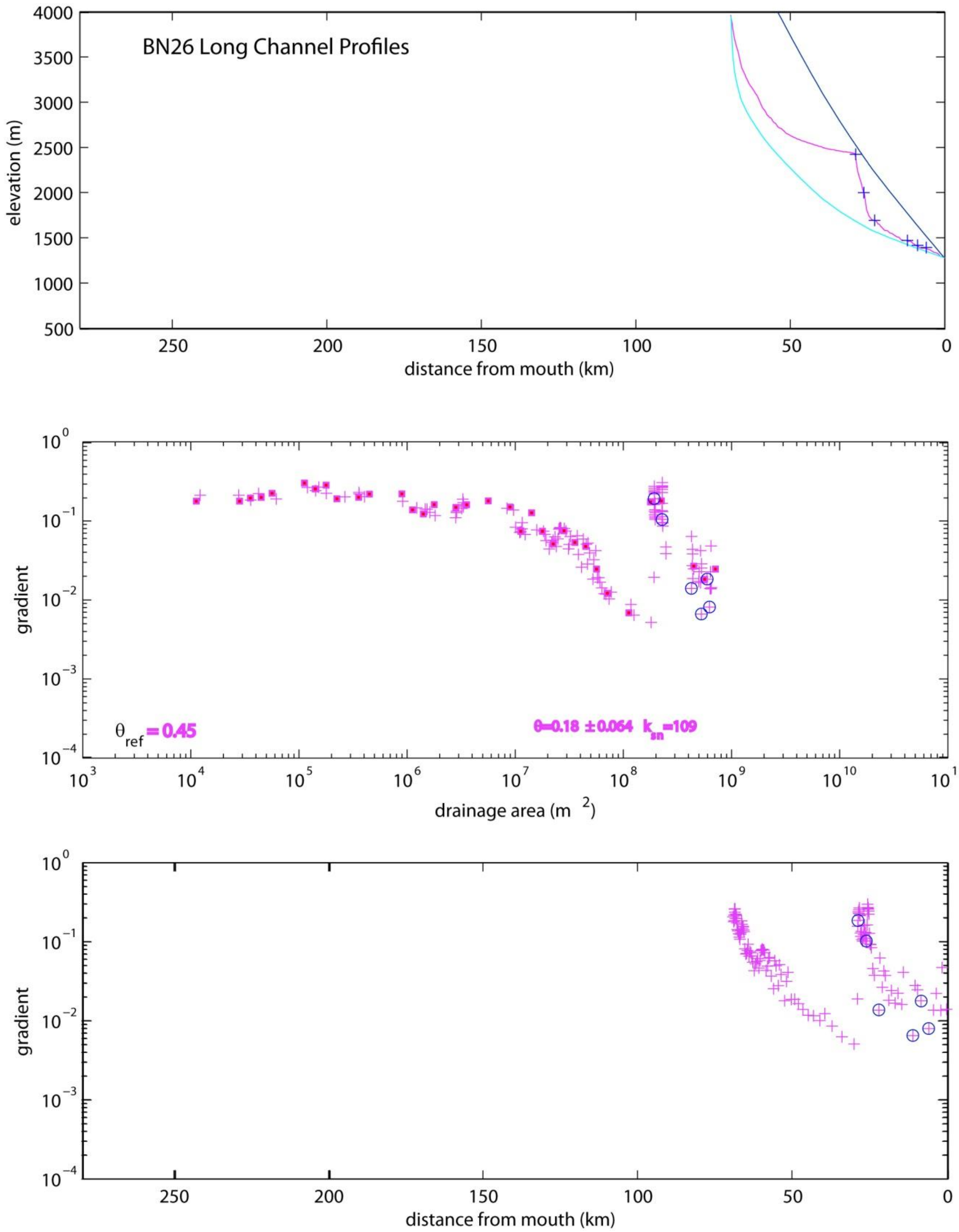
BN26 Long Channel Profiles
elevation (m)
distance from mouth (km)
gradient
θref = 0.45
θ=0.18 ±0.064 ksn=109
drainage area (m 2)
gradient
distance from mouth (km)

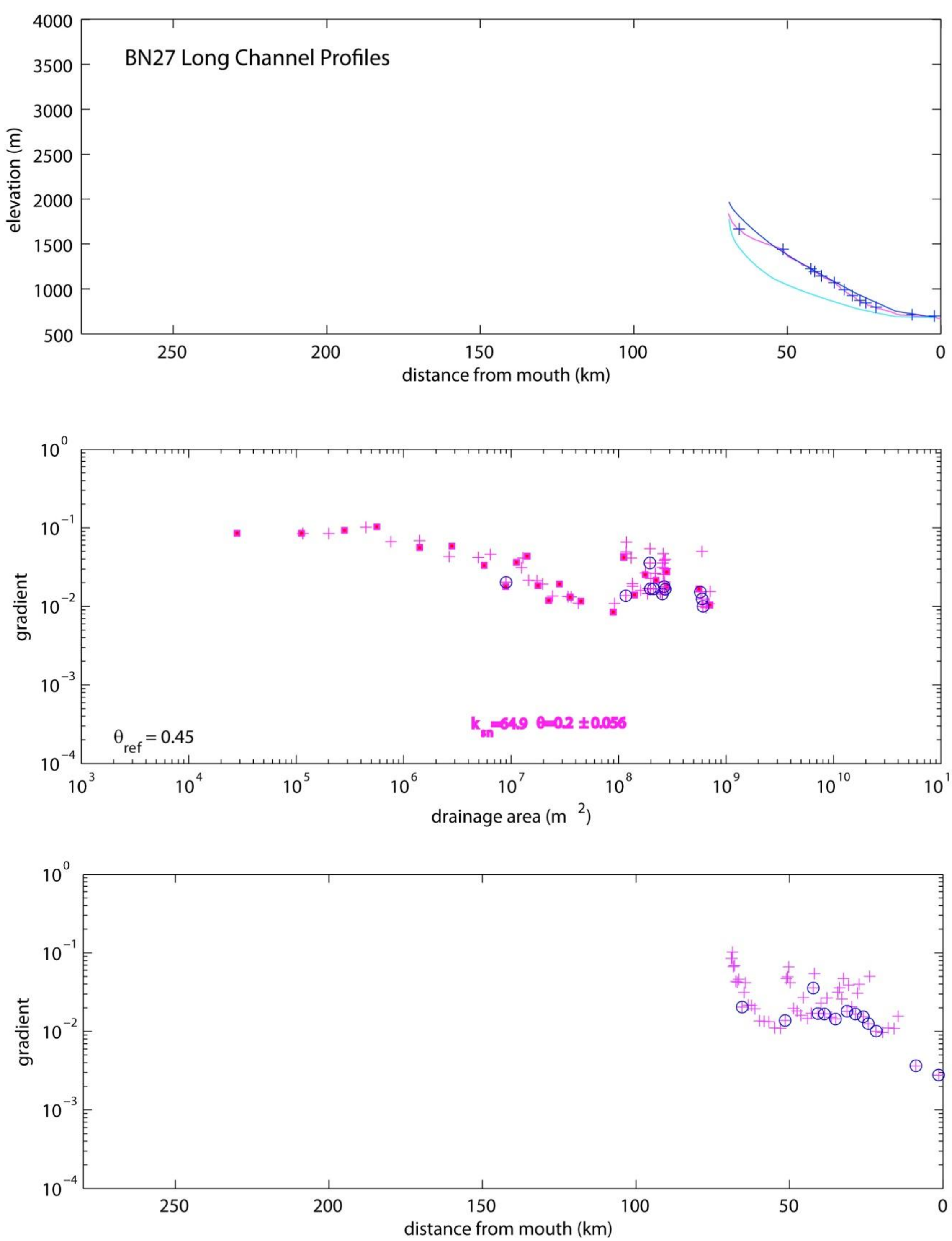
BN27 Long Channel Profiles
elevation (m)
distance from mouth (km)
gradient
θref = 0.45
ksn=64.9 θ=0.2 ±0.056
drainage area (m 2)
gradient
distance from mouth (km)

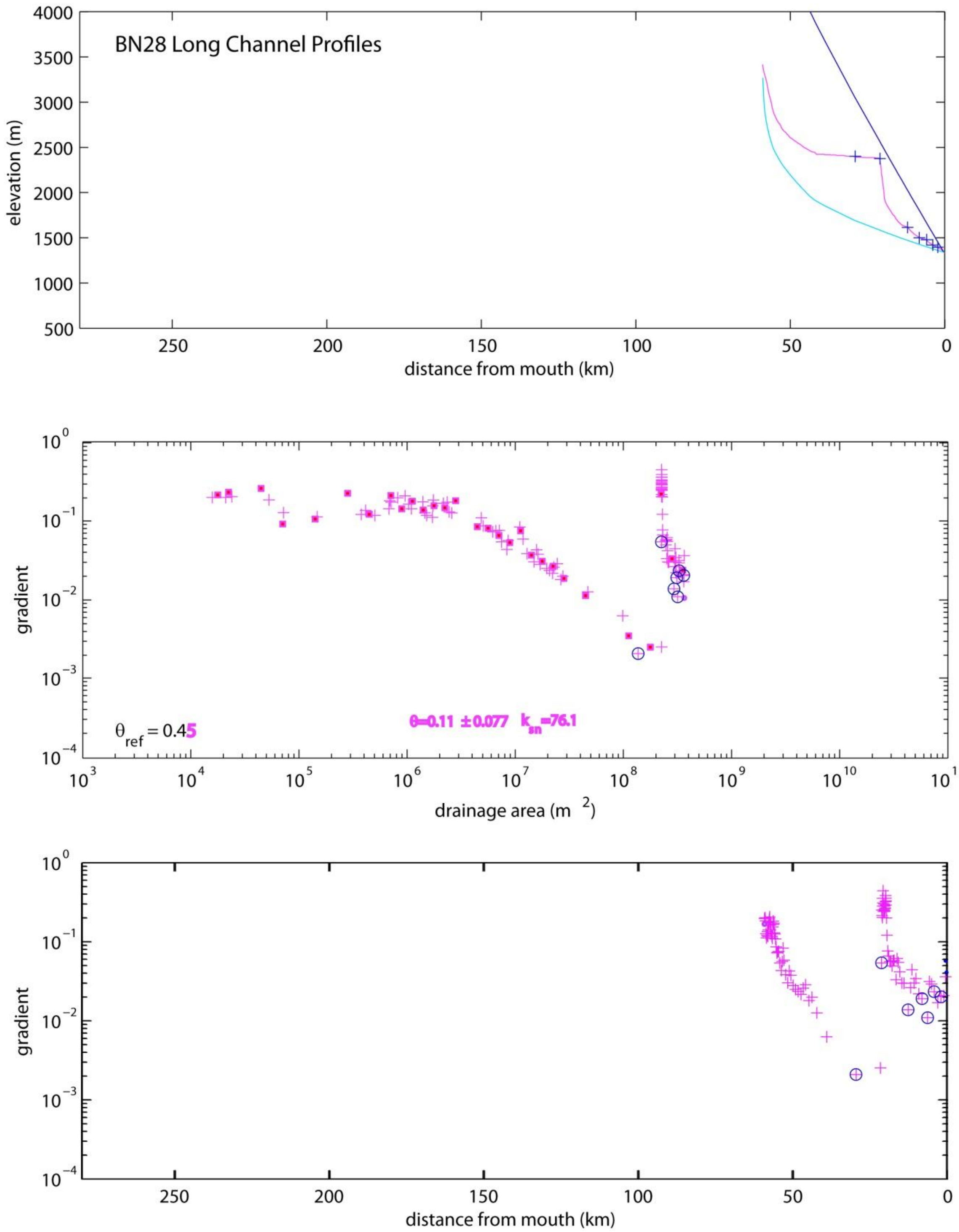
BN28 Long Channel Profiles
elevation (m)
4000
3500
3000
2500
2000
1500
1000
500
250
200
150
100
50
0
distance from mouth (km)
gradient
10^0
10^{-1}
10^{-2}
10^{-3}
10^{-4}
θ_{ref} = 0.45
θ=0.11 ±0.077 k_{sn}=76.1
10^3
10^4
10^5
10^6
10^7
10^8
10^9
10^{10}
10^{11}
drainage area (m^2)
gradient
10^0
10^{-1}
10^{-2}
10^{-3}
10^{-4}
250
200
150
100
50
0
distance from mouth (km)

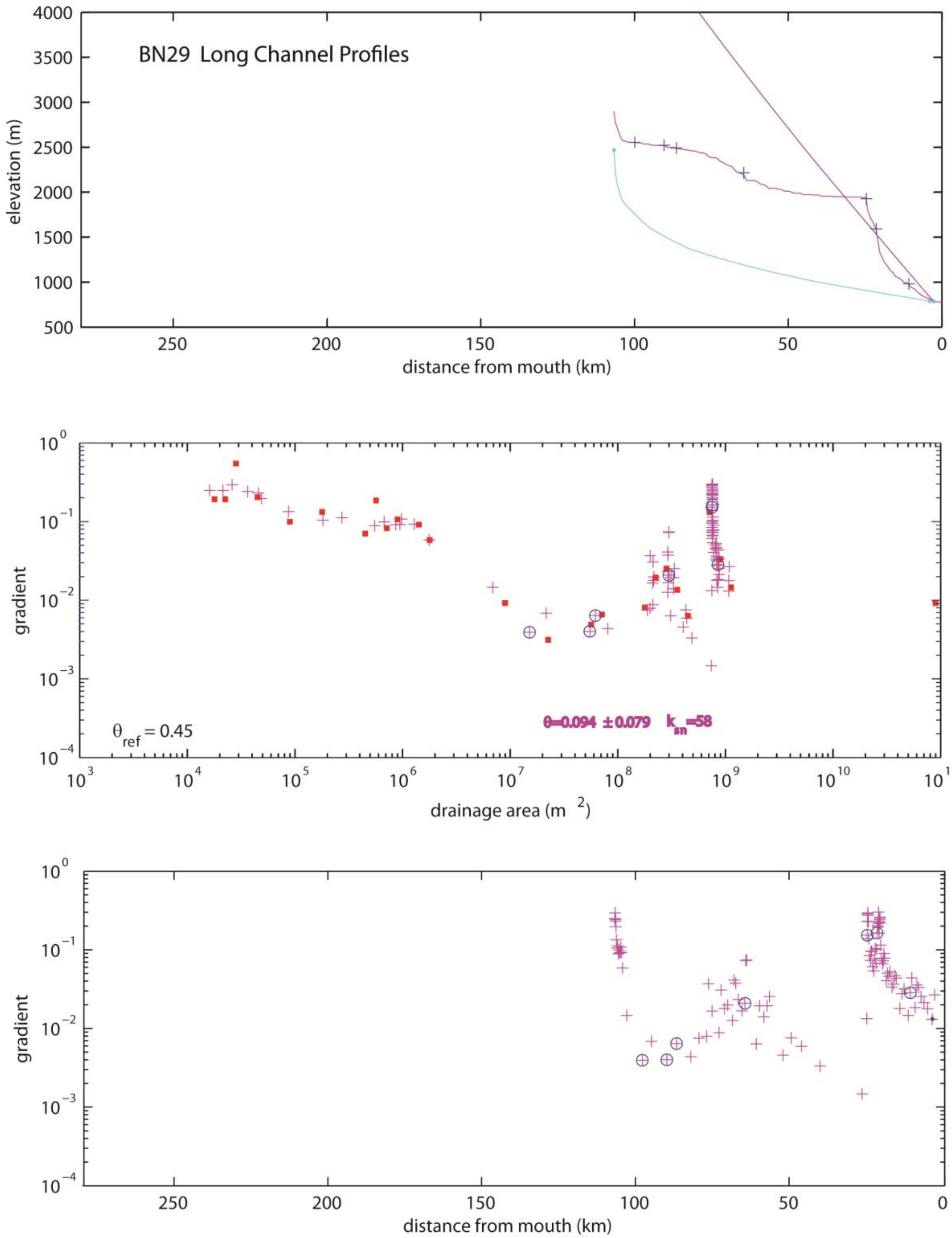
BN29 Long Channel Profiles
elevation (m)
distance from mouth (km)
gradient
drainage area (m 2)
θ=0.094 ±0.079 k_sn=58
θ_ref = 0.45
gradient
distance from mouth (km)

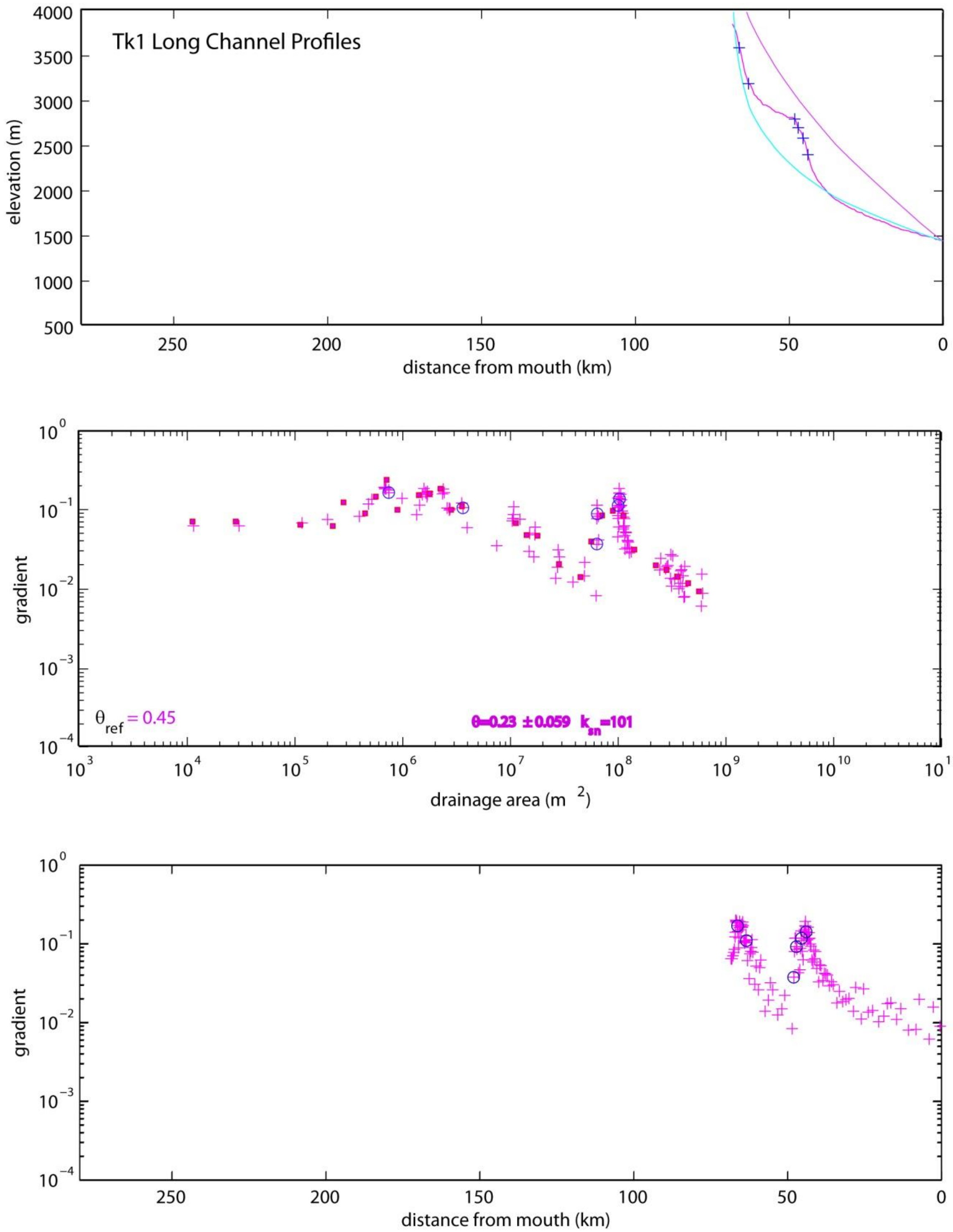
Tk1 Long Channel Profiles
elevation (m)
distance from mouth (km)
gradient
drainage area (m 2)
θref = 0.45
θ=0.23 ±0.059 ksn=101
gradient
distance from mouth (km)

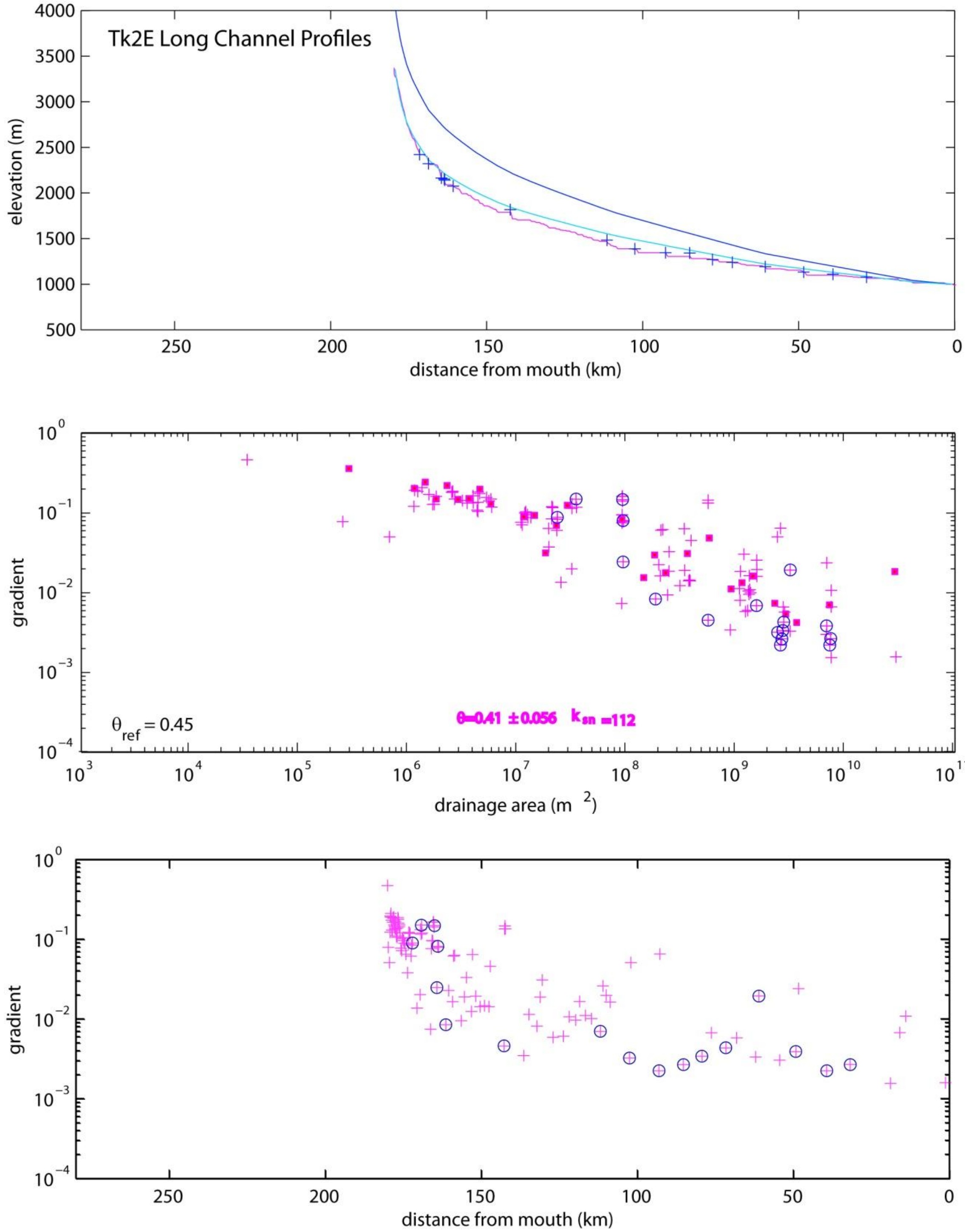
Tk2E Long Channel Profiles
elevation (m)
distance from mouth (km)
gradient
θ_{ref} = 0.45
θ=0.41 ±0.056 k_{sn} =112
drainage area (m^2)
gradient
distance from mouth (km)

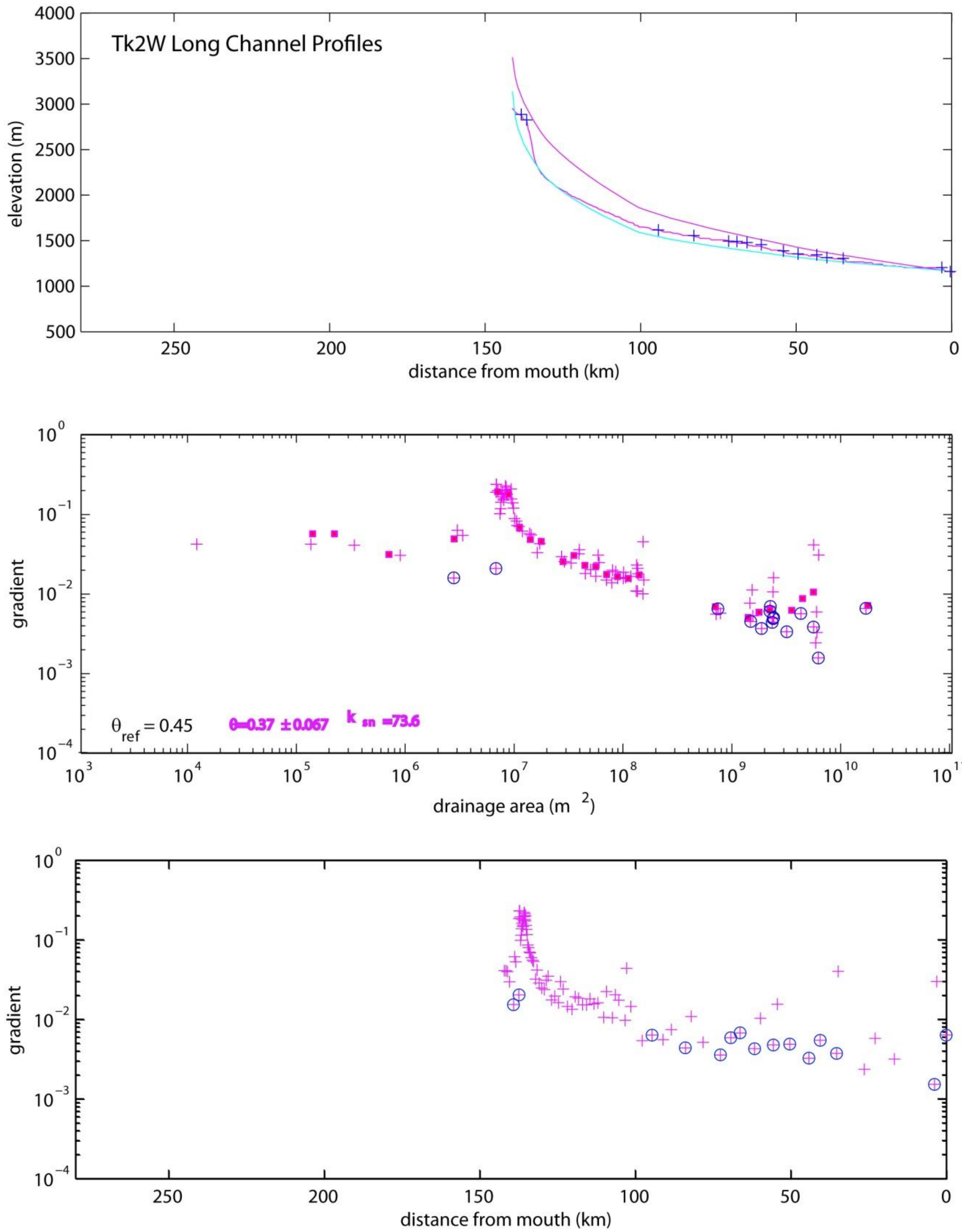
Tk2W Long Channel Profiles
elevation (m)
distance from mouth (km)
gradient
drainage area (m 2)
θref = 0.45
θ=0.37 ± 0.067
k sn =73.6
gradient
distance from mouth (km)

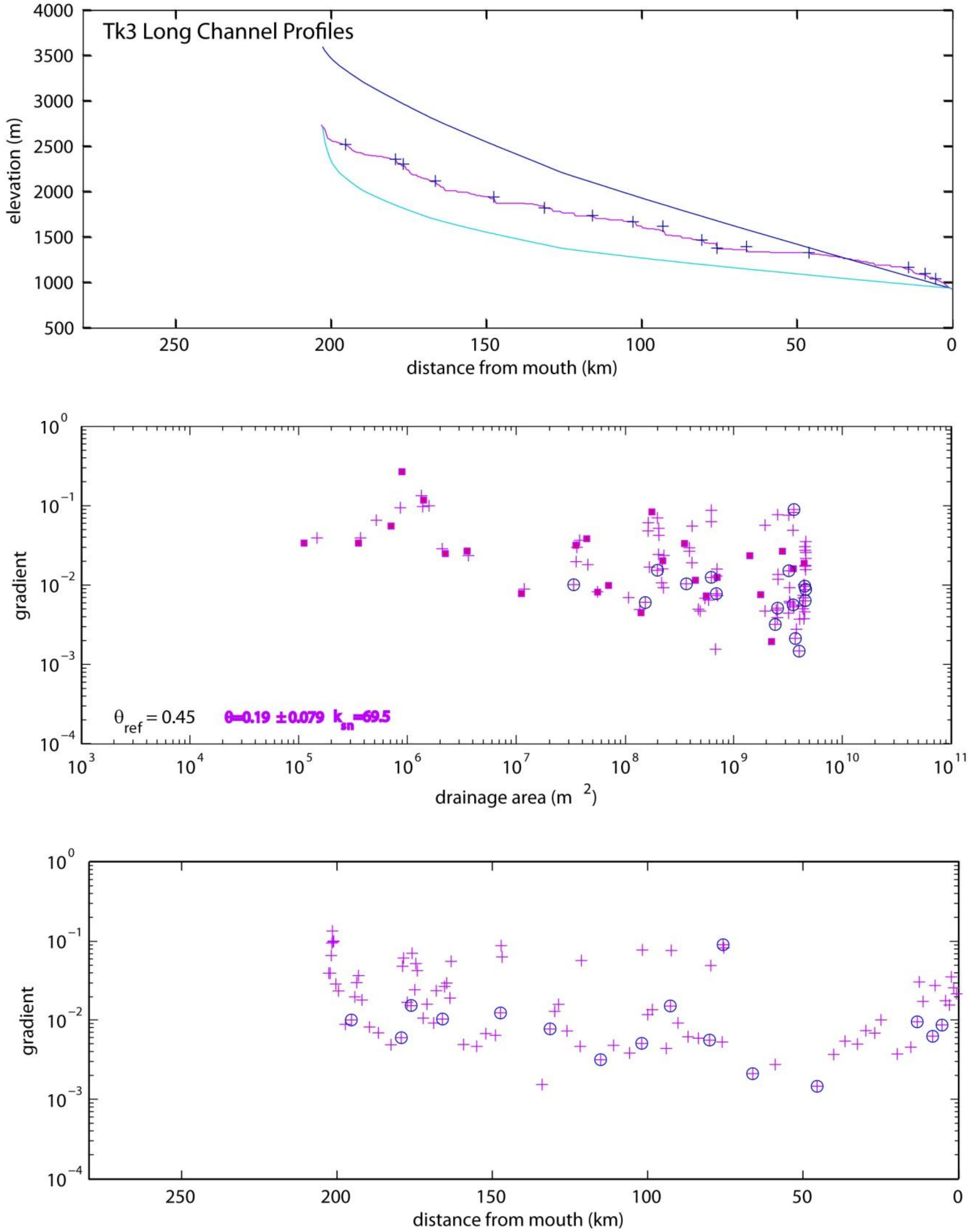
Tk3 Long Channel Profiles
elevation (m)
distance from mouth (km)
gradient
drainage area (m 2)
θ_{ref} = 0.45
θ=0.19 ±0.079 k_{sn}=69.5
gradient
distance from mouth (km)

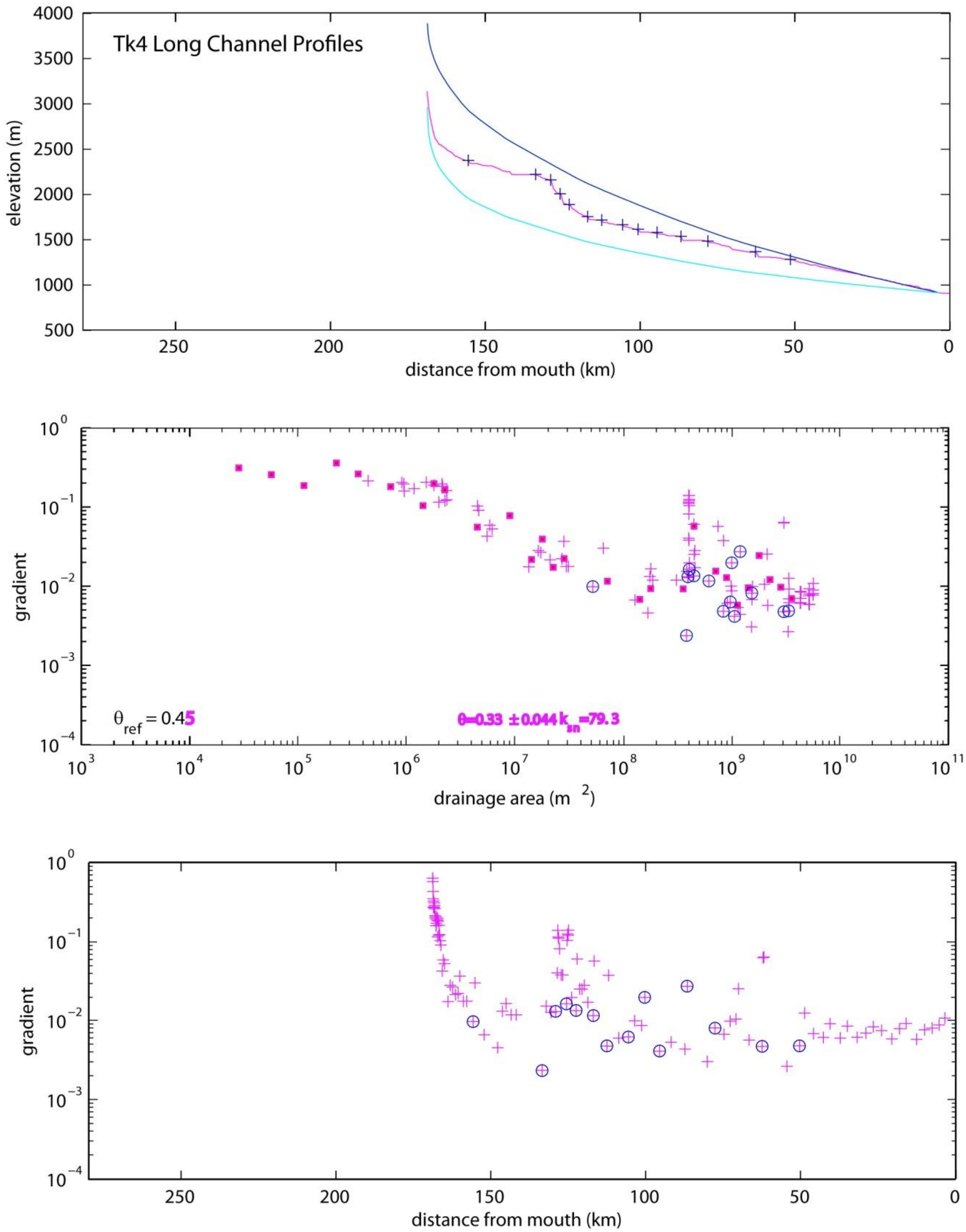

Tk4 Long Channel Profiles
elevation (m)
distance from mouth (km)
gradient
drainage area (m 2)
θ_{ref} = 0.45
θ=0.33 ±0.044 k_{sn}=79.3
gradient
distance from mouth (km)

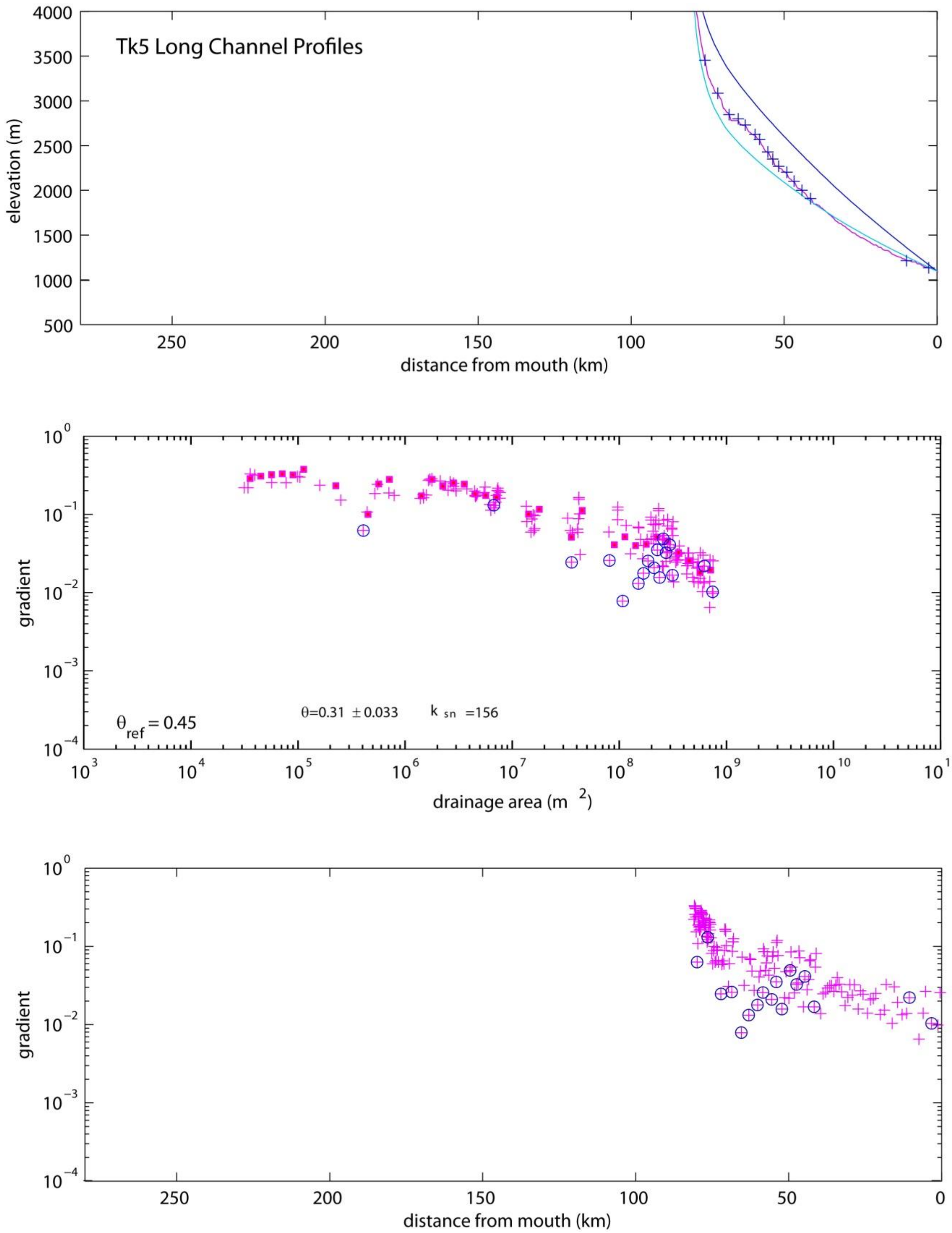

Tk5 Long Channel Profiles
elevation (m)
distance from mouth (km)
gradient
θ=0.31 ± 0.033
k sn =156
θ_{ref} = 0.45
drainage area (m 2)
gradient
distance from mouth (km)

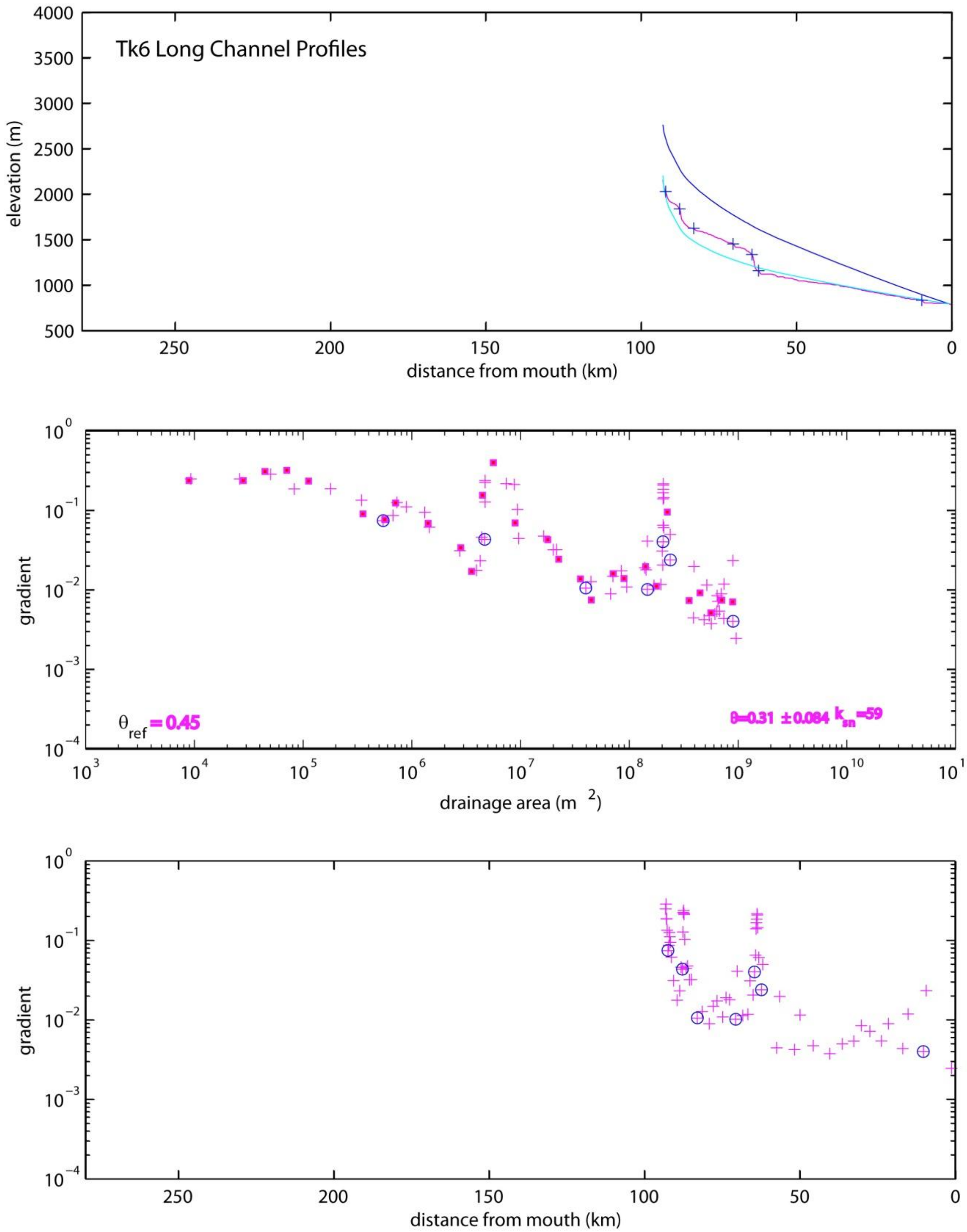
Tk6 Long Channel Profiles
elevation (m)
distance from mouth (km)
gradient
drainage area (m 2)
θref = 0.45
θ=0.31 ± 0.084 ksn=59
gradient
distance from mouth (km)

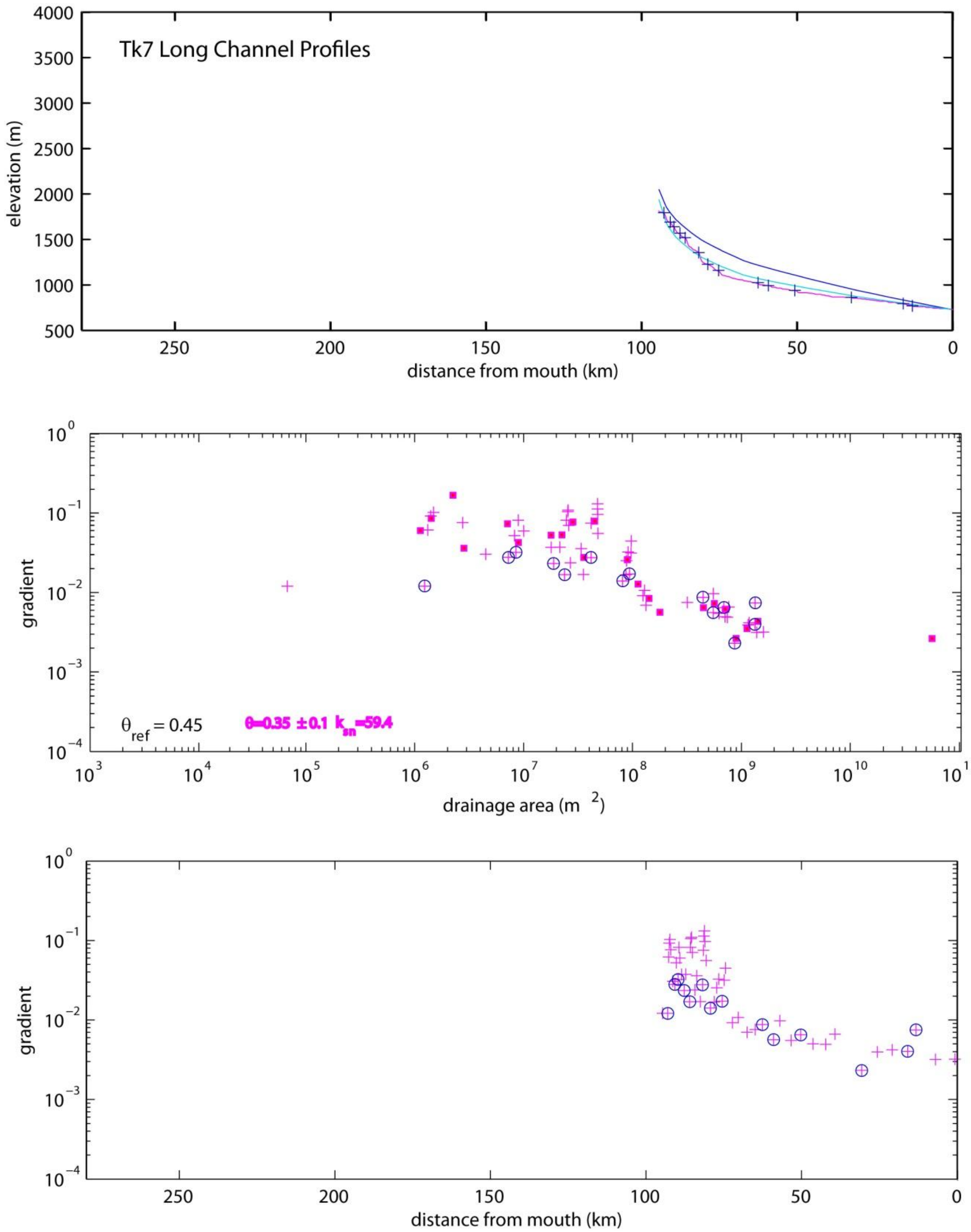

Tk7 Long Channel Profiles
elevation (m)
distance from mouth (km)
gradient
drainage area (m 2)
θ_{ref} = 0.45
θ=0.35 ±0.1 k_{sn}=59.4
gradient
distance from mouth (km)

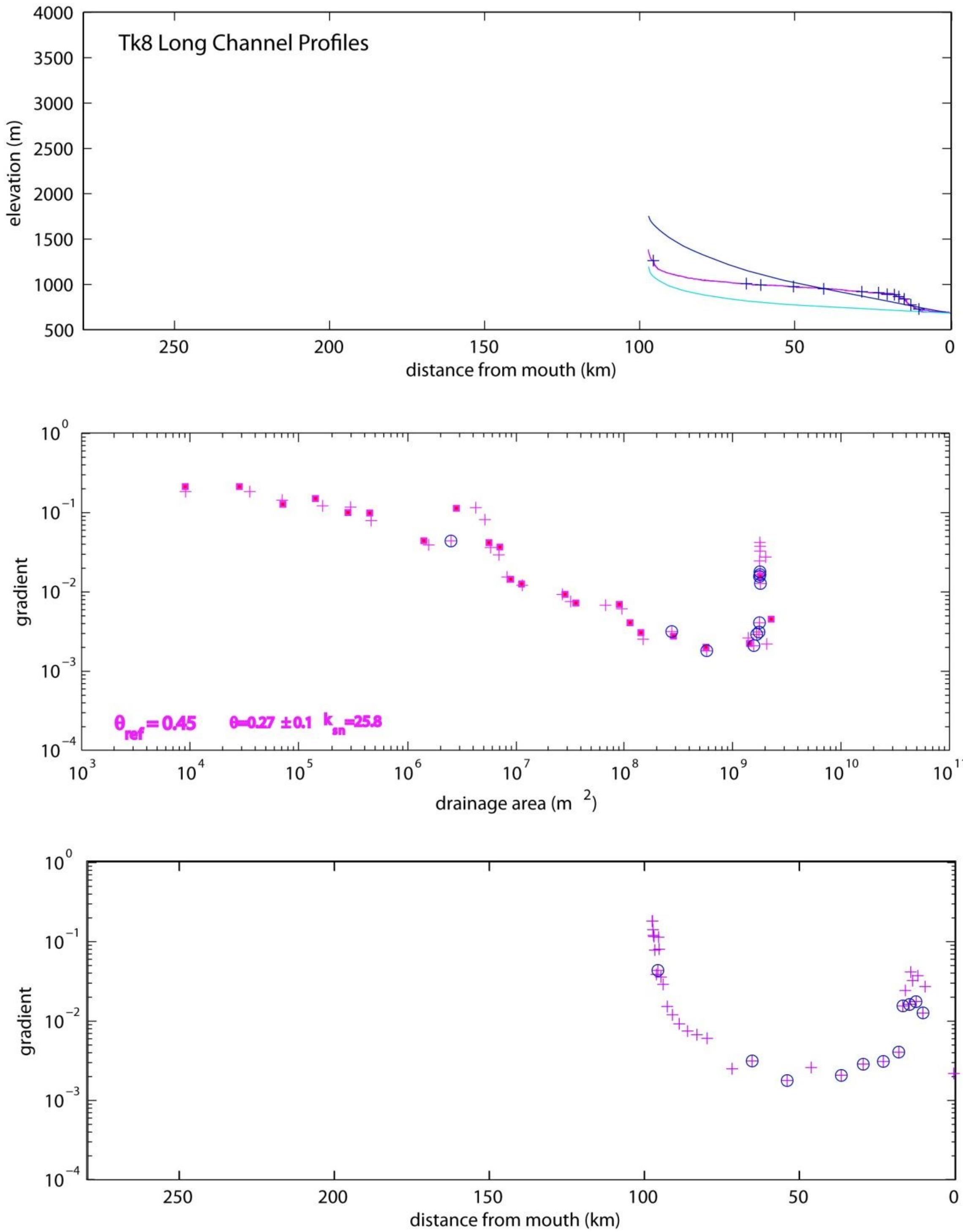
Tk8 Long Channel Profiles
elevation (m)
distance from mouth (km)
gradient
drainage area (m 2)
θref = 0.45
θ=0.27 ±0.1 ksn=25.8
gradient
distance from mouth (km)

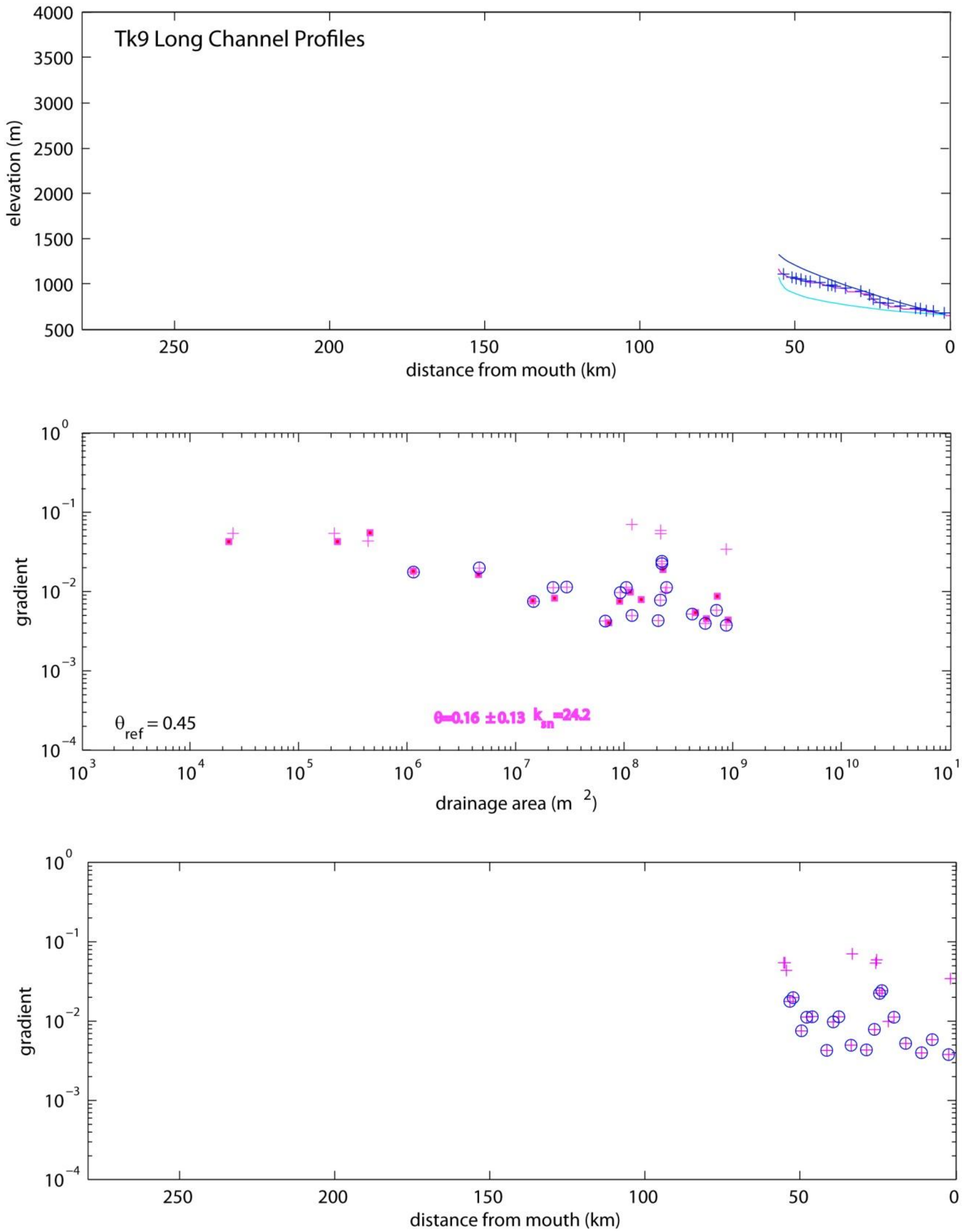
Tk9 Long Channel Profiles
elevation (m)
distance from mouth (km)
gradient
drainage area (m 2)
θ=0.16 ±0.13 k sn=24.2
θ ref = 0.45
gradient
distance from mouth (km)

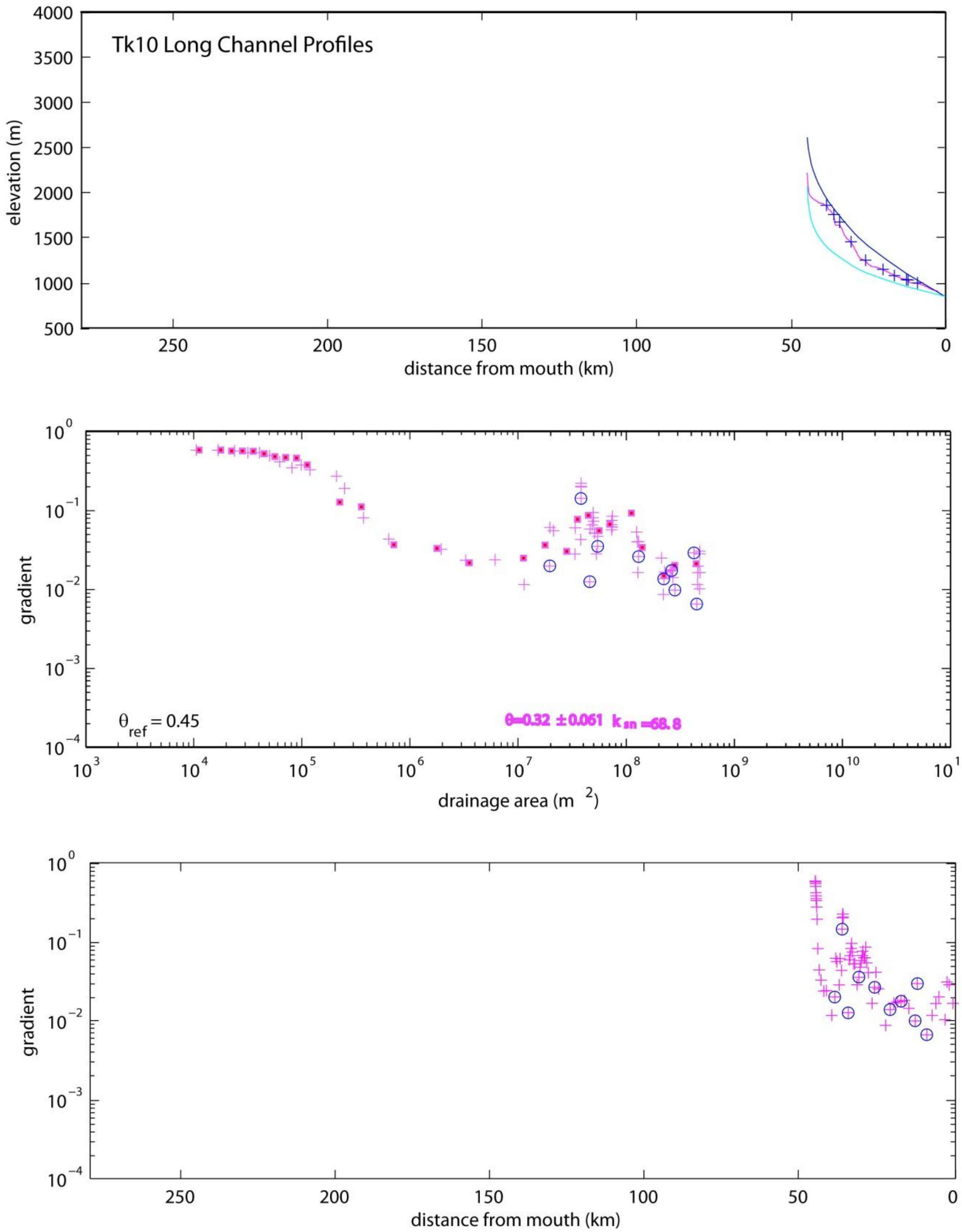
Tk10 Long Channel Profiles
elevation (m)
distance from mouth (km)
gradient
drainage area (m 2)
θref = 0.45
θ=0.32 ±0.061 ksn =68.8
gradient
distance from mouth (km)

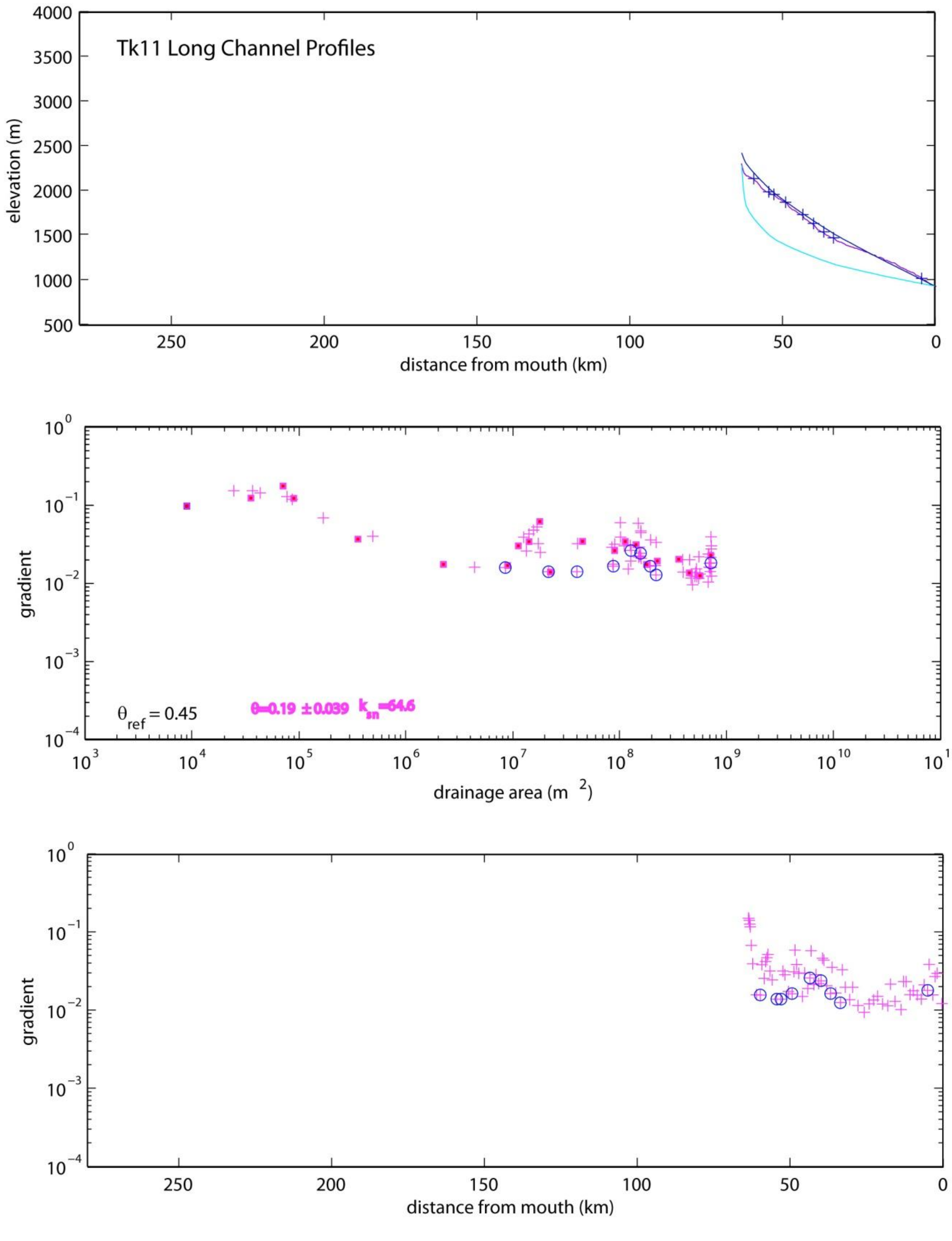
Tk11 Long Channel Profiles
elevation (m)
distance from mouth (km)
gradient
drainage area (m 2)
θref = 0.45
θ=0.19 ± 0.039 ksn=64.6
gradient
distance from mouth (km)

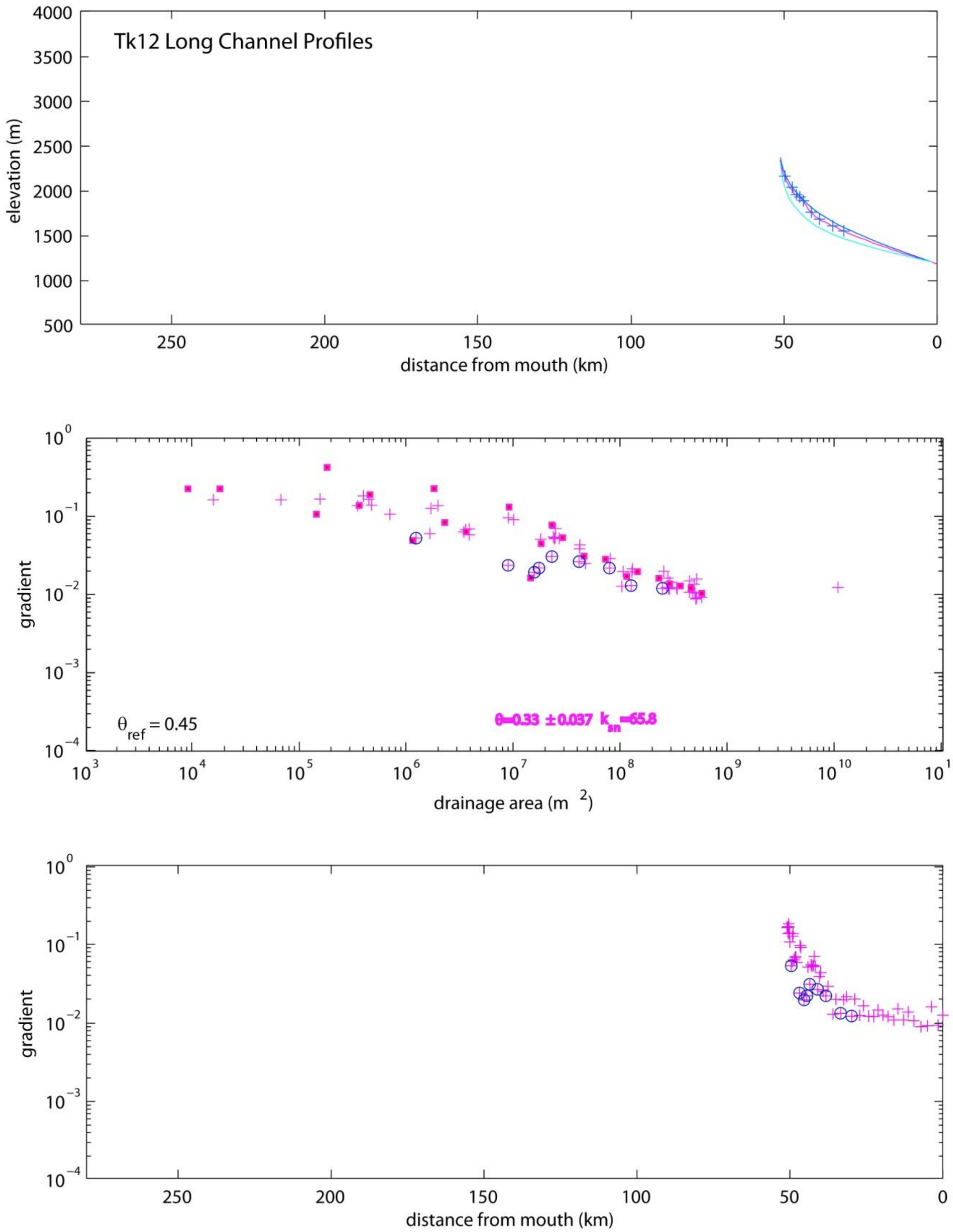
Tk12 Long Channel Profiles
elevation (m)
distance from mouth (km)
gradient
drainage area (m 2)
θref = 0.45
θ=0.33 ±0.037 ksn=65.8
gradient
distance from mouth (km)

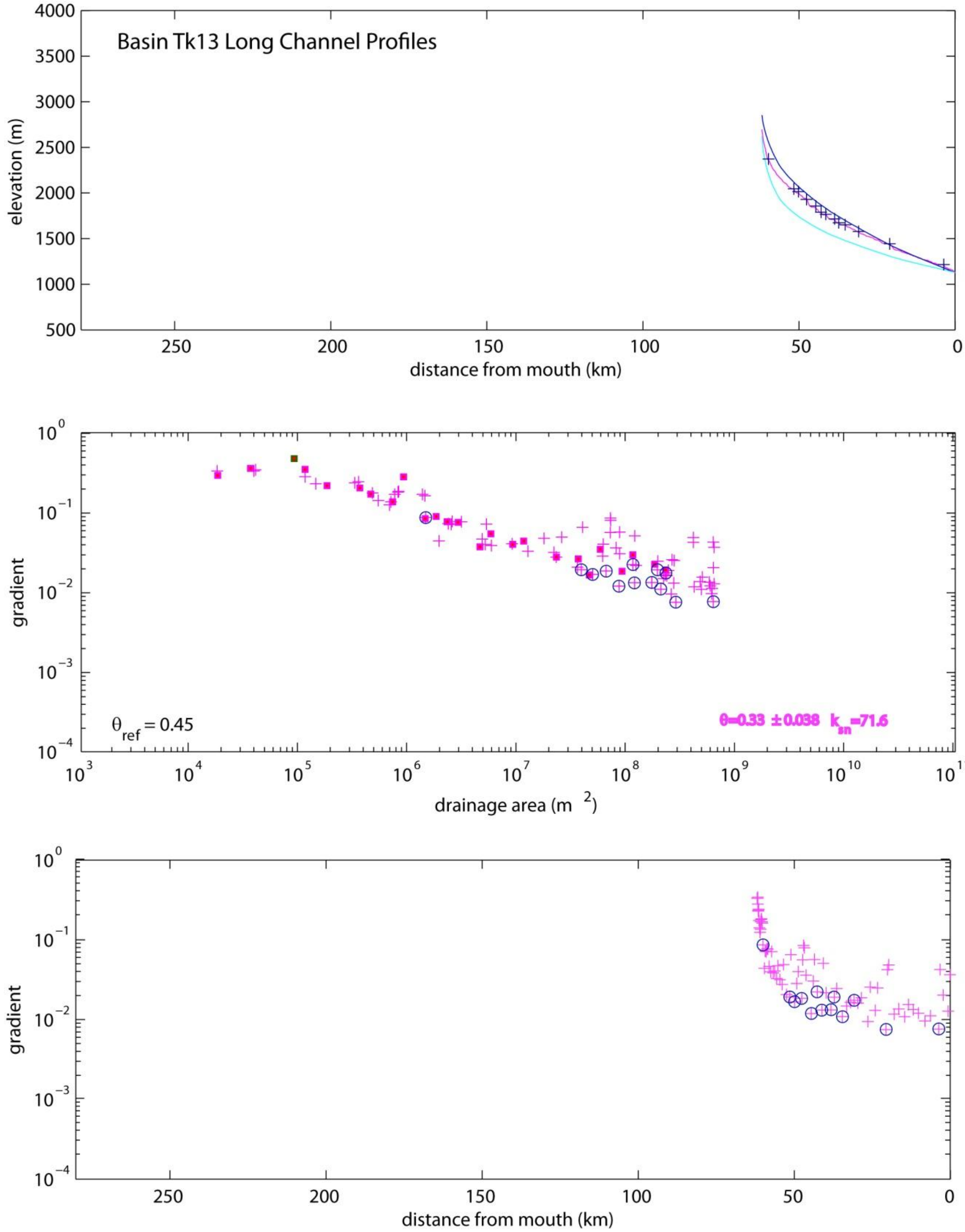
Basin Tk13 Long Channel Profiles
elevation (m)
distance from mouth (km)
gradient
drainage area (m 2)
θref = 0.45
θ=0.33 ±0.038 ksn=71.6
gradient
distance from mouth (km)

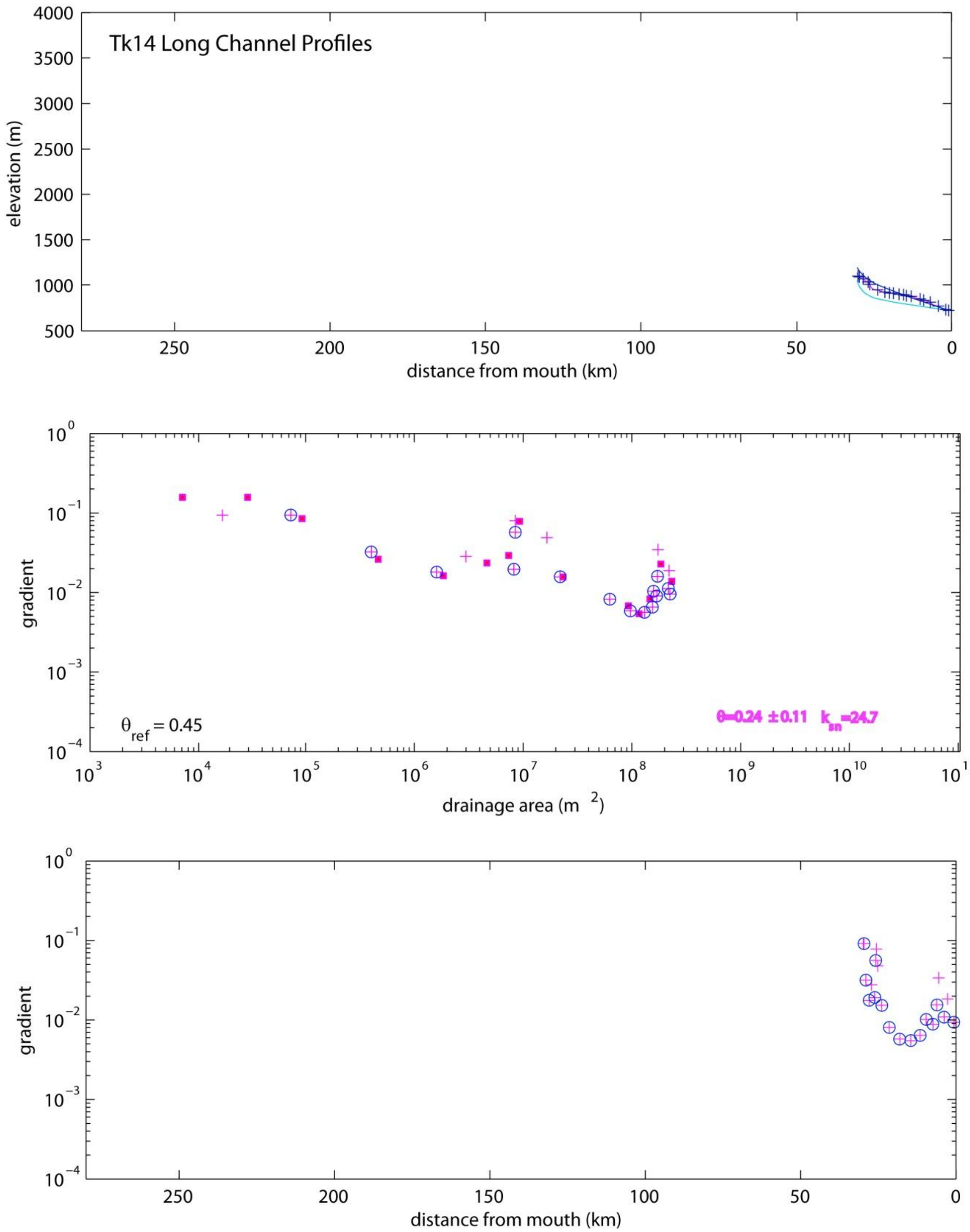

Tk14 Long Channel Profiles
elevation (m)
distance from mouth (km)
gradient
drainage area (m 2)
θref = 0.45
θ=0.24 ±0.11 ksn=24.7
gradient
distance from mouth (km)

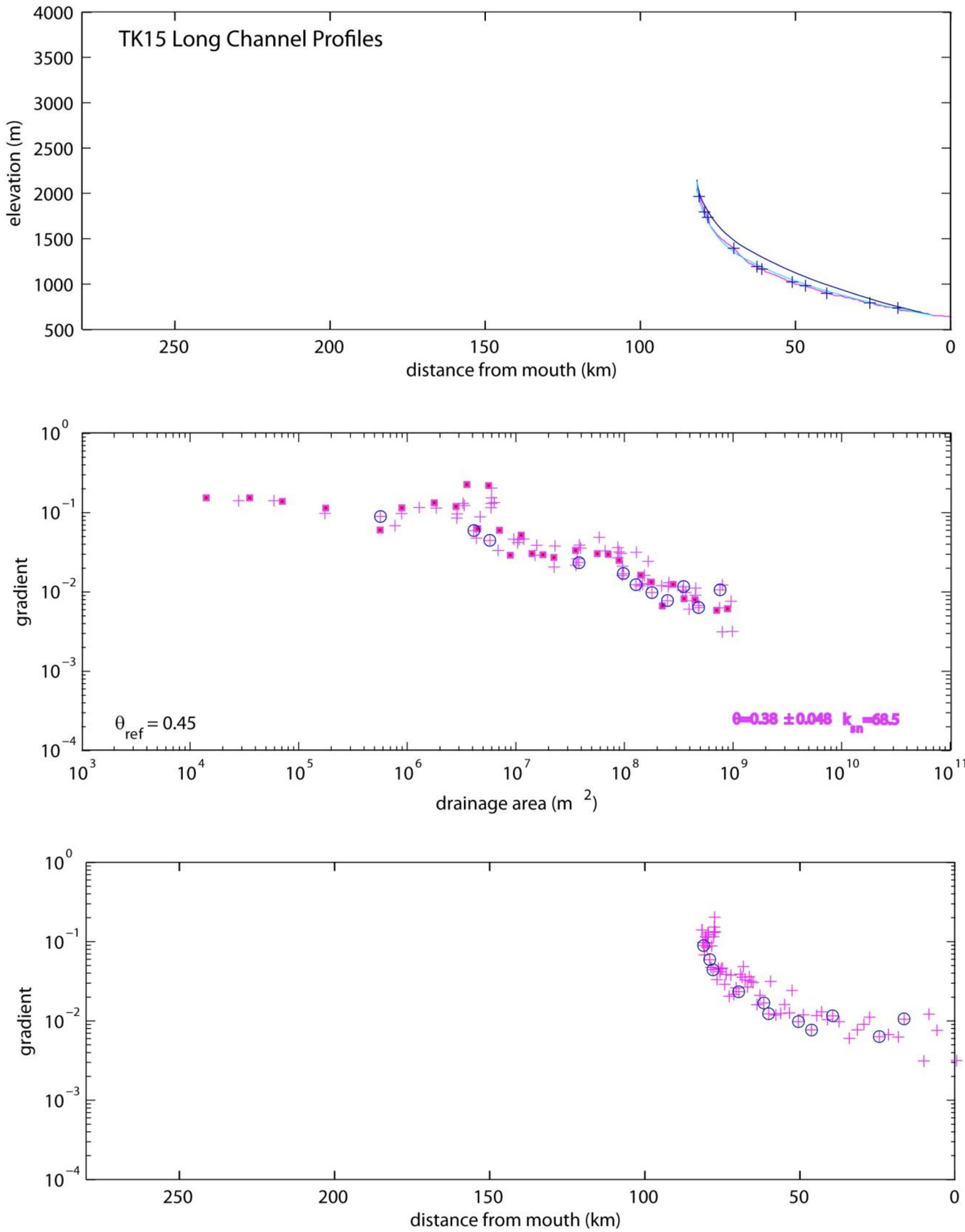
TK15 Long Channel Profiles
elevation (m)
distance from mouth (km)
gradient
drainage area (m 2)
θref = 0.45
θ=0.38 ± 0.048 ksn=68.5
gradient
distance from mouth (km)

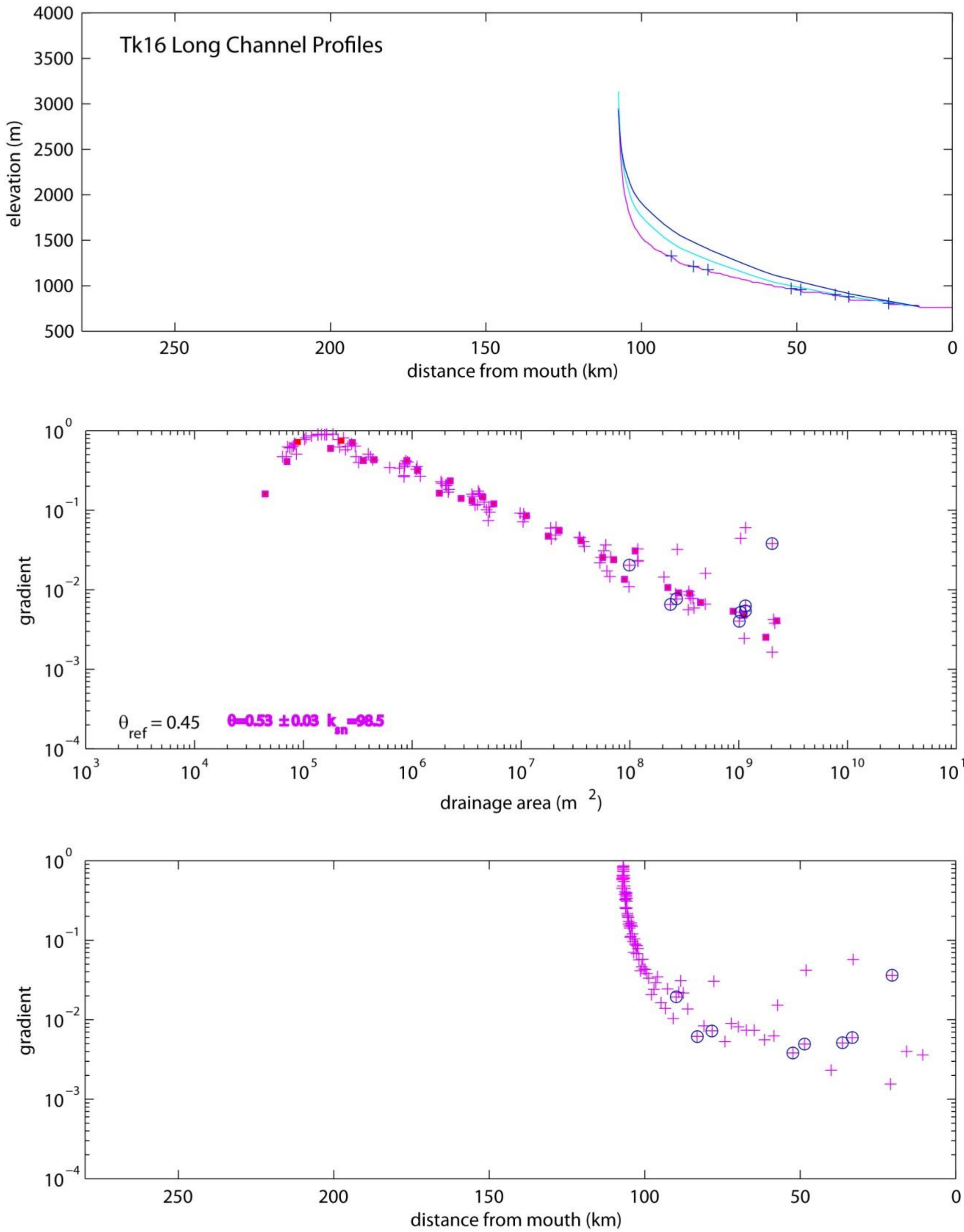
Tk16 Long Channel Profiles
elevation (m)
distance from mouth (km)
gradient
drainage area (m 2)
θ_{ref} = 0.45
θ=0.53 ±0.03 k_{sn}=98.5
gradient
distance from mouth (km)

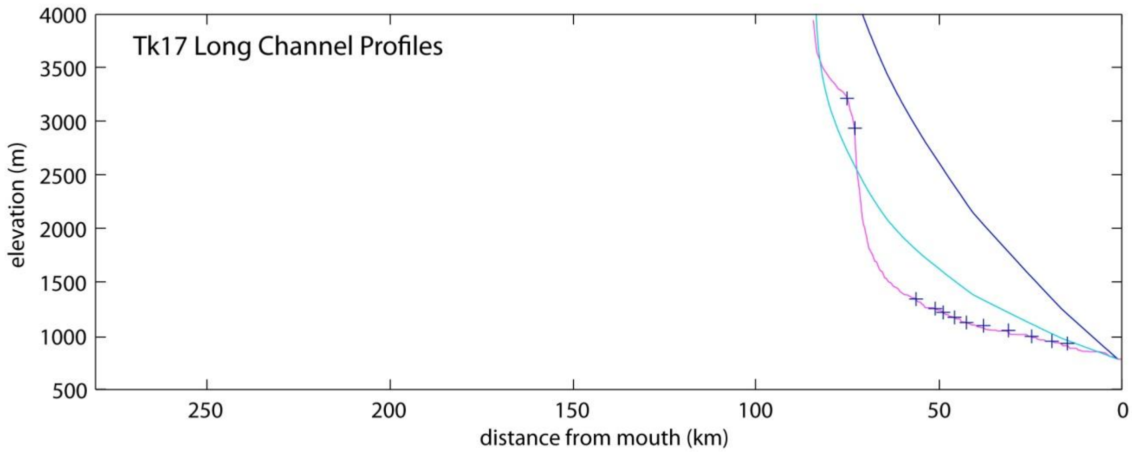
Tk17 Long Channel Profiles
elevation (m)
distance from mouth (km)

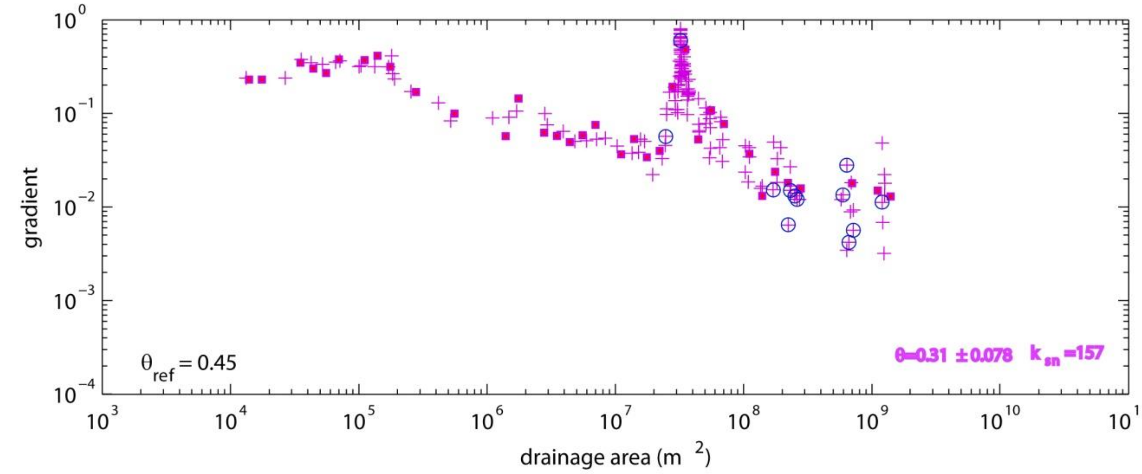
gradient
drainage area (m 2)
θref = 0.45
θ=0.31 ±0.078 ksn =157

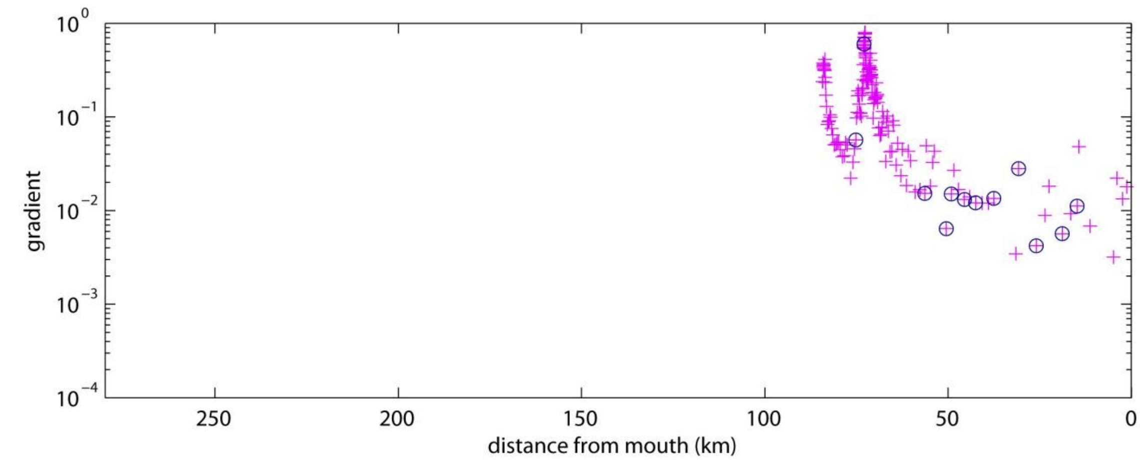
gradient
distance from mouth (km)

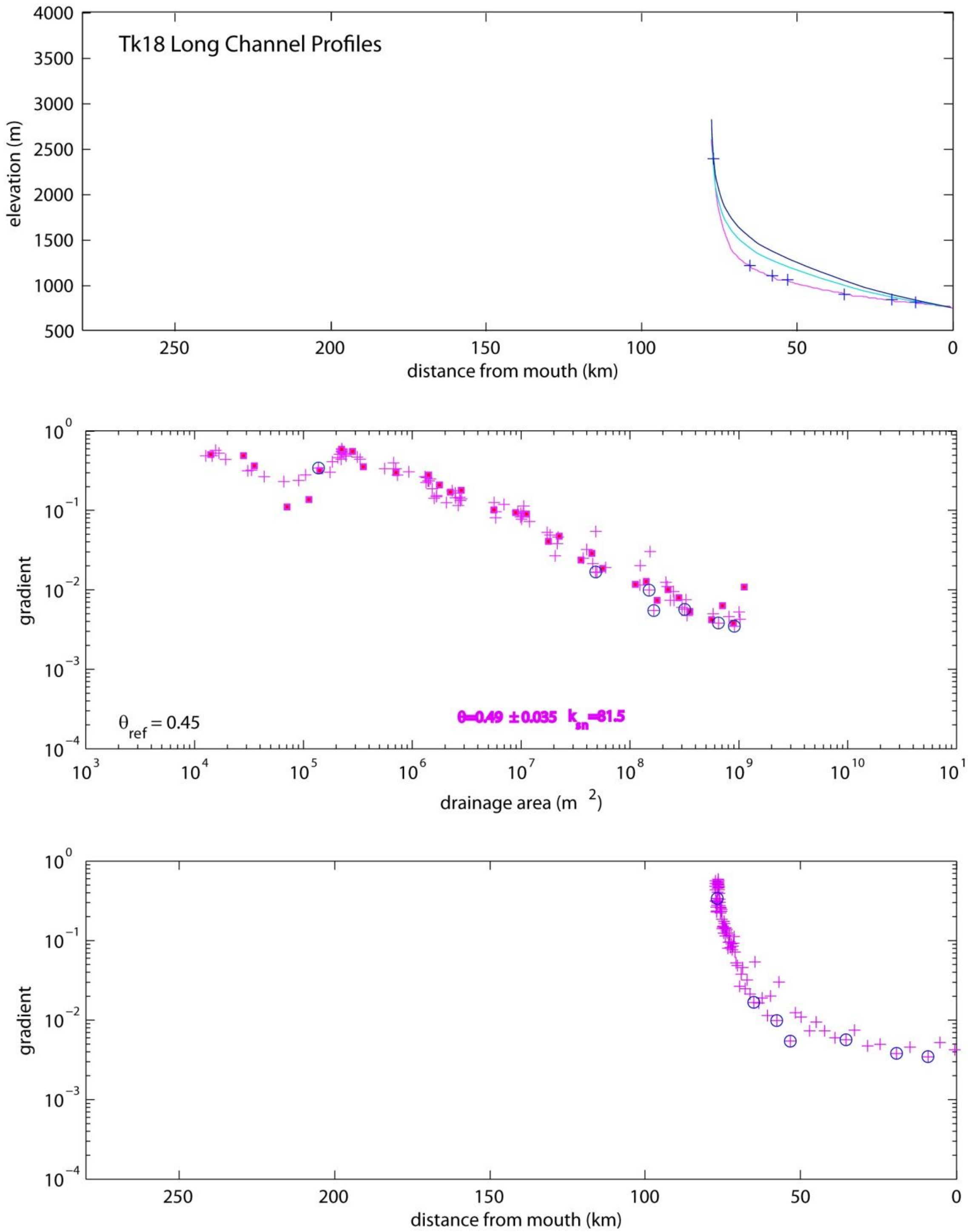
Tk18 Long Channel Profiles
elevation (m)
4000
3500
3000
2500
2000
1500
1000
500
250
200
150
100
50
0
distance from mouth (km)
gradient
10^0
10^-1
10^-2
10^-3
10^-4
θref = 0.45
θ=0.49 ±0.035 ksn=81.5
10^3
10^4
10^5
10^6
10^7
10^8
10^9
10^10
10^11
drainage area (m 2)
gradient
distance from mouth (km)

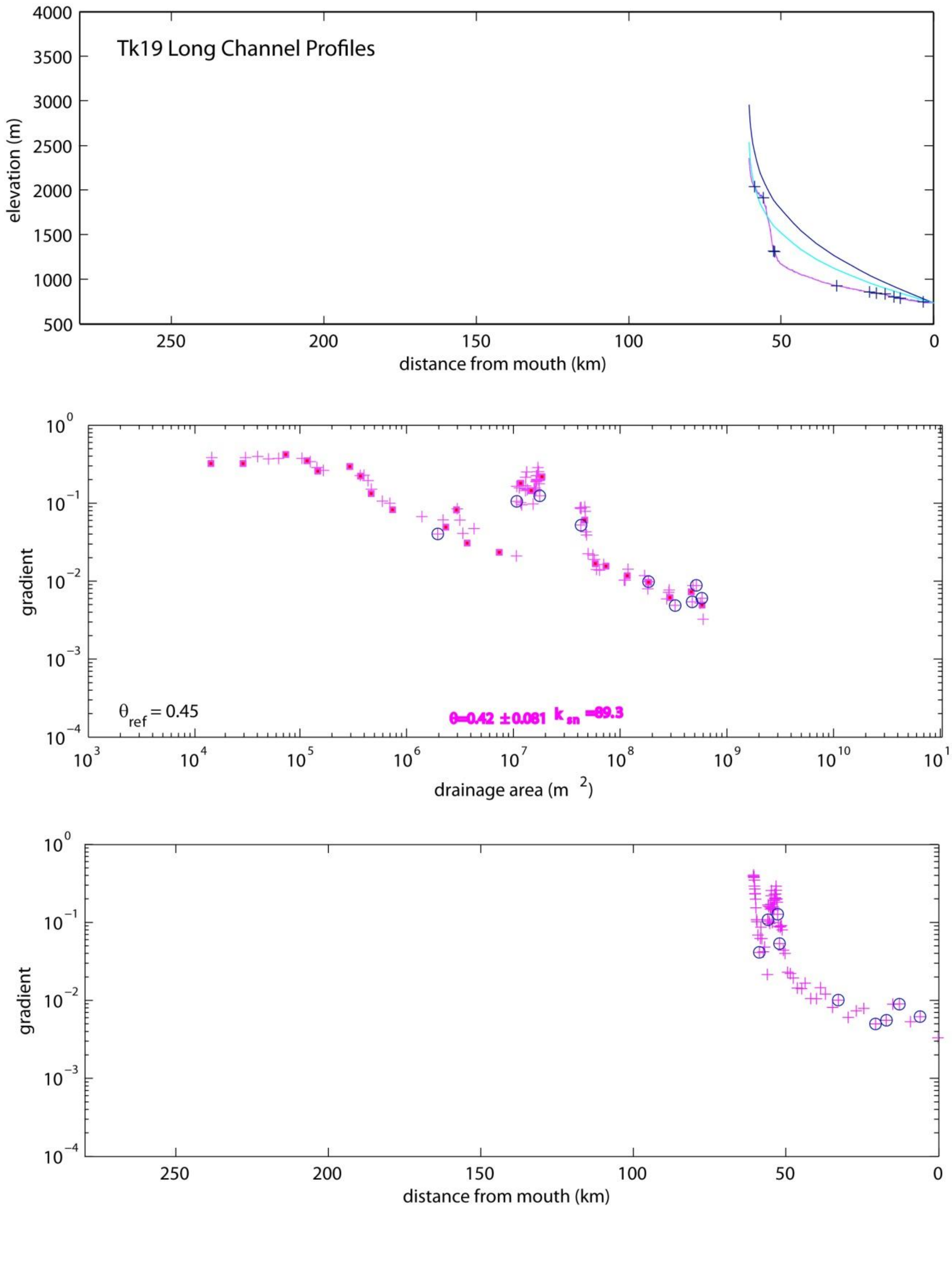

Tk19 Long Channel Profiles
elevation (m)
distance from mouth (km)
gradient
θref = 0.45
θ=0.42 ± 0.081 k sn =89.3
drainage area (m 2)
gradient
distance from mouth (km)

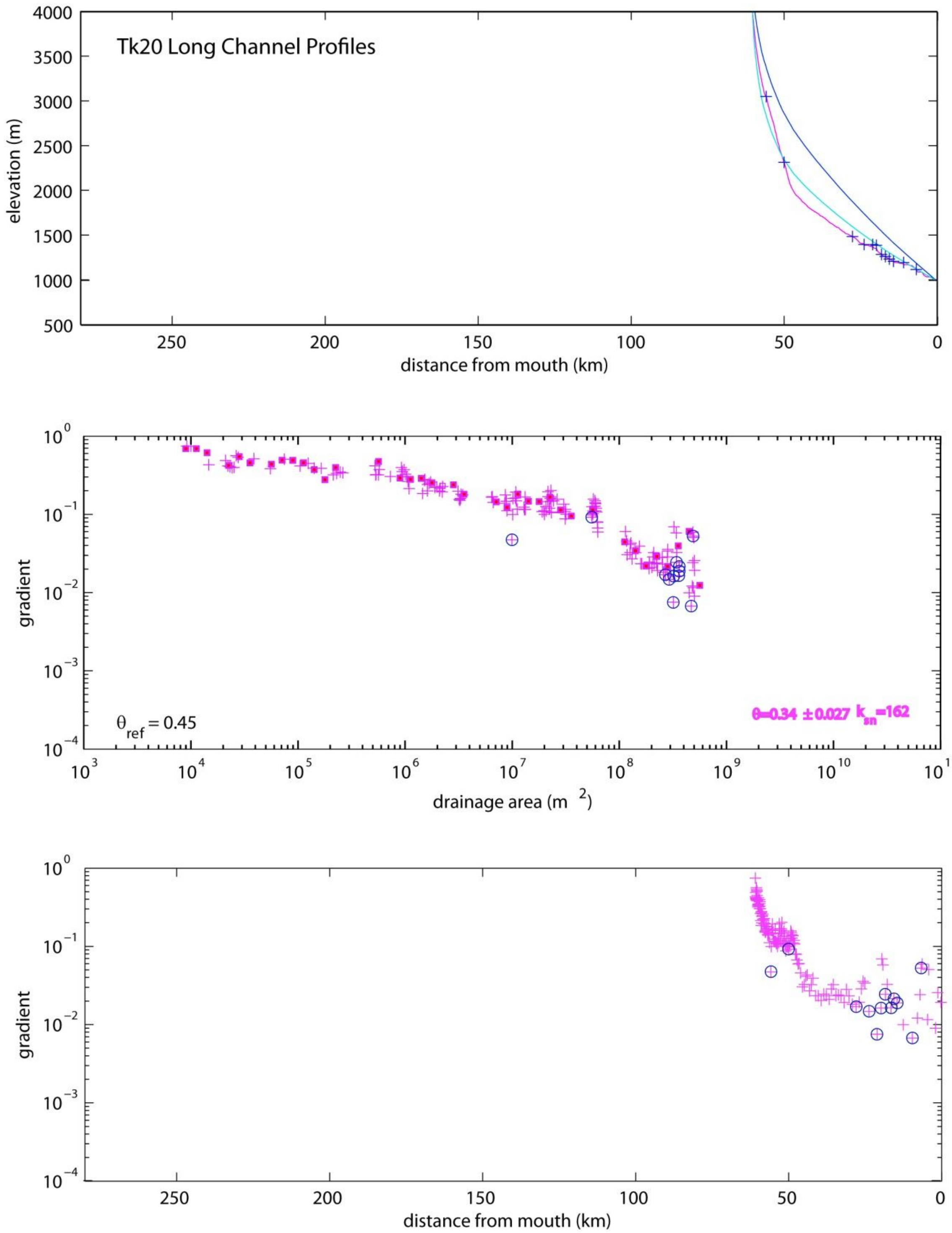
Tk20 Long Channel Profiles
elevation (m)
distance from mouth (km)
gradient
θref = 0.45
θ=0.34 ± 0.027 ksn=162
drainage area (m 2)
gradient
distance from mouth (km)

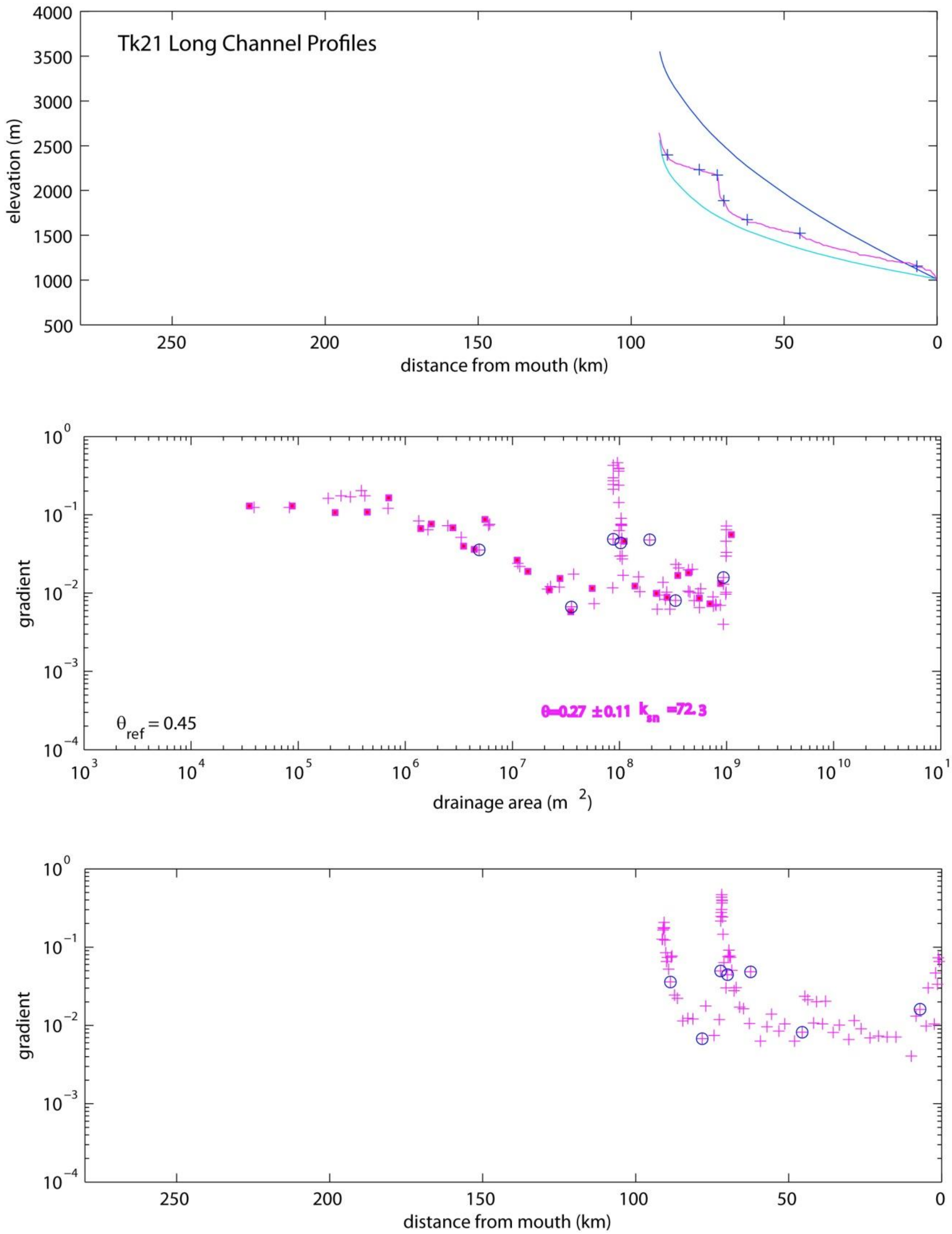
Tk21 Long Channel Profiles
elevation (m)
distance from mouth (km)
gradient
θ=0.27 ±0.11 k_sn =72.3
θ_ref = 0.45
drainage area (m 2)
gradient
distance from mouth (km)

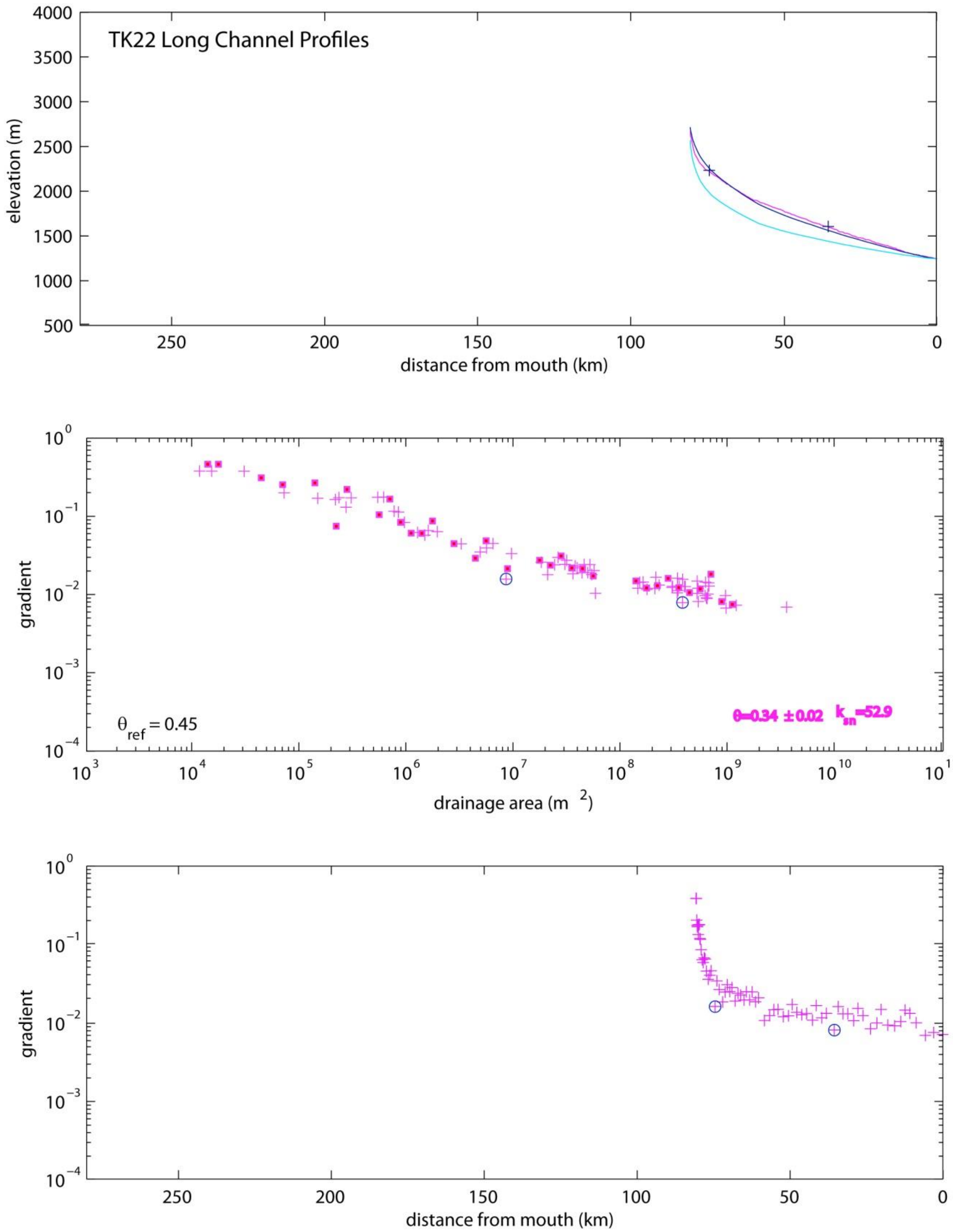
TK22 Long Channel Profiles
elevation (m)
distance from mouth (km)
gradient
drainage area (m 2)
θref = 0.45
θ=0.34 ± 0.02 ksn=52.9
gradient
distance from mouth (km)

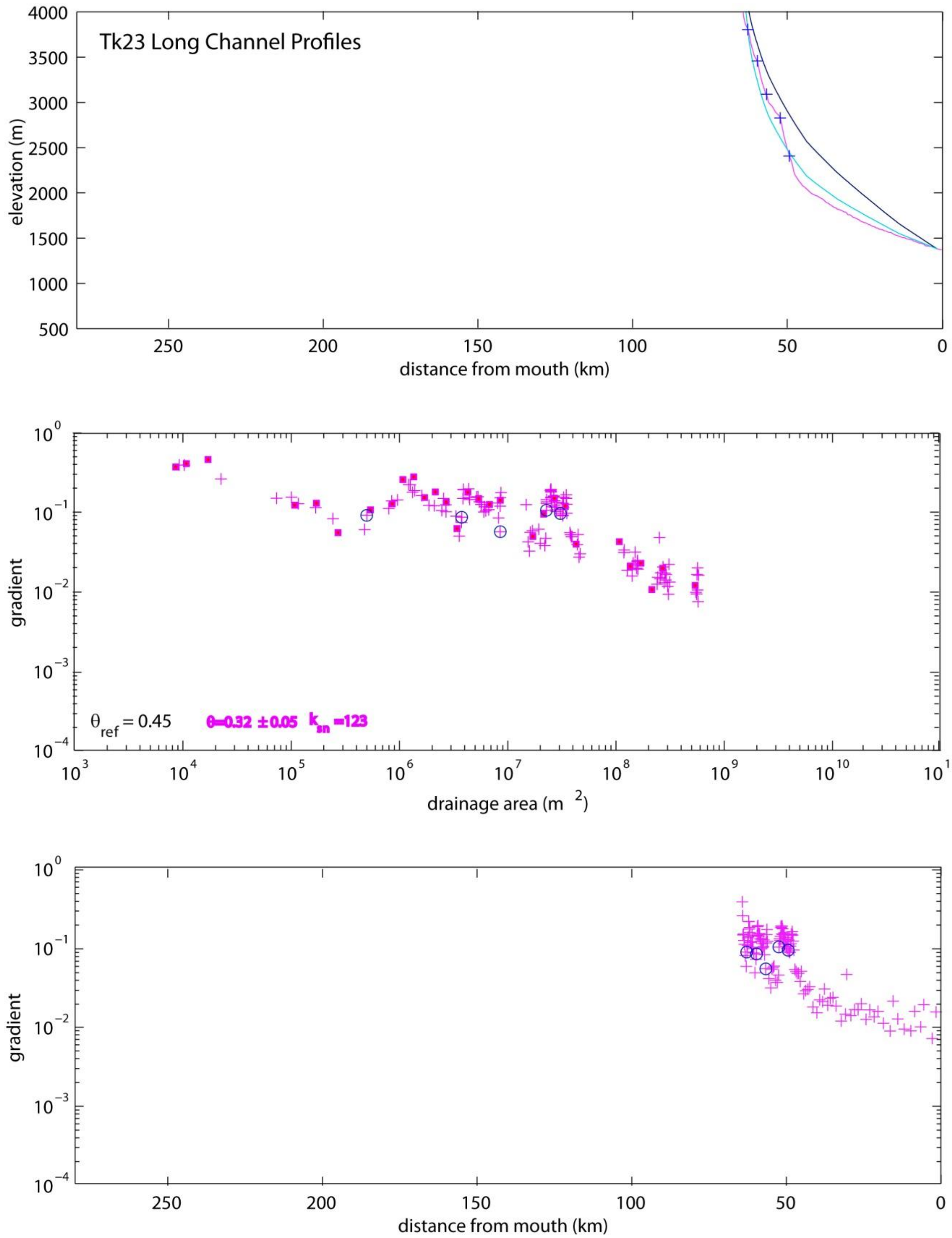
Tk23 Long Channel Profiles
elevation (m)
distance from mouth (km)
gradient
$\theta_{ref} = 0.45$
θ=0.32 ±0.05 k_{sn} =123
drainage area (m 2)
gradient
distance from mouth (km)

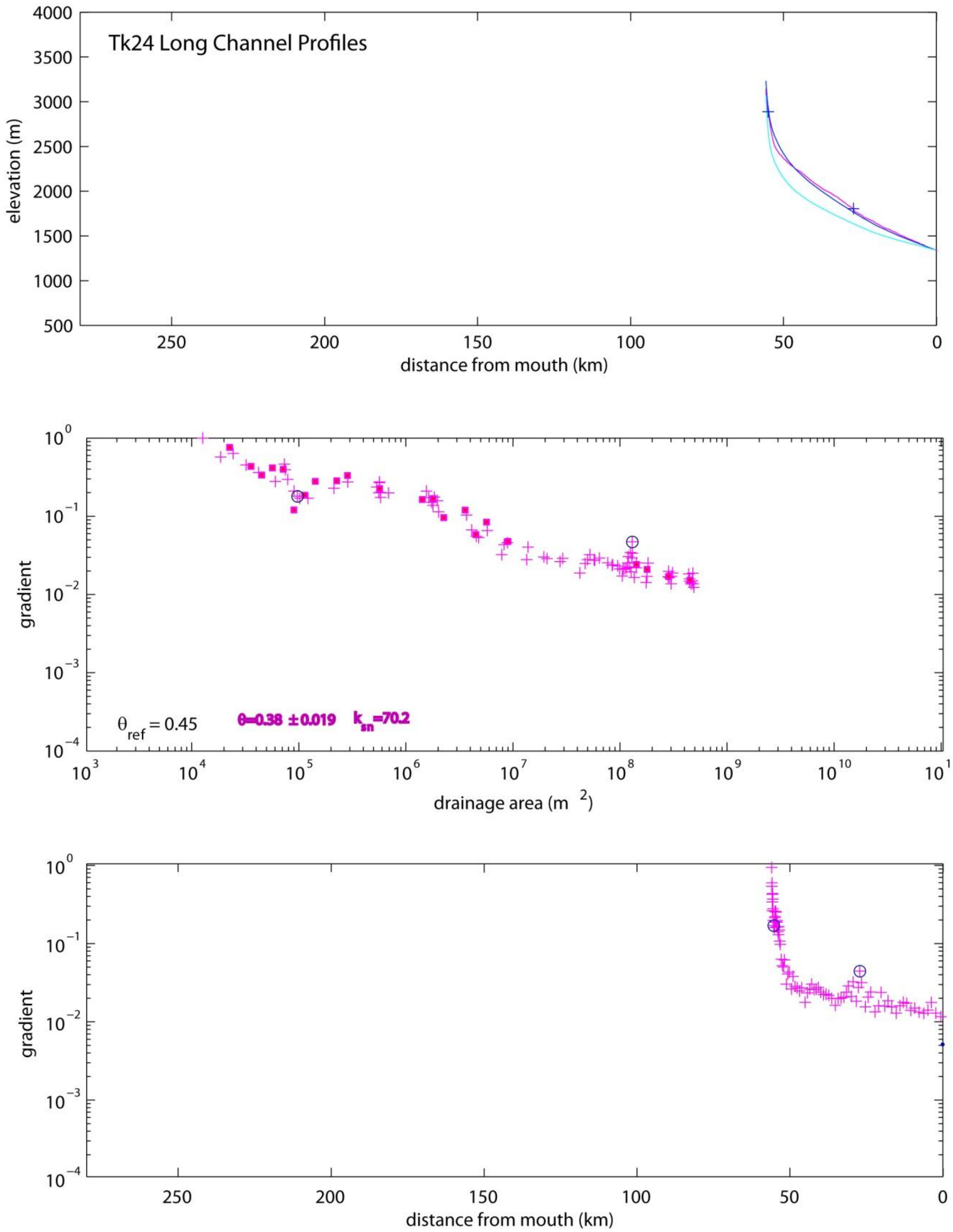

Tk24 Long Channel Profiles
elevation (m)
distance from mouth (km)
gradient
drainage area (m 2)
θ_{ref} = 0.45
θ=0.38 ± 0.019 k_{sn}=70.2
gradient
distance from mouth (km)

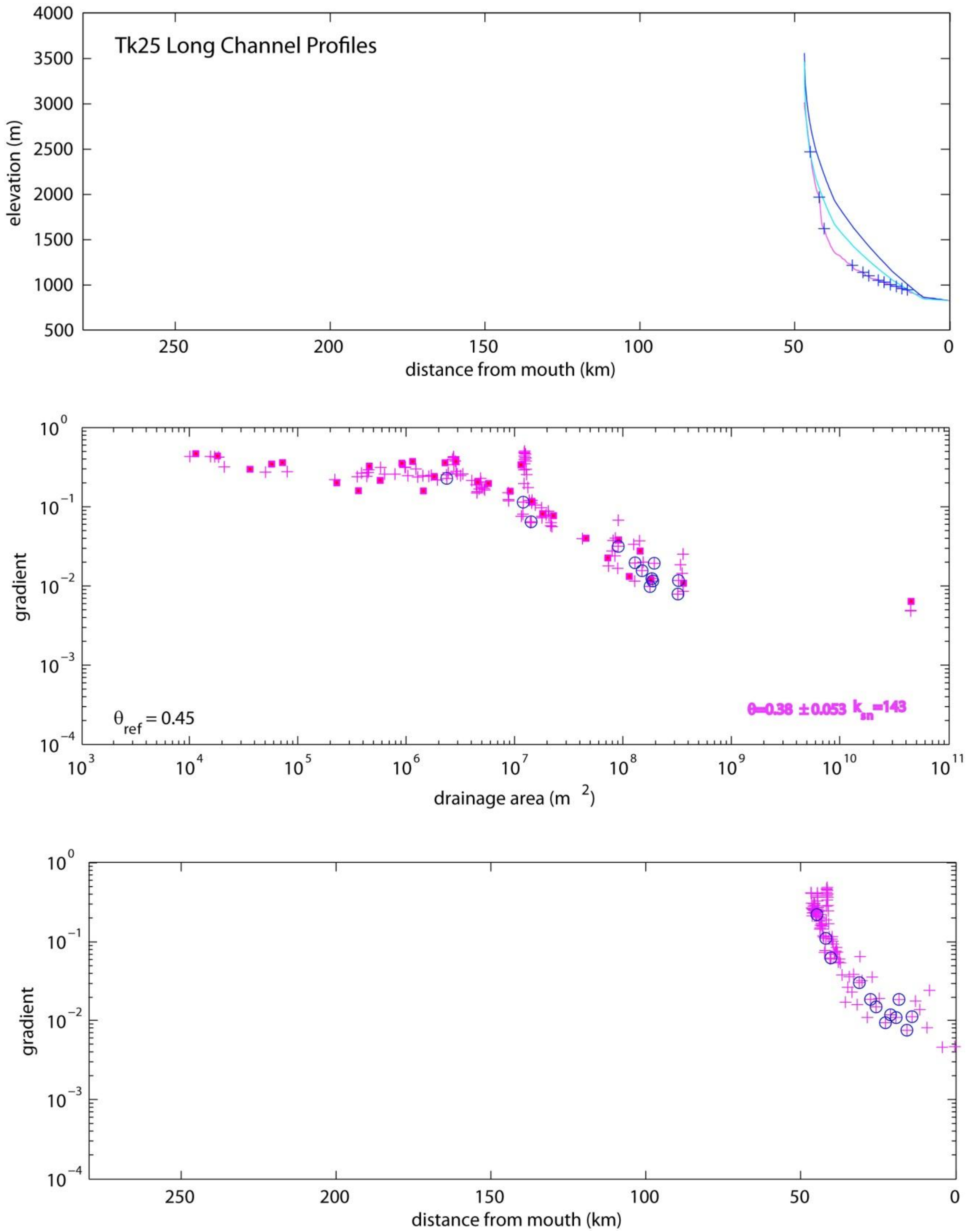
Tk25 Long Channel Profiles
elevation (m)
distance from mouth (km)
gradient
drainage area (m 2)
θref = 0.45
θ=0.38 ± 0.053 ksn=143
gradient
distance from mouth (km)

BIBLIOGRAPHY

Beyene, A., and Abdelsalam, M., 2005, Tectonics of the Afar Depression: A review and analysis: Journal of African Earth Sciences, v. 41, p. 41-59, doi: 10.1016/j.jafrearsci.2005.03.003.

Beyth, M., 1972. The Paleozoic-Mesozoic Sedimentary Basin of the Mekele Outlier, Northern Ethiopia. J. Basins sedimentaires du litforal African. Sedimentary basins of the African coasts, issue p2, 1973, pages 179-190.

Burbank, D., and Anderson, R., Tectonic Geomorphology, 2001, Blackwell Publishing, Victoria 3053, Australia, ppgs. 274, ISBN 978-0-632-04386-6.

Burbank, D.W., and Pinter, N., 1999, Landscape evolution: the interaction of tectonics and surface processes, Basin Research (1999) 11, 1-6.

Capaldi, G., Chiesa, S., Manetti, P., Orsi, G., and Poli, G., 1987, Tertiary anorogenic granites of the Western border of the Yemen Plateau: Lithos, v. 20, p. 433-444, doi: 10.1016/0024-4937(87)90028-4.

Chen, Y., Sung, Q., Cheng, K., 2003. Along-strike variation of morphotectonic features in Western Foothills of Taiwan: tectonic implications based on stream gradient and hypsometric analysis. Geomorphology 56 (2003) 109-137.

Clark, M., Schoenbohm, L., Royden, L., Whipple, K., Burchfiel, B., Zhang, X., Than, W., Wang, E., and Chen, L., 2004, Surface uplift, tectonics, and erosion of eastern Tibet from large-scale drainage patterns: Tectonics, v. 23, TC1006, doi: 10.1029/2002TC001402.

Collet, B., Taud, H., and Parrot, J., 1999, Altimetric anomalies in the Afro-Arab zone: Ecolgae Geolgicale Helvateae, v. 92, p. 275-284.

Crosby, B., and Whipple, K., 2006, Knickpoint initiation and distribution within fluvial networks: 236 waterfalls in the Waipaoa River, North Island, New Zealand: Geomorphology, v. 82, p. 16–38.

Cunha, P., Martins, A., Daveau, S., and Friend, P., 2005. Tectonic control of the Tejo river fluvial incisión during the late Cenozoic, in Ródao-central Portugal (Atlantic Iberian border). Geomorphology 64, 271–298.

Cry, J., Granger, D., Olivetti, V., and Molin, P., 2010, Quantifying rock uplift rates using channel steepness and cosmogenic nuclide-determined erosion rates: Examples from northern and southern Italy, Lithosphere, v. 2 Number 3, p. 188-198.

Davis, P., and Slack, P., 2002, the uppermost mantle beneath the Kenya dome and relation to melting, rifting, and uplift in East Africa: Geophysical Research Letters, v. 29, doi: 10.1029/2001GL013676.

Gani, N., 2006, Geological evolution and incision history of the Gorge of the Nile on Ethiopian Plateau from remote sensing and geographic information system analysis, and field studies, PhD dissertation: University of Texas at Dallas, 128 p.

Gani, N., Abdelsalam, M., Gera, S., and Gani, M., 2008, Stratigraphic and structural evolution of the Blue Nile Basin, Northwestern Ethiopian Plateau, Geol. J. (2008), John Wiley & Sons, Ltd, DOI: 10.1002/gj.

Gani, N., Gani, M., and Abdelsalam, M., 2007, Blue Nile Incision on the Ethiopian Plateau: pulsed plateau growth, Pliocene uplift and hominin evolution, GSA Today: v. 17, no. 9, doi: 10.1130/GSAT01709A.1

Gani, N., and Abdelsalam, M., 2006, Remote sensing analysis of the Gorge of the Nile, Ethiopia with emphasis on Dejen–Gohatsion region: Journal of African Earth Sciences, v. 44 (2006) 135-150.

Goldstein, E., and Kirby, E., 12/2006, Testing fluvial incision models in landscapes undergoing differential rock uplift, American Geophysical Union, Fall Meeting2006, abstract #H51G-0557, http://adsabs.harvard.edu/abs/2006AGUFM.H51G0557G.

Harmar, O.P., and Clifford, N.J., 2007, Geomorphological explanation of the long profile of the Lower Mississippi River, Geomorphology 84 (2007) 222–240.

Hay, w., Soeding, E., DeConto, R., Wold, C., 2002, The Late Cenozoic uplift – climate change paradox: International Journal of Earth Sciences, v. 91, p.746-774, doi: 10.1007/s00531-002-0263-1.

Hofmann, C., Courtillot, V., Feraud, G., Rochette, P., Yirgu, G., Ketefo, E., and Pik, R., 1997. Timing of the Ethiopian flood basalt event and implications for plume birth and global change. Nature, v. 389, p. 838-841, doi: 10.1038/39853.

Howard, D., 1994, modeling fluvial erosion on regional to continental scales, journal of geophysical research, vol. 99, No. B7, p. 13,971-13,986, July 10, 1994.

http://www.geomorphtools.org/: Web site developed by Dr. Benjamin Crosby, Idaho State University for geomorphic tools used in the analysis of stream profiles.

Jordan, G., Meijninger, B., van Hinsbergen, J., Meulenkamp, J., and van Dijk, P., 2005, Extraction of morphotectonic features from DEMs: Development and applications for study areas in Hungary and NW Greece, International Journal of Applied Earth Observation and Geoinformation 7 (2005) 163–182, doi:10.1016/j.jag.2005.03.003

Keller, E., 1986, Investigation of Active Tectonics: Use of Surficial Earth Processes, Active Tectonics Studies in Geophysics, National Academy Press, Washington, DC., 1986.

Kieffer, B., Arndt, N., Lapierre, H., Bastien, F., Bosch, D., Pecher, A., Yirgu, G., Ayalew, D., Weis, D., Jerram, D., Keller, F., and Meugniot, C., 2004. Flood and Shield Basalts from Ethiopia: Magmas from the African Super swell. J. of Petrology. 45, 793-834.

Knuepfer, P., 2004, Extracting tectonic and climatic signals from river terrace long profiles in active Orogens, Taiwan and New Zealand, Geological Society of America Abstracts with programs, vol. 36, No. 5, p. 307, 2004 Denver Annual Meeting (November 7-10, 2004), Colorado, Paper No. 126-8.

Koons, P., 1995, Modeling the topographic evolution of collisional belts, Ann. Rev. Earth Planet. Sci. 1995. 23:375-408.

Larue, J., 2007, Effect of tectonics and lithology on long profiles of 16 rivers of Southern Central Massif border between the Aude and Orb (France), Geomorphology 93 (2008) 343-367.

Masek, J., Isacks, B., Gubbels, T., and Fielding, E., 1994, Erosion and tectonics at the margins of continental plateaus, Journal of geophysical research, vol. 99, No. B7, p. 13,941-13,956, July 10, 1994.

McDougall, I., Morton, W., William, M., 1975, Ages and rates of denudation of trap series basalts at the Blue Nile Gorge, Ethiopia. Nature 254: 207–209.

McMillan, M., 2003, Basinfill erosion surfaces and tilted markers: Evidence of Late Cenozoic tectonic uplift of the Rocky Mountain Orogenic Plateau: PhD Dissertation, University of Wyoming, Laramie, p. 1-127.

McMillan, M., Heller, P., and Wing, S., 2006, History and causes of post-Laramide relief in the Rocky Mountain orogenic plateau: Geological Society of America Bulletin, v. 118, p. 393–405.

Miller, R., Baldwin, L., and Fitzgerald, G., 2008, Surface uplift and disequilibrium geomorphology of metamorphic core complexes in the D'Entrecasteux Islands and Dayman-Suckling Massif, Papua New Guinea, American Geophysical Union, Fall Meeting 2008, abstract #T11B-1864, Bibliographic Code: 2008AGUFM.T24C..07S, http://adsabs.harvard.edu/abs/2005AGUFM.T11B-1864M.

Mohr, P., and Zanettin, B., 1988, the Flood Basalt Province, in McDougall, J.D., eds., Continental Flood Basalts: Dordercht, Netherlands, Kluwer Academic Publishers, p. 63-110.

Molin, P., Pazzaglia, F., and Dramis, F., 2001, Relif drainage integration as geomorphic expression of regional uplift and local footwall flexure in portion of Sila Massif, Southern Apennines (Calabria, Italy), American Geophysical Union, Fall Meeting, abstract #T52B-0937, Bibliographic Code: 2001AGUFM.T52B0937M, http://adsabs.harvard.edu/abs/2001AGUFM.T52B0937M.

Molnar, P., 2003, Nature and landscape, Nature, v. 426, p. 612-614, doi: 10.1038/426612a.

Montgomery, D., and Brandon, M., 2002, Topographic controls on rates in tectonically active mountain ranges, Earth and planetary science letters 201 (2002) 481-489.

Pederson, J., Mackley, R., Eddleman, J., 2002, Colorado Plateau uplift and erosion evaluated using GIS: GSA Today, v. 12 (8), p. 4-10.

Pedrera, A., Perez-Pena J., Galindo-Zaldivar, J., Azanon, J., and Azor, A., Testing the sensitivity of geomorphic indices in areas of low-rate active folding (eastern Betic Cordillera, Spain), 2009, Geomorphology 105 (2009) 218-231, doi: 10.1016/j.gemorph.2008.09.026.

Pik, R., Marty, B., Carignan, J., and Lave, J., 2003, Stability of Upper Nile drainage network (Ethiopia) deduces from (U–Th)/He thermochronometry: Implication of uplift and erosion of the Afar plume dome: Earth and Planetary Science Letters, v. 215, p. 73–88.

Schoenbohm, L., Whipple, K., Burchfield, B., and Chen, L., 2004, Geomorphic Constrains on surface uplift, exhumation, and plateau growth in the Red River region, Yunnan Province, China: Geological Society of America Bulletin, v. 116, p. 895-909, doi: 10.1130/B25364.1.

Sengor, A., 2001, Elevation as indicator of mantle-plume activity, in Ernest, R.E., and Buchan, K., eds., Mantle Plumes: Their Identification through time: Geological Society of America Special Paper 352: 183–225.

Seta, M., Del Monte, M., Fredi, P., and Palmieri, E., 2004, Quantitative morphometric analysis as a tool for detecting deformation patterns in soft-rock terrains: a case study from southern Marches, Italy, Gemorphologie: relif, processus, environment, 2004, no 4, p.267-284.

Snyder, N., Whipple, K., Trucker, G., and Merritts, D., 28 September 1999, Landscape response to tectonic forcing: Digital elevation model analysis profiles in Mendocino triple junction region, northern California, Geological Society of America, http://gsabulletin.gaspubs.org/content/112/8/1250.abstract.

Sougnez, N., and Vanacker, V., 2010, Spatial variability in channel and slope morphology within the Ardennes Massif, and its link with tectonics, Hydol. Earth Syst. Sci. Discuss., 7, 6981-7006, 2010, doi: 10.5194/hessd-7-6981-2010.

Studnicki-Gizbert, C., Wang, Y., Burchfiel, C., and Chen, L., 2005, The Yulong Mountains structural culmination: Tectonic and geomorphic controls on localized uplift rates and exhumation, American Geophysical Union, Fall Meeting 2005, abstract #T24C-07, Bibliographic Code: 2005AGUFM.T24C..07S, http://adsabs.harvard.edu/abs/2005AGUFM.T24C..07S.

Tefera, M., Chernet, T., and Haro, W. 1996. Geological map of Ethiopia at 1:2,000,000 scale. Ethiopian Institute of Geological Surveys.

Tucker, G., and Slingerland, R., 1997, Drainage basin responses to climate change: Water Resources Research, v. 33, no. 8, p. 2031-2047, doi: 10.1029/97WR00409.

Tucker, G., and Whipple, K., 2002, Topographic outcomes predicted by stream erosion models: sensitivity analysis and intermodal comparison, Journal of geophysical research, vol. 107, No. B9, 2179, doi: 10.1029/2001JB000162, 2002.

Weissel, J., and Seidl, M., 1998, Inland propagation of escarpments and river profile evolution across the Southeast Australia passive Continental margin, in Tinkler, K., and Wohl, E., eds., Rivers over rock: Fluvial processes in bedrock channels: American Geophysical Union Geophysical Monograph 107, p. 189-206.

Weissel, J., Malinverno, A., and Harding, D., 1995, Erosional development of the Ethiopian plateau of Northeast Africa from fractal analysis of topography, in Barton, C.C., and Pointe, P.R. eds, Fractals in Petroleum Geology and Earth Processes: New York, Plenum Press, p. 127-142.

Whipple, K., 2004, Bedrock Rivers and the geomorphology of active Orogens, Annu. Rev.Earth Planet. Sci.2004. 32:151-85, doi: 10.1146/annurev.earth.32.101802.120356.

Whipple, K., and Tucker, G.E., 1999, Dynamics of the stream-power river incision model: Implications for height limits of mountain ranges, landscape response timescales, and research needs: Journal of Geophysical Research, v. 104, p. 17,661-17,674, doi: 10.1029/1999JB900120.

Wobus, C., Whipple, K., Kerby, E., Snyder, N., Jhonson, J., Spyropolou, K., Crosby, B., and Sheehan, D., 2006, Tectonics from topography: Procedures, promise, and pitfalls, Geological Society of America, Special Paper 398, Penrose Conference Series, p. 55-74, doi:10.1130/2006.2398(04).

Wolfenden, E., Yirgu, G., Ebinger, C., Deino, A., and Ayalew, D., 2004, Evolution of the northern M Ethiopian Rift: birth of a triple junction. Earth and Planetary Science Letters 24: 213–228.

VITA

Elamin Ismail was born in Khortaqqat, Sudan in 1952, the fourth among ten brothers and sisters. He grew up and studied in Khartoum. Elamin graduated from Khartoum University in 1978 with BS in Chemistry and Geography. He was employed as soil and water chemist and rural development inspector at the Ministry of Agriculture and Natural resources, the Sudan. He joined an MS degree program at the Institute of Environmental studies, University of Khartoum and obtained master degree in environmental studies in 1982. He joined the department of geography, King Saud University in Saudi Arabia as a lecturer from 1983 to 2001, where he taught physical and regional geography and directed for the GIS and computer cartography laboratory, the soil and water analysis laboratory and the department's climatic station.

He migrated to USA in 1999 and started a computer business in Columbus, OH and Brooklyn, NY. He worked as GED and computer instructor at Allen School in Brooklyn, NY and as machine operator, computer component inspector in Grove City, OH. He worked for Central Parking Systems as parking attendant at Madison Square Garden, Manhattan, NY then moved to Manchester, NH to work for Easter Seals NH. He supervised and was caretaker for clients with mental, physical and psychological disabilities.

He enrolled in the PhD degree program in geospatial information sciences at the University of Texas at Dallas in 2006, where he spent one year and then transferred to Missouri University – Rolla in 2007. He earned his M.S degree in Geology and Geophysics from Missouri University of science and Technology in August 2011.